Universidad
Carlos III de Madrid

BIOENGINEERING AND AEROSPACE
ENGINEERING DEPARTMENT

BACHELOR THESIS

# RESOLUTION STUDY OF OPTICAL TOMOGRAPHY SYSTEMS IN MICROSCOPY

**Author: Álvaro Gomariz Carrillo**

**Supervisor: Jorge Ripoll Lorenzo**

Reading date: 4th July 2014

# Acknowledgements

First and foremost, I would like to gratefully acknowledge the enthusiastic supervision of professor Jorge Ripoll during this work, who besides providing me his patient guidance and enthusiastic encouragement, he has been a key part in the decisions regarding my professional future. I should like to express my gratitude to professor Miguel Moscoso, who has also been a source of inspiration for this project. I would also like to extend my thanks to the technicians of the bioengineering laboratory, for their help in offering me the resources in running some of the experiments. This thesis would not have been possible without these people and their enormous knowledge.

Last but not least, I wish to thank my family, as they have done their best for helping me find my pathway and go further. The only way I got here today is through my parents' support and understanding. A special thank you to Victor for helping me start writing this work and being a model of perseverance, and Laura for sharing with me all my successes and failures. Of course, a final word of thanks to all my friends, especially those who despite the distance have been close to me these four years.

# Abstract

Optical microscopy has been used in biomedical studies for more than three centuries, but the limitations imposed by light scattering restricted it to superficial studies. However, novel systems have led to the acquisition of 3D images by means of novel laser techniques, thus making it possible to examine features at depths and resolutions that were impossible before. They are referred as optical tomography systems, and they are of special interest in developmental biology studies, where fluorescent proteins are to be identified in transgenic animals for determining cell and tissue behavior.

The main problem resides in the fact that although it is a noninvasive technique the sample should be transparent. For this purpose different methods have been developed, all of them based on the idea that water inside the sample has to be replaced with a liquid that has the same refractive index that proteins and lipids for preventing light scattering effects.

The resolution obtained with these techniques is such that a gap which was previously uncovered by other techniques is hence possible. This is due to the fact that techniques like confocal microscopy have a higher resolution, but consequently a smaller Field of View (FOV). On the other hand, there are tomographic techniques like Computed Tomography that cover a much larger FOV, but they have a smaller resolution, being in this way more appropriate for large animal or humans.

Nevertheless, each imaging modality uses a different technique for obtaining the 3D image, and depending on the technique used, it will be more appropriate for an specific study. However, it is still not clear in the literature which advantages one technique has over another, and more importantly, under which conditions is it more convenient to use each technique.

In this project, different methods are studied for characterizing optical tomography systems, so that a reliable procedure can be used for determining the advantages and disadvantages of each of these techniques. The resolution of an image system is mainly determined by analyzing its Point Spread Function (PSF). This PSF is defined as the response of the system to a point object, and its degree of spreading determines the quality of the imaging system. However, the method used for measuring it can diverge leading to unreliable results, substantially due to difficulties for handling imperfections that usually arise when imaging a sample.

Although the analysis presented here is valid for different systems, it is mainly focused in Selective Plane Illumination Microscopy (SPIM), which consists in the use of a sheet of light for illuminating the sample from the side and perpendicular to the direction of observation, so the camera can detect the whole side. As a fluorescent microscopy technique, SPIM allows the detection of fluorescent proteins in small alive and transparent specimens, and allows in toto optical sectioning of whole cleared organs.

Fluorescent beads were used for the study of the resolution, as they are small enough to be considered point-like emitters and thus recover the PSF of the system. The procedure mainly consists in identifying different particles in the sample by making use of an image processing software developed in MATLAB, which use them for a latter mathematical analysis that results in the desired parameters. With this analysis, it was proven that the resolution of SPIM is not influenced by the magnification used, at the same time that the PSF was characterized according to the position of the fluorescent beads inside the 3D image.

In addition, a numerical study was carried out for comparing the resolution of two of the most popular systems at this time: SPIM and Optical Projection Tomography (OPT). In contrast to SPIM, OPT illuminates the whole volume within the FOV, and by rotating the sample in small steps, data is acquired from different perspectives. By integrating the tools developed for the characterization of an optical system, it was concluded that SPIM is a better option for the study of small structures given in biological samples, whereas OPT offers isotropic resolution and is more robust in the presence of scattering.

These tools were then used for creating a protocol that results in the quantification of some parameters of interest for the characterization of an optical system. In this way, the main results of this study can be obtained by following a series of easy steps.

This protocol was finally put into practice for analyzing the effect of scattering in the resolution of SPIM. By using different samples that contained different amount of scattering material, it was concluded that scattering affects negatively to the resolution in the lateral plane, that is, in the direction of the sheet of light. However it does not affect to the axial resolution, because it depends on the sectioning capability of the lightsheet. The contrast resolution was also considered, and it was seen to worsen when the scattering coefficient increases.

All in all, besides having created a theoretical model for characterizing an optical system, it was put into practice by means of a software that analyzes the 3D image for obtaining the desired results and quantifying the resolution of the system. Furthermore, after having tested it and concluding that the results were accurate, it was also proved to be useful when used for studying the effect of scattering on the PSF. The fact that this model is also incorporated in an easy to implement protocol that can be put into practice by a standard user gives account of the scope of the future applications in which it can be used.

# Contents

# 1 INTRODUCTION

## 1.1 OPTICAL MICROSCOPY

### 1.1.1 History of microscopy

Although it is not clear when the first microscope was invented, it is commonly attributed to Zacharias Janssen in 1590 [1]. Hans Lippershey is also proposed in some studies as the inventor of the microscope, as he was a competitor of Janssen. The system that both of them proposed is referred as the compound microscope, because it was the first system that included more than one lens. However, the name of microscope was first given to the system that Galileo Galilei developed in 1609, consisting in a convex and a concave lens.

The quality of microscopes existing up to the nineteenth century was limited by optical aberrations, blurred images, and poor lens design, until Lister and Amici developed an achromatic objective that could reach a numerical aperture of 0.65 for dry objectives [2]. These lenses were corrected for being able to focus different wavelengths, so that chromatic and spherical aberrations were limited. Nowadays they are widely used because they are one of the most inexpensive options available. These aberrations were further improved in 1886 with the apochromatic objectives developed by Carl Zeiss, being able of providing a good correction even at high numerical apertures [3]. Other innovations allowed a fast grow of the optical microscopy field at the end of the nineteenth century, like metallographic microscopes, which was useful for the study of the metals structure, binocular microscopes, which included for the first time two eyepieces instead of one, or the stereomicroscope, which made use of reflected light instead of the transmitted one. All these novelties allowed for a more reliable inspection of small structures that was not possible before. Furthermore, parfocal lenses were started to being commercialized at the beginning of the twentieth century. These lenses were able to be maintained in focus even when either magnification or focal length was changed.

Soon after, phase contrast microscopes were created by Zeiss. These microscopes are based on a technique by which light crosses a sample for then analyzing the phase shifts created, that are finally converted into brightness in the image. Phase shifts give information about scattering and absorption of light by the sample, so that they are especially useful in biology, as they reveal some cellular structures that cannot be detected by other microscopy techniques.

Another significant innovation was done in 1955 with the development of Nomarski interference contrast (NIC) or differential interference contrast (DIC) microscopy. It enhances the contrast of unstained and transparent samples by means of the principle of interferometry, in which different waves are superimposed for obtaining

information about the optical path length of the sample, which at the same time gives information about the phase, so that some structures that were invisible before could be analyzed with this technique [4].

From that moment on, different microscopes were proposed that were adapted to different purposes. It is worth mentioning fluorescence microscope, which captures the light emitted by fluorescent probes designed to remain fixed in specific structures within a cell, so that depending on the probe used, different structures can be imaged in the same sample. In contrast to other techniques, in fluorescence microscopy the sample is illuminated with a narrow set of wavelengths, specific for producing the excitation of the probe. In this way the probe emits light at a wavelength slightly longer than the one with which it has been excited. An spectral emission filter is used in order to capture this specific wavelength, that separates it from other wavelengths that are not needed for the image [5]. Fluorescent microscopes are usually epifluorescence microscopes, what means that both excitation and detection of the fluorescence take place through the same light path specified by the objective. The technique became even more important with the development of novel chemical fluorescent stains that bound to DNA, so that different processes related with genetic material could be studied. An example of these stains is DAPI, that can be used both for live and fixed cells [6].

More advanced microscope designs were developed using the principle of fluorescent microscopy. Confocal microscopy has as main difference the use of a pinhole in the spatial space of the light path, so that out-of-focus light is removed. Consequently, only structures placed in the focal plane are imaged, what allows the acquisition of images in different planes for a later reconstruction resulting in a 3D image. An additional advantage of this technique is the possibility of using a controllable depth of field.

Another technique that makes use of the advantages of fluorescent microscopy is total internal reflection fluorescence microscope (TIRFM). This technique makes use of an evanescent wave, which is defined as a wave whose intensity decays exponentially with the distance from the boundary at which it was formed. This wave make it possible to image thin regions of a surface, specifically a distance equal to one light wavelength or less [7], making this modality especially useful for detecting fluorophores that are bound to the specimen surface.

### 1.1.2 Image formation

In the optical microscope, light is generated in an illumination source for then crossing a condenser before reaching the sample. The function of the condenser is to concentrate light for focusing it through the object. Then light can cross the object in different ways. Direct light is the one that travels both around (background light) and through the specimen without being disturbed in its path [8]. On the other hand,

scattering is produced by the deviation of light when it encounters parts of the specimen. Light scattering is defined as light that is deflected from its straight path due to heterogeneities in the medium it traverses. This happens because of the interaction of an electromagnetic wave (light) with the electric charges of which matter is composed (protons and electrons). When such interaction occurs, these electric charges start oscillating, and as a consequence they radiate electromagnetic energy in all directions, and this energy forms scattered light [9].

In the next step, light travels through an objective lens, whose function is gathering light for focusing it and producing a real image. There are two important parameters defining the characteristics of the objectives. The first one is magnification, which is the factor by which the actual size of the sample is enlarged; it usually ranges from 4x to 100x. It is important to note that the actual angular magnification of the system is equal to the product of both the objective magnification and the eyepiece magnification, where the former is equal to its focal length divided by the distance between its back focal plane and the focal plane of the eyepiece (or tube length). The magnification of the focal length depends on its focal length.

The second important parameter defining an objective lens is the numerical aperture (NA), which is a dimensionless number that defines the range of angles over which the lens can gather light or emit it. It can also be understood as the acceptance cone of an objective, because when all the angles that it accepts are drawn, it forms a cone. NA is calculated as the product of the index of refraction of the medium and the sine of the maximum angle at which the objective can accept light. An important application of this concept is that a medium with higher refractive index than air is used between the objective and the sample, like immersion oil (with index of refraction equal to 1.52), the effective NA is much greater and thus the resolution is improved compared to a dry objective. This principle can also be explained by means of the Snell's law, which explains the relationship between the incidence and refractive angles when light hits an interface between two media. These angles are related with the refraction indices of the media by the expression in Formula 1.1.

$$\frac{\sin\theta_1}{\sin\theta_2} = \frac{n_2}{n_1} \qquad 1.1$$

Where $\theta_1$and $\theta_2$ are the angles of incidence for each media, and $n_1$ and $n_2$ are the refractive indexes for each media.

Although it may be thought that it is always a good idea to use a high NA, another concept should be taken into account. The working distance is defined as the distance between the objective lens to the closest surface of the sample to be imaged when it is in sharp focus [10]. Figure 1.1 shows how these specifications are detailed in the objective, at the same time that a graphical explanation of working distance appears.


*Figure 1.1: Objective lens specifications by [10].*

In this way, direct light then travels through an objective lens that produces a magnification, for later being spread across the image plane at the diaphragm of the microscope. The diaphragm is an opaque structure with an aperture at its center, so that depending on the diameter of this aperture, some rays of light can be stopped, and thus the amount of light that will finally form the image can be regulated. Scattering is brought to focus at different places of the same image plane, thus producing noise.

Once these concepts are understood, the resolution of a system can be expressed by means of the Rayleigh relationship [11] shown in Formula 1.2.

$$d = 1.22 \cdot \frac{\lambda}{2 \cdot NA} \qquad 1.2$$

Where d is the minimum distance between two points for them to be perceived as separate, λ is the wavelength of excitation light, and NA is the already defined numerical aperture of the objective lens. If the separation between two objects is smaller than defined by the Rayleigh equation, they will be imaged as a single object that is bigger than the original one. As a direct consequence of this formula, when light with shorter wavelength is used, the resolution is better. However the wavelength is usually a requisite of the desired image, as most of the probes require a specific range of wavelength for being excited. On the other hand, objectives with higher NA result in systems with a better resolution, and this is one of the reasons why the election of the objective is crucial for determining the quality of the image. The problem arises when long working distances are desired, as it is not possible when high NA or high magnifications are required, so a tradeoff should be done.

Another important factor regarding the resolution of the system is the depth of field. It is measured parallel to the optical axis and gives account of the distance between the nearest and the farthest features of the sample that appear considerably sharp when imaged. In this way the depth of field is used for defining the axial resolution.

Finally, light reaches the eyepieces or oculars, and a further magnification of the image is produced. The focal length of this eyepiece is important for determining the total magnification of the system as explained before.

The development of photomicrography led to the acquisition of the images created in a microscope. The first media used for this technique were films coated with a light-sensitive emulsion of silver salts or dyes. In this way, when light hits this film, a latent image is formed that must be developed with different photographic chemicals. Some examples are mentioned in [12].

The use of electronic cameras was not popular until last decade, when they started to be affordable for these purposes. It allowed the storage of images in computers, what besides facilitating their distribution, it made possible the use of new image processing techniques for a deeper study of microscopic images. Tube cameras were the first option for converting an optical image into an electrical signal, but nowadays they have been replaced by charge-coupled device (CCD) cameras and complementary metal oxide semiconductor (CMOS) cameras. CCD sensors consist in an integrated circuit with a number of capacitors that can transfer their charge. In this way, the charge can be manipulated and converted into the digital image that will be stored in the computer. In CMOS sensors, each pixel contains a photodetector and an amplifier, so that pixels can be read individually.

It is important to understand the advantages of each camera so that a good election can be done based on some parameters like their quantum efficiency, signal to noise ratio (SNR), dynamic range or acquisition speed. Their main difference is that CCD sensors are less susceptible to noise and have a better light sensitivity than CMOS sensors, but they are more expensive and the power they require to work is much higher. One of the greatest advantages of CMOS cameras is that they can acquire an image faster than a CCD camera. Furthermore, CMOS cameras are relatively new and they are being improved rapidly, with the goal of obtaining images with a quality comparable to that obtained by CCD cameras.

## 1.2 STATE OF THE ART IN OPTICAL IMAGING

The microscopic techniques mentioned up to now are useful for imaging many structures that cannot be observed by other means. However, they have a number of limitations that favored the development of novel techniques, especially in the field of three-dimensional (3D) optical microscopy. This leads to optical tomography, where the same optical principles are used for obtaining images, it is, capturing light that is both transmitted and scattered through a sample. The main difference is that in optical tomography different images are obtained for a later analysis that allows the obtaining of a volumetric model of the sample being imaged.

Two of the most popular optical tomography techniques are SPIM (Selective Plane Illumination Microscopy) [13]–[18] and OPT (Optical Projection Tomography) [19], [20], which produce 3D image by means of different laser techniques. The resolution obtained with these systems is such that a gap that was previously uncovered by other techniques is hence possible. This is due to the fact that techniques like confocal microscopy have a higher resolution, but consequently a smaller FOV (Field Of View); and moving just one step beyond there are tomographic techniques like CT (Computed Tomography) [21]–[23], which cover a much larger FOV, but they have a smaller resolution, being in this way more appropriate for large animal or humans.

In SPIM a sheet of light is used for illuminating the sample stack by stack, in such a way that a camera perpendicular to the focus plane can catch the fluorescence emitted by the excitation laser. The mentioned sheet of light is created by placing a cylindrical lens in the path of the excitation laser, so that a plane is created. This plane produces the effect known as optical sectioning, which leads to a higher contrast by reducing the background signal at the same time that photobleaching is enormously reduced because the laser only illuminates a plane at a time. However, this lightsheet is unfortunately not exactly a plane, but it usually has a Gaussian shape. This drawback is avoided by placing the narrowest part of the beam in the FOV, so that it is focused. Of course, when the FOV is large, the resolution is notably better in the center than far from it. Although SPIM was first proposed in 1902 by [24], it is nowadays a growing technique for a lot of biological research.

In contrast to SPIM, OPT illuminates the whole FOV at a time, and by rotating the sample in small steps, acquisitions are taken at different perspectives by a camera that is placed in the same conformation than in SPIM. Then a sinogram is obtained which allows to obtain the image by using reconstruction techniques, what makes this modality similar to CT. The main disadvantage of this technique is that the photobleaching effect is much more notable than in SPIM, since the whole sample is illuminated for every angle. However, as acquisitions have been taken around the whole sample, resolution is notably more isotropic.

Both techniques have been of interest for developmental biology studies, in which fluorescent proteins are to be identified in transgenic animals for determining cell and tissue behavior. The problem resides in the fact that although it is a non-invasive technique the sample should be transparent, for what different methods have been developed. All of them are based on the idea that water inside the sample has to be replaced with a liquid that should have the same refractive index that proteins and lipid inside the sample, for preventing in this way light scattering effects. This effect was first described by [25] at the same time that BABB mixture was proposed as a protocol for clearing the sample. BABB stands for Benzyl Alcohol and Benzyl Benzoate and serves as an organic solvent, which can be used to clear samples (called Murrays clearing); but this method is quite aggressive and denaturalizes proteins, so it must be taken carefully.

Its index of refraction is 1.51, near those of fats. Although it dates from 1911, it is one of the most popular methods used nowadays, but its use is limited because some of the sample proteins are denaturalized, so that some important features are lost and the sample is made smaller.

SPIM and OPT are just two examples of the huge number of techniques used for obtaining 3D images with optical techniques. In fact, most of the techniques are very similar to SPIM in the sense that they also use a sheet of light. These are called light sheet fluorescence microscopy (LSFM) techniques. The principle of all light sheet techniques is based on the idea of using a paralleled excitation and perpendicular excitation, leading to a higher signal to noise ratio, and minimizing photobleaching by rejecting out-of-focus light. The main inconvenience of this orthogonality between excitation and detection is that a smaller numerical aperture (NA) is required, producing an image with an axial resolution up to four times worse than lateral resolution. Some techniques have been implemented for overcoming this anisotropy, but most of them are very slow and produce photobleaching effects, losing in this way the main advantage of light sheet techniques. Two of the most promising ideas in this sense are the iSPIM (Inverted Selective Plane Illumination Microscopy) by [26] and the diSPIM (dual-view iSPIM) developed by [27].

iSPIM is a light sheet technique very similar to SPIM, with the main difference that it incorporates an inverted microscope as shown in Figure 1.2, so that it takes advantage of the features existing in both systems. On the one hand, it is able of creating a 3D image by means of the plane illumination, and on the other hand, it maintains the flexibility and sample geometry of a normal inverted microscope.

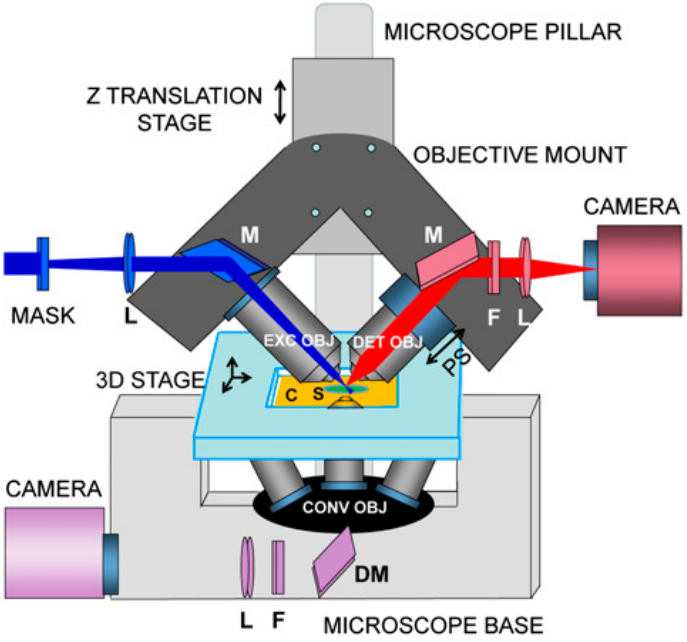


*Figure 1.2: Conformation of iSPIM by [26]. As in SPIM, it contains both an excitation objective (EXC OBJ) that emits the lightsheet, and a detection objective (DET OBJ) that gathers*

*the light emitted by the fluorescent probes inside the sample. The inverted microscope is in the base of the system.*

diSPIM also uses the principle of SPIM for perpendicular illumination and detection objectives. The main novelty of diSPIM is that the two objectives make the function of either excitation or detection objectives. In this way, when the image is being acquired, they rapidly interchange their function, and when one objective illuminates the sample with a lightsheet, the perpendicular one captures the fluorescence emitted, and vice versa. As they have to change their behavior very rapidly between excitation and detection, CMOS cameras are used instead of CCD ones, as they are much faster for this purpose. This technique is similar to iSPIM in the sense that it also incorporates a third objective for an inverted microscope, which allows finding and screening samples. All in all this technique can acquire an image with an isotropic resolution, as the problems with the axial direction are solved by means of a perpendicular camera. At the same time it can acquire images much faster than other techniques, so that it is appropriate for in-vivo studies.

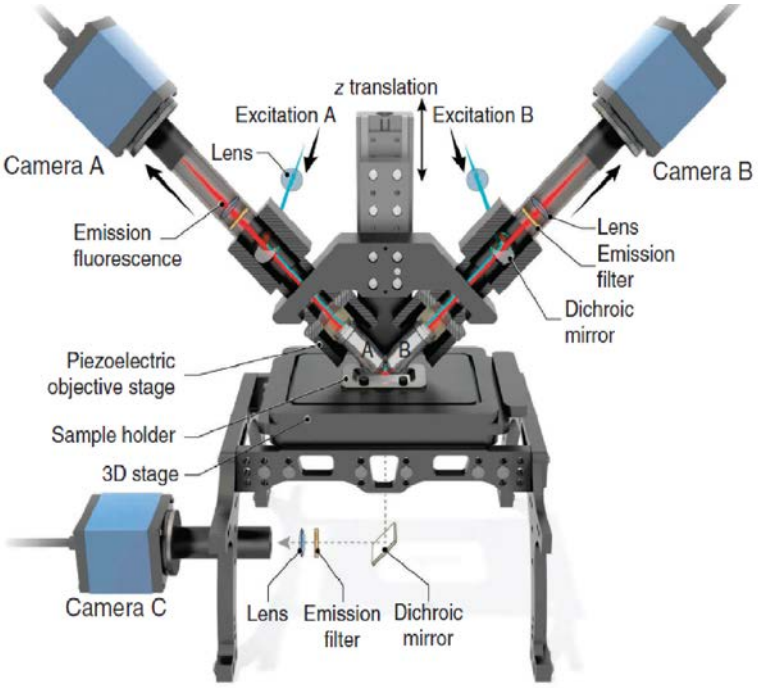


*Figure 1.3: Conformation of diSPIM by [27]. Objectives A and B can act either in emission mode or in acquisition mode. Excitation A and excitation B are the light sources for each objective respectively, at the same time that camera A and camera B can capture an image when each of them is supposed to work in detection mode. Camera C is in charge of capturing the light path corresponding to the inverted microscope.*

## 1.3 STATE OF THE ART IN RESOLUTION STUDIES FOR OPTICAL TOMOGRAPHY

It has already been remarked in the previous section the importance of novel techniques in the field of optical imaging, especially light sheet techniques. However, most of these techniques have not been exploited yet. In order to make use of all the possibilities of a system, a thorough knowledge of all its technical aspects is required. Between these parameters, it is of special importance a complete understanding of the resolution of a system, it is, how it can be determined, and which of the elements in the setup have an influence on it. Only in this way new proposals can be studied for improving the characteristics of a system. This section is devoted to the discussion of the current state of the art in the study of the SPIM resolution, as well as some techniques used for improving it without major changes in the system.

The concept of PSF (described in section 4.1) has been extensively used for defining the resolution of an optical system. Some theoretical models have been proposed for properly defining it. In 1969 a deep analysis was published involving the relation between the PSF of an optical system and its focusing characteristics [28]. Later, in 1989, a similar study was carried out for formulating this function in 3D and applying it to fluorescence microscopy. Empirical studies then lead to the application of the PSF for improving the possibilities of the systems. In [29] the properties of three dimensional image formation in an epifluorescence microscope were used for obtaining very high resolution images of biological structures, at the same time than in [30] the theoretical models mentioned before for the PSF were compared with the experimental results obtained. In this way, the results in their analysis can be used for reconstructing images by means of theoretical models that correspond to their sample.

Consequently, the PSF can be used in the field of fluorescence microscopy for reconstruction purposes by deconvolution techniques, in which the intensity distribution of the images obtained by the system is repaired once the PSF of this system is characterized. In [31] the PSF of an imaging system is obtained by measuring fluorescent microspheres. They apply a Maximum Likelihood Expectation Maximization (MLEM) algorithm for reducing the effect of noise and the influence of the microsphere size, since theoretically it should be infinitesimally small. However the method they propose for doing it has some drawbacks. One of these drawbacks is the fact that it is based on the estimation of some parameters and some assumptions are done for this purpose, including that the image of the fluorescent bead should be spherical. This leads to results that may not correspond to reality. Furthermore the method is only useful for the specific case of fluorescent microscope, thus limiting the scope of this technique.

Similar studies in this field had led to a more precise knowledge of the characterization of the PSF of a system [32]–[35]. A protocol was published in [36] for measuring and interpreting the PSF of a confocal microscope, for then being able of

determining its resolution. They made use of fluorescent microspheres, which are small enough for considering them as a point. The main inconvenient of this protocol is that fluorescent beads are imaged individually, so that a lot of images should be taken for having statistically reliable results, and this would imply a lot of time.

When SPIM started to gain importance, a deep study of the resolution in this system was published by [37], emphasizing the fact that axial resolution should be studied separately, as it was determined by the sectioning capability of the lightsheet. For measuring the cross-section of the illumination beam they used the experimental arrangement shown in Figure 1.4, where a fluorescent cover slip was placed at the focal line of the cylinder lens. In this way they were able of measuring this parameter at various distances from the focal point. With this technique they got a good theoretical model for the PSF in SPIM, at the same time that they modelled the response of the system when the distance between two points is as small as possible for them to be distinguished. For this model they used the Rayleigh criterion and the Nyquist theorem for constructing Figure 1.5. The minimum distance for the points to be distinguished is thus defined as the distance between the maximum and the first minimum of the PSF.

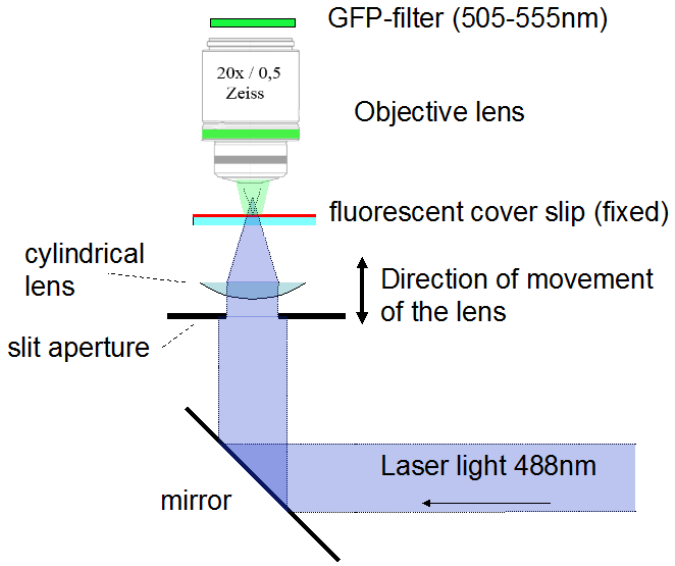


*Figure 1.4: Experimental setup for measuring the cross-section of the illumination beam (by [37]).*

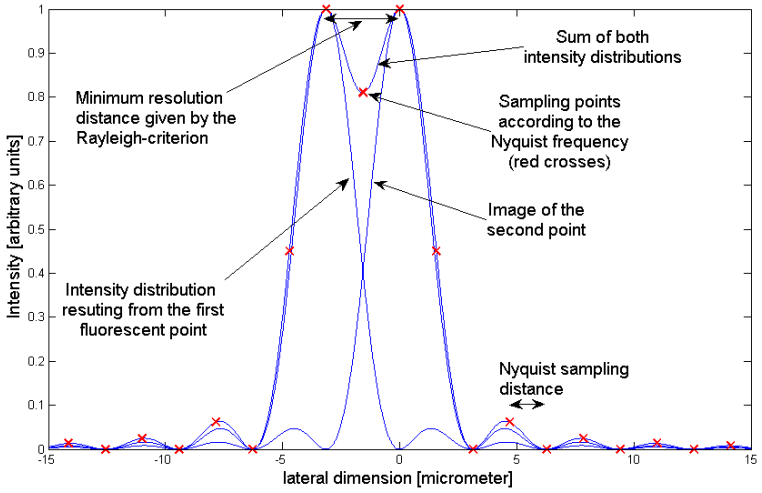


*Figure 1.5: Response of a SPIM system when two points are very close in space (by [37]).*

Some of the most important formulas resulting from the study of the resolution of SPIM explain that the axial resolution is mainly determined by the excitation and detection NA, as expressed in Formula 1.3. The first term is related with the thickness of the illumination light sheet (the subscript *exc* means excitation), and the second term with the detection objective (the subscript *det* means detection and *em* means emission). $\theta_{det}$ describes half the angle of light collection, and n is the refractive index. It is also important to note that there is a trade-off between the length of the lightsheet and its thickness, as the thickness should be nearly constant over the FOV. In this way, it is considered that it changes by a factor of $\sqrt{2}$ over a distance defined by Formula 1.4, where the Rayleigh criterion is used.

$$\left(\frac{2 \cdot NA_{exc}}{\lambda_{exc}} + \frac{n \cdot (1 - \cos\theta_{det})}{\lambda_{em}}\right)^{-1} \qquad 1.3$$

$$\frac{\pi {w_0}^2}{\lambda_{exc}} \qquad 1.4$$

In [38] a new model was proposed for the PSF that took into account the mismatches occurring between the refracting indices of the media of the objective lens and the specimen. Previous mathematical approaches assumed that a perfect spherical wave was emitted when an electric, magnetic or mixed dipole was excited by an electromagnetic wave. However, the real situation for the generation of the PSF is depicted in Figure 1.6 where three different interfaces are considered. In Figure 1.7 this situation is studied by using two cover glasses with different thicknesses, so that when the refraction mismatches increase considerably, the PSF acquires an asymmetrical shape (Figure 1.7b).

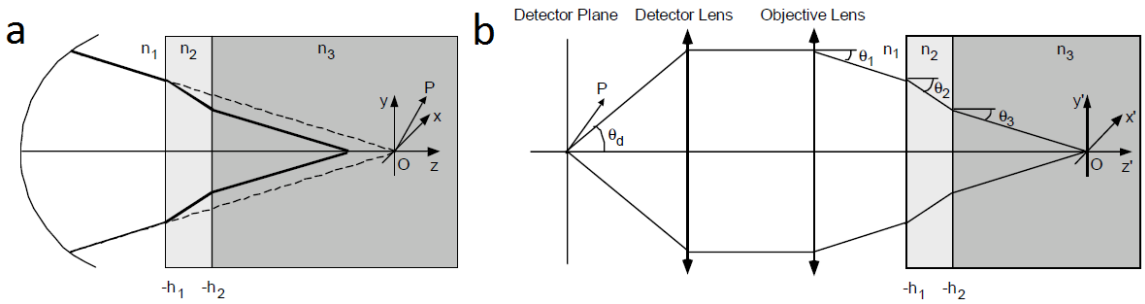


*Figure 1.6: a) Focusing of an electromagnetic wave when it crosses three different interfaces. b) Dipole radiation imaged in (a). (by [38]).*

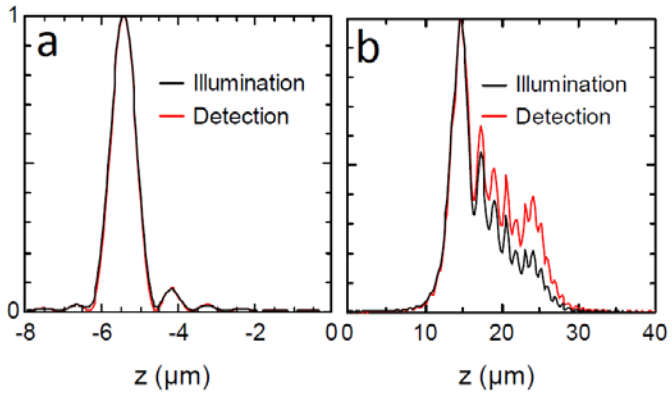


*Figure 1.7: Illumination and detection PSF for a fluorescent nanosphere with different cover glass thicknesses. a) Thickness = 120 μm. b) Thickness = 170 μm. (by [38]).*

It has already been remarked that in LSFM the resolution is quite dependent on the lightsheet used. Although the common profile is the Gaussian shape, different options are considered in [39]. They considered that 3D live fluorescence imaging requires a balance between spatial resolution, imaging speed, optical sectioning, photobleaching and other factors. For overcoming the trade-off between the length and thickness of Gaussian 2D beams defined by Formula 1.4, they propose the different operational modes of Bessel beam plane illumination microscopy shown in Table 1.1. They finally conclude that Bessel beam plane is an excellent option for achieving high speed in 3D fluorescence imaging, what leads to new possibilities in in-vivo studies.

| Operation modes | Bessel beam plane illumination | Bessel SIM | TP Bessel beam plane illumination | TP Bessel SIM |
|---|---|---|---|---|
| Illumination pattern (*xz* cross-section) | 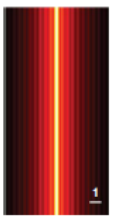 |  |  |  |
| Typical spatial resolution | *x* ~230 nm | *x* ~180 nm | *x* ~230 nm | *x* ~180 nm |
| | *y* ~230 nm | *y* ~230 nm | *y* ~230 nm | *y* ~230 nm |
| | *z* ~600 nm | *z* ~350 nm | *z* ~450 nm | *z* ~450 nm |
| Optical sectioning capability | Fair | Good | Excellent | Excellent |
| Typical imaging speed | ~40 planes/s | 10–20 planes/s | ~40 planes/s | 10–20 planes/s |
| Multicolor imaging | Yes | Yes | No | No |
| Fluorophore brightness requirement | Low | Low | High | High |
| Photodamage | Low | Fair | Low | High |

*Table 1.1: Comparison of different operational modes of Bessel beam plane illumination microscopy (by [39]).*

# 2 PROJECT DESCRIPTION

## 2.1 MOTIVATION AND OBJECTIVES

The development of novel optical tomography systems such as SPIM and OPT allows the study of novel features in biological samples that have led to great advances in the biomedical field. Some of the most important experiments that have been possible with these system are gene expression studies in the mouse embryo [20] and *Caenorhabditis elegans* [40] or studies of internal structures of adult *Drosophila melanogaster* [41], [42]. They have also been used in human samples for studies of breast cancer biopsies [43] and melanoma [44].

Although optical microscopy has been used in biological studies for more than three centuries, it was mainly used to superficial investigations due to limitations imposed by light scattering. It has been already highlighted in [45] the fact that the new techniques in this field make it possible to obtain images at depths and resolutions that were impossible before. Having reached this stage, it is of first importance which imaging modality should be used for each specific study. In Figure 2.1 a model is proposed for choosing the appropriate system as a function of the penetration depth and the resolution desired.

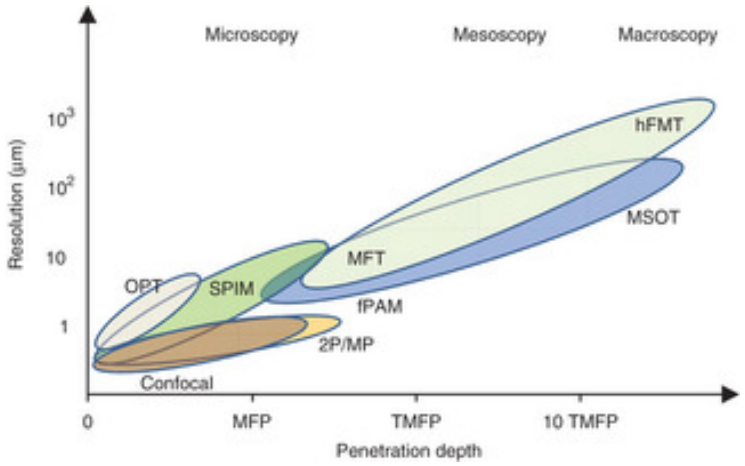


*Figure 2.1: Penetration depth and resolution of modern photonic imaging techniques (by [45]).*

In this sense, it is clear that the resolution of a system is of great importance for determining the scope of a biological study, as most of the features to be analyzed are only visible when some resolution requirements are fulfilled.

In this project a deep study of the resolution for optical tomography systems is carried out, so that different methods are proposed for quantifying this parameter, at the same time that it is measured under different circumstances that are applicable to real situations that are usually implicit in biomedical imaging studies. Although this study

has been mainly used for SPIM, it is applicable to most light sheet fluorescence microscopy (LSFM) techniques and other systems like OPT.

In a first stage, a model is proposed for characterizing an optical system in terms of its resolution. For this purpose, the response of the system to an infinitesimal point, or PSF, is obtained by means of fluorescent beads that are small enough for being considered as a delta function. A software was also developed which facilitated the analysis of these particles at the same time that resulted in a quantification of both the spatial resolution and the contrast of the system.

For the specific case of SPIM, an additional experiment was performed for characterizing the lightsheet used for acquisition. In this way different steps were followed that resulted in a fast and easy method for determining the sectioning capability of the sheet of light in use. This parameter was useful for further characterizing the axial resolution of the system.

Being both SPIM and OPT two of the most important systems in the field of optical tomography, a resolution comparison was carried out. As their operation mode is very different in terms of how the 3D image is produced, a theoretical study was used for determining the maximum resolution achievable for each of them as a function of the size of the sample. It was then seen that the resolution in SPIM is not influenced by this parameter, whereas in OPT it worsens drastically as the size of the sample increases. It was concluded that SPIM is a better option when the sample of study is bigger, thus limiting the use of OPT to small samples. However it is also important to take into account that OPT is much better in terms of isotropy, as the axial resolution is usually four times worse than the lateral one in SPIM.

Once the tools for the analysis were ready, a protocol was proposed for applying them in a correct way. The need of such a protocol resides in the fact that some standards are needed for the analysis to give comparable results when used in different systems or different laboratories. Furthermore, some of the steps require some knowledge in different areas such as biology, chemistry, mathematics or programming, and it can be difficult for a team without knowledge in these areas to use this analysis tool. In this way, the protocol proposed here describes a sequence of steps that can be carried out without the need of understanding them.

By following this protocol, the analysis tools proposed were put into practice for studying the effect of scattering on the PSF of a SPIM system. For doing it, different samples were used whose amount of scattering differed between them. The experimental results showed that as the scattering increases, the lateral resolution of the system (it is, in the plane of the lightsheet, or perpendicular to the detection axis) worsens, but the axial resolution (it is, in the direction parallel to the detection axis) is maintained constant, as it depends on the sectioning capability of the lightsheet.

## 2.2 PROJECT PLANNING

This section details the different stages of the project as well as the time spent for each of them. The estimated time for this project is one year, starting on 3rd June 2013, and considering that the time employed is 8 hours per week on average.

Figure 2.2 shows the Gantt chart, in which the different sections and subsections of the project are depicted with the period of time in which they were developed.

A first stage consisted in the project preparation, in which the theoretical concepts and the state of the art were deeply studied for considering the possibilities in this field.

As the project mainly consisted in a resolution study of the SPIM, an appropriate software was needed for this purpose. Such a program was developed through three iterations, because although each of them seemed to work properly when tested, they did not work as expected with some applications. In this way, the software was continuously renewed in order for it to give the expected results in the different scenarios that can be found in practice.

The study of the characterization of optical systems also consisted in three different phases. As opposed to the software development, the problems in this part were usually detected when the results were evaluated. After an evaluation for detecting the problem, it was corrected both by changing some of the steps in the protocol for the creation of the samples and by modifying some of the parts in the SPIM setup.

Once the software was shown to work perfectly, and a deep study of the characterization of optical systems was carried out, a protocol was proposed for establishing the PSF of a system. In fact, most of the steps of the protocol came from the different experiments done before this.

An additional experiment was done in parallel to the rest of studies, consisting in the study of the effect of scattering on PSF. It was carried out discontinuously because it greatly depended on the accuracy of the methods that were being studied. In fact, the effectiveness of the methods was tested with this experiment. However, it was frequently put aside because a priority was given to the other stages, as they had to work properly for applying them to this work.

A final study was carried out, in which SPIM and OPT were compared in terms of resolution. It was part of the study of the characterization of optical systems, but in this case the methods used were different from before, since this study was done theoretically.

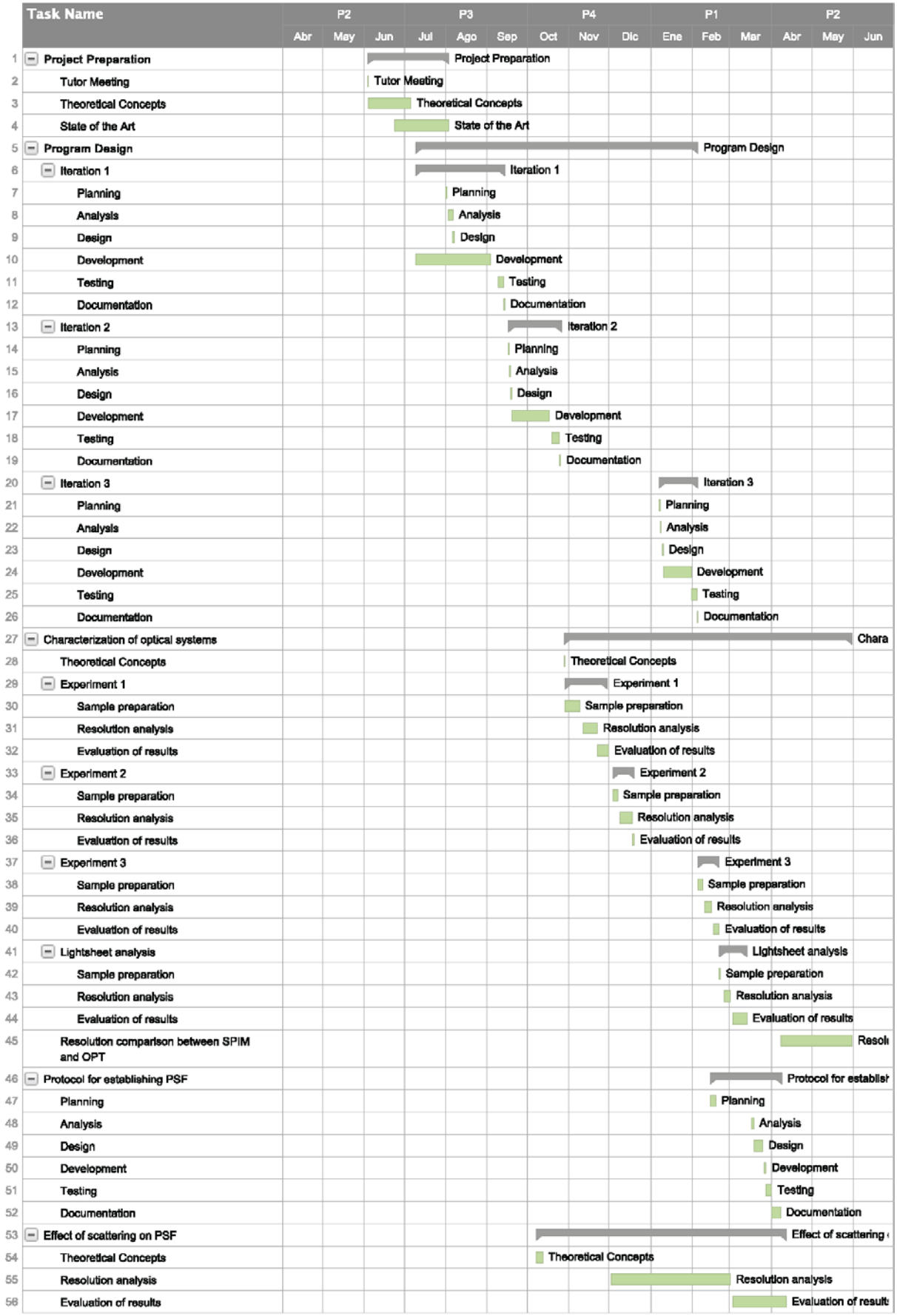


*Figure 2.2: Gantt Chart.*

## 2.3 COST PROJECTION

The costs involved in the project can be analyzed separately as human resources and equipment resources.

Table 2.1 shows the costs for human resources, which are composed by a project manager that worked in the project the same time than the student. More details about the time invested are given in the previous section.

| Roles | Cost/Hour | Working Hours | Total Cost |
|---|---|---|---|
| Project Manager | 35 € | 416 | 14,560 € |
| Student | 25 € | 416 | 10,400 € |
| | | | 24,960 € |

*Table 2.1: Cost projection for human resources.*

The costs generated by the equipment resources are listed in Table 2.2. Regarding the hardware, the SPIM used has an average lifetime of 10 years (depreciation of 10% per year), whereas the personal computer is considered to have an average lifetime of 5 years (depreciation of 20% per year). The costs of the software are due to licenses, which come to 139 € for two years in the case of Office 2010, and 500 €/year for Matlab. The software used for controlling the SPIM is offered at 1000 €/year. The choice of ImageJ as an image analysis tool is a good option for slightly reducing the cost projection, since it is free.

| Equipment | Unit Cost | Units | Depreciation per Month | Months employed | Total Cost |
|---|---|---|---|---|---|
| Personal computer | 850 € | 1 | 14 € | 12 | 170.40 € |
| Office 2010 license | 139 € | 1 | 5.80 € | 12 | 69.60 € |
| ImageJ | 0 € | 1 | 0 € | 12 | 0.00 € |
| Matlab license | 500 € | 1 | 41.67 € | 12 | 500.00 € |
| SPIM | 120,000 € | 1 | 1,000 € | 9 | 9,000.00 € |
| SPIM software license | 1,000 € | 1 | 83.33333 | 9 | 750.00 € |
| | | | | | 10,490.00 € |

*Table 2.2: Cost projection for equipment resources.*

The total cost projection is shown in Table 2.3, where both the human resources and the equipment resources are considered.

| Concept | Total Cost |
|---|---|
| Human Resources | 24,960 € |
| Physical Resources | 10,490.00 € |
| | 35,450 € |

*Table 2.3: Total cost projection.*

# 3 EXPERIMENTAL SETUP OF THE SPIM

The experimental setup for the SPIM used in this project is very similar to the hOPT setup described in [46]. Figure 3.1 depicts all components of the SPIM setup, including the stages allowing both rotation or translation of the sample under study, with the sample (S) placed in a bath of dissolved agarose (B), or a different component depending on the experiment to be carried out, the detection objective (OLd) and tube lens (TL) assembly featuring an emission filter (Fd) and an iris diaphragm (I), and an EMCCD camera (iXon DV885, Andor Corp, Belfast, Northern Ireland, with 13μm x 13μm physical detector size and a 1004 x 1002 sensor; a 2 x 2 binning was used for all the studies included here) thermoelectrically cooled to -70ºC so that electronic noise is reduced. The whole setup is assembled on an optical table (Vere, New Kensinton, U.S.A.) with a passive vibration isolation system.

The SPIM arm consisted on a 473nm 100mW laser (Roithner LaserTechnik, Vienna, Austria), directed through mirrors (M) towards the illumination objective (OLi) after passing through a cylindrical lens (CL) of focal length f = 10mm. The function of the mirrors is to position the laser for it to hit the cylindrical lens in the central point. In this way the cylindrical lens creates a lightsheet that is correctly localized in the FOV. Finally the illumination objective adjusts the distance at which the sheet of light will have the thinnest section, which should coincide with the region of study.

A detailed close-up of the movement and rotation stages together with the glass cuvette is shown in Figure 3.1c. Depending on the fluorophores used, appropriate light sources (and filters) can be automatically selected. The SPIM illumination objective is an infinity corrected 5x long-working distance objective (Mitutoyo, Kawasaki, Japan; NA 0.14, WD 34 mm, DF 14 μm). The detection optics consisted in three different infinity-corrected long working distance objectives (Mitutoyo, Kawasaki, Japan). Each of them is defined by a different magnification:

- 5x illumination objective: numerical aperture (NA) 0.14, working distance (WD) 34 mm and depth of focus (DF) 14 μm.
- 10x illumination objective: numerical aperture (NA) 0.28, working distance (WD) 33.5 mm and depth of focus (DF) 3.5 μm.
- 20x illumination objective: numerical aperture (NA) 0.42, working distance (WD) 20 mm and depth of focus (DF) 1.6 μm.

A 605 ± 70nm bandpass filter (Chroma, Bellows Falls, VT) is incorporated, what allows the detection of the characteristic emission wavelength of the fluorescent beads used. A 531 ± 40nm bandpass filter (Semrock, Rocherster, NY) is also incorporated, which is more appropriate for studies involving GFP, because the wavelength of the

light emitted by this protein is in this range. Exposure times were in the range of 0.02s. Sample movement is controlled with three translation stages (8MT167-100, Standa, Vilnius, Lithuania) and one rotation stage (8MR190-2, Standa, Vilnius, Lithuania). The rotation stage is not usually used for the acquisition of SPIM images, but it can be useful for finding specific features of the sample more easily. It can be also used for obtaining OPT images in the same system.

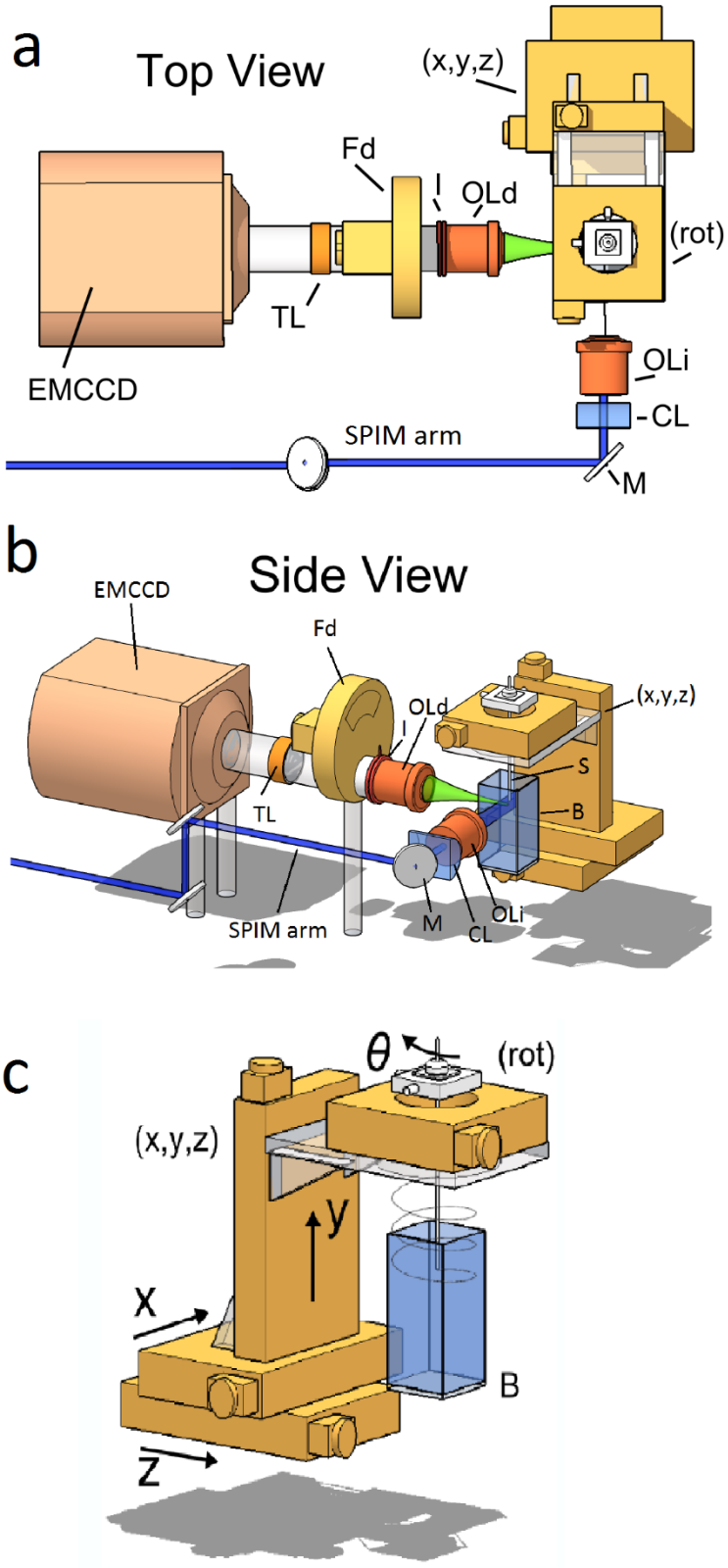


*Figure 3.1: Description of the SPIM set-up (a, b and c), its main components consisting of a detection objective (OLd), a tube lens (TL), an emission filter (Fd), an iris (I) which is projected to an EMCCD camera and an excitation filter (Fi). The SPIM arm consists of a 473nm laser, mirrors (M), a cylindrical lens (CL) and an excitation objective (OLi). The rotation/translation module allows for both rotation and translation (d). Samples (S) are imaged in an agarose bath (B).*

Figure 3.2 shows a real image of the system setup. A joystick (J) with three degrees of freedom is included for controlling the movement of the camera and two the movements of the sample by means of the translation stages and the rotation stage. The third translation axis (z) is controlled by combining the 'z' key in the keyboard with the scroll wheel of the mouse.

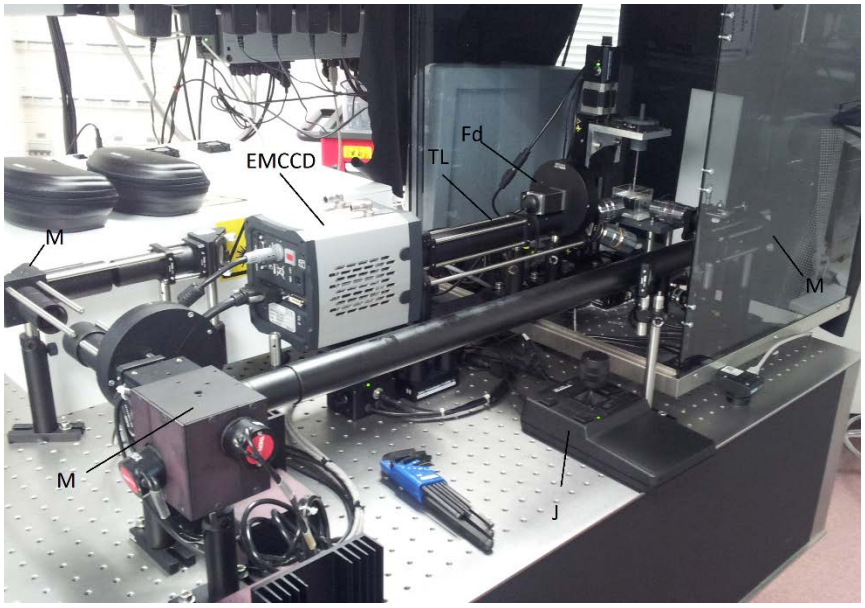


*Figure 3.2: Real implementation of the SPIM used. A joystick (J) is included in this image.*

The sheet of light created by the illumination objective goes through the bath and the sample as shown in Figure 3.3. In this way the fluorescent probes in the sample are excited and emit a light that can be detected by the camera placed perpendicular to it.

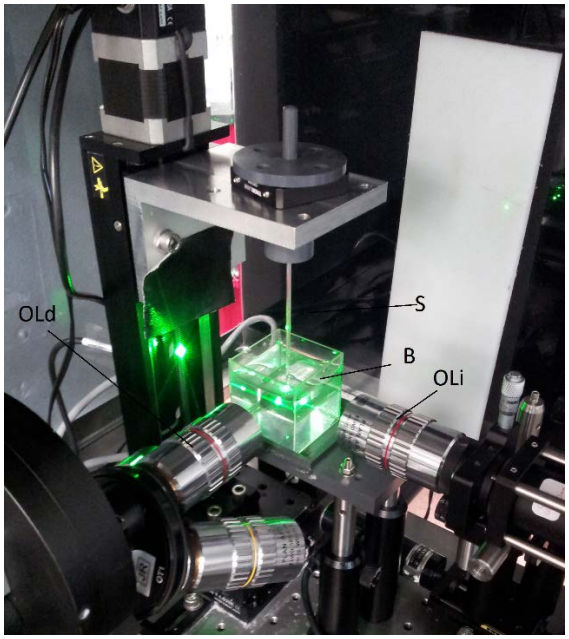


*Figure 3.3: Illumination area of the real SPIM.*

# 4 CHARACTERIZATION OF OPTICAL SYSTEMS

## 4.1 PSF TRANSFER FUNCTIONS

Although most imaging systems have some intrinsic parameters defining the resolution, they are often based on theoretical models including parameters such as the pixel size of the detector. However, the experimental resolution of a system is usually worse than the one obtained by using theoretical models. In this way, different procedures exist for calculating the real resolution capabilities of an imaging system.

One of the most commonly used parameters is the MTF (Modulation Transfer Function). It describes the response of a system to different spatial frequencies, it is, how much the system attenuates each specific frequency. A good imaging system has a wide MTF, indicating that it produces a faithful image up to high spatial frequencies. For this reason, the value of the MTF at 10% of the maximum value has become a standard measure for determining how good the system is in terms of its spatial resolution. This value is given in line pairs per millimeter (lp/mm), and the greater it is, the better the spatial resolution is.

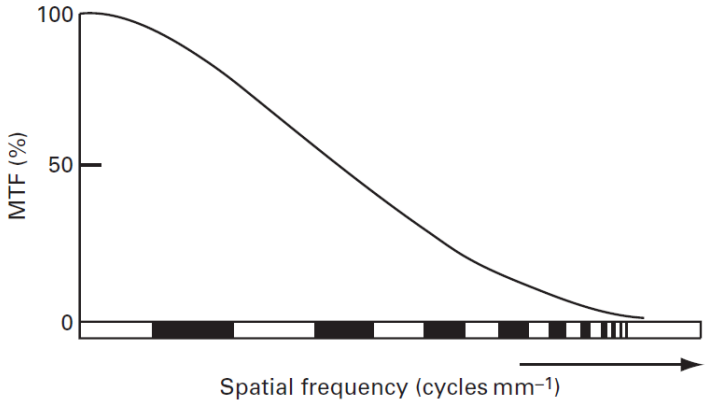


*Figure 4.1: The MTF relates the attenuation of intensities for each spatial frequency.*

However obtaining this value is not always an easy task, and different procedures exist based on other parameters related with the transfer function of the system. One of the most common procedures is taking an image of an object with a sharp edge (for instance, an aluminum sheet in X-ray). The ERF (Edge Response Function) is obtained by taking a profile across this edge. It defines the response of a system to an edge, and allows the calculation of the PSF (Point Spread Function) by using Equation 4.1, which is one of the most useful parameters for studying the resolution of a system.

$$PSF(x) = \frac{d}{dx} ERF(x) \tag{4.1}$$

The PSF is described as the response of a system to a point source or delta function, or in other words, how a point is seen in an image obtained by such a system. It usually

has the shape of a Gaussian function because it is the result of doing a convolution of a point with a circle (most of the image acquisition systems have a circular shape). In contrast to the MTF, which gives account of the frequency response of the system, the PSF is used for the study of the spatial domain. In this way a narrow PSF implies that the spatial blurring is less notable, and consequently that the spatial resolution of the system is better.

Finally, the MTF is calculated as the magnitude of the Fourier Transform of the PSF. The reason why the Fourier Transform is applied is that both the MTF and the PSF express the same parameter in different spaces, since the PSF represents the response of the system in the space domain, and the MTF in the frequency domain.

When a tomography system is to be analyzed, a different method should be used for studying the resolution in a 3D image. A common procedure in CT is to use a cylinder instead of a sheet of aluminum, so that the same analysis can be carried out. However the ERF is not very useful in SPIM, since it is not easy to have a structure with a sharp edge to be analyzed.

For this reason fluorescent particles are used in this study, as they are small enough for considering them as a delta function. In this way, when they are excited, they emit light in a slightly longer wavelength, which is captured by the camera and represented in the image as the PSF of the system in 3D. Thereafter, the FWHM (Full Width at Half Max) of this PSF is calculated. By taking into account that the shape of the PSF is very similar to a Gaussian distribution, the FWHM is defined as the width of the Gaussian in the region where the intensity is equal to half its maximum value. This parameter is used as an indicator of the width of the PSF, and thus as an indicator of the resolution of the SPIM.

The Gaussian to be studied was fitted over the PSF of the system, which in this case is interpreted as the transfer function of the microscope when all components are well aligned. Formula 4.2, described as the normal distribution formula, was used for the fitting.

$$f(x) = \frac{1}{\sigma\sqrt{2\pi}} exp\left[-\frac{(x - x_0)^2}{2\sigma^2}\right] \quad 4.2$$

Being σ defined as the standard deviation, and measured as the width of the Gaussian fitted, the FWHM is calculated with Formula 4.3.

$$FWHM = 2\sqrt{2\log 2\,\sigma} \quad 4.3$$

With the same protocol the contrast resolution, defined as the ability for appreciating small differences in intensity, can also be determined by means of the

Michelson contrast formula expressed in Formula 4.4, where $I_{max}$ is the maximum intensity in the image, and $I_{min}$ is the minimum non-zero value.

$$Contrast = \frac{I_{max} + I_{min}}{I_{max} - I_{min}} \quad 4.4$$

## 4.2 MATERIALS AND METHODS

### 4.2.1 Sample preparation

Fluorescent beads with a diameter of 500 nm were used for this study, as they are small enough to be considered point-like emitters and thus recover the PSF the system. A well-established procedure for imaging biological tissues such as whole organs in SPIM consists on clearing them by immersing in BABB, a mixture of Benzyl Alcohol and Benzyl Benzoate that was described in section 1.2. However, it was found that this clearing method is not possible when sub-micron beads for resolution studies are used, since they either are dissolved or tend to migrate to the edges.

Consequently, the fluorescent beads were dissolved in agarose following the steps described with detail in section 5.3. It is important to highlight that mismatches between refraction indices are not desired, as they produce abnormal shapes in the axial PSF because of the deviations that light suffers at the boundaries between different media (further details in [38]). For this reason the sample is pushed out from the capillary tube as shown in Figure 5.3, and agarose is used for the bath in which the sample is to be immersed.

### 4.2.2 Resolution analysis

For the analysis of the fluorescent beads, a software was developed that allows the selection of the desired particles in the image for then analyzing them one by one, so that at the end, different data related with the resolution of the system are obtained. This software is attached in Appendix A.

There are some programs available for similar tasks, especially in ImageJ, where some plugins for particles analysis can be found. A clear example is the tool “Analyze particles” for ImageJ, which looks for different particles in a binary image and segment them. The problem for this kind of tools is that they are optimized for 2D microscopy, as they have been developed for being used in the segmentation of cells and similar particles. The problem when using 3D images is that the user does not only look for the features found in a single stack, but the features existing in the surrounding stacks are also important for determining the parameters he is interested in. Furthermore, this kind of tools do not take into account some features of the particles used here, like the fact that they are similar to Gaussian functions in 3D, and the center of mass correspond to

the peak of such Gaussian. However, the most important reason why a custom software have been developed is that some of the criteria used for determining if a particles should be selected are very difficult to be automatized. For the task to be developed it is more reasonable to provide an interface in which a user can select the particles according to his own criteria. Some of the characteristics a user should take into account are:

1. Some of the particles form a cluster, and although both their size and intensity look normal, there are some features that indicate if they should not be selected. This effect is more easily detected when the profile is seen in different planes, since it may have odd shapes in some cases. A common example is a Gaussian that has two peaks instead of one.
2. If the particles are near the edge of the image, they should not be selected. Although the program correctly fits the Gaussian function over them, it does so assuming they are symmetrical, but the information lost can be crucial, for instance if the point corresponds to a cluster of particles and they cannot be seen with the information available.
3. Some of the fluorescent beads seem to be separate enough for selecting them, but it is important to take into account that these particles appear in the image as a Bessel sinc as has been explained. This Bessel sinc has some local minima that in some cases can be interpreted as the edge of the particle in the image. However, the nature of the Bessel sinc is to increase again (although with progressively decreasing local maxima), and these peaks can interfere with a particle that is relatively far from it. In this way, it is recommendable to select particles that are reasonably far for interfering between them.
4. Do not select particles that are saturated. This should not happen if a correct protocol for acquiring the image is followed (see section 5.5), but if there are suspicions that this could be the case, it is a good option to take a profile of the particle. If the particle is saturated, the peak will be flat instead of having the correct shape of a Gaussian function.

For starting using the software for the analysis of the fluorescent beads, the Matlab script “particles_selection.m” should be opened. The functioning of the program is described in the flowchart shown in both Figure 4.2 and Figure 4.3.

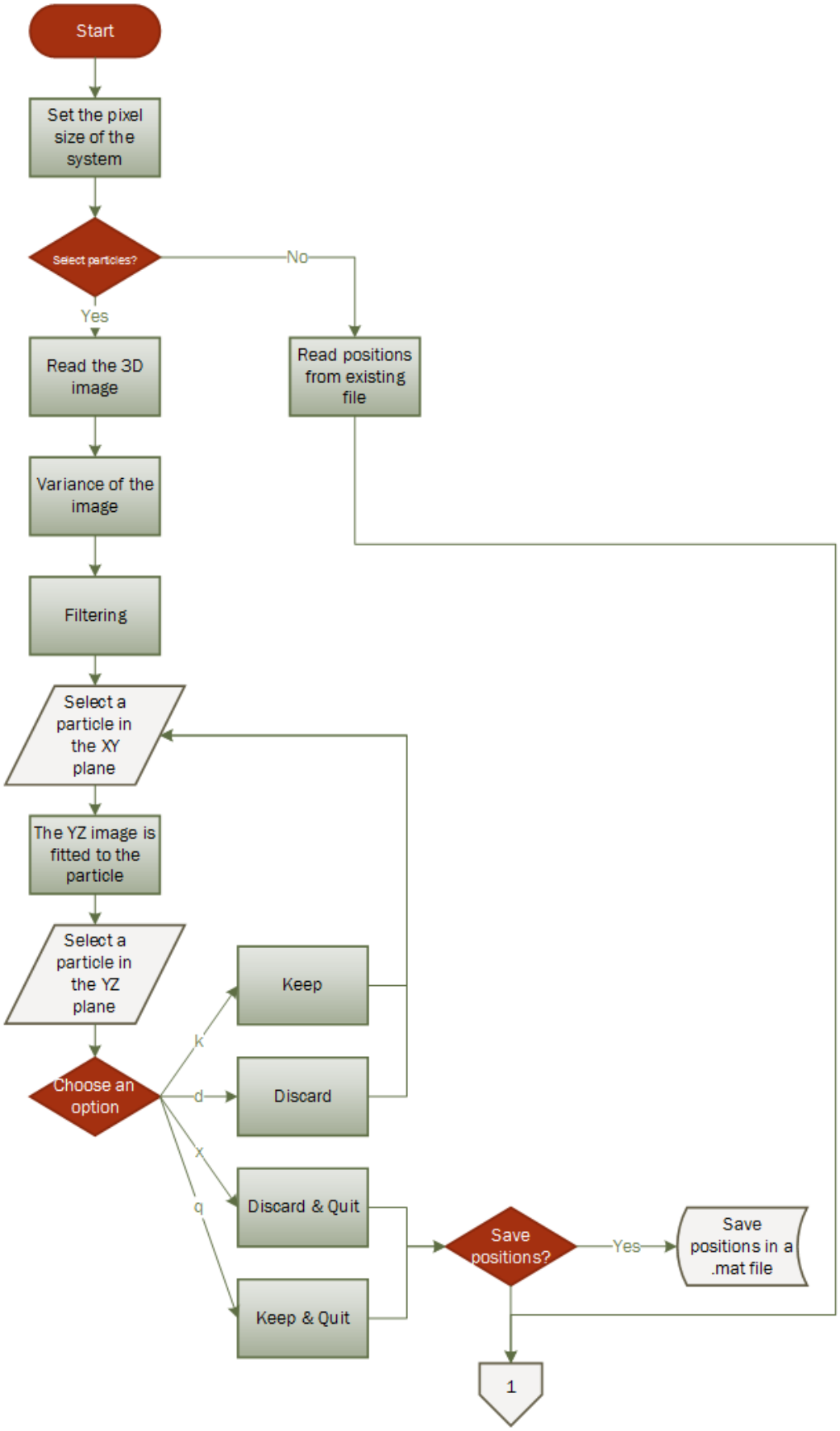


*Figure 4.2: Flowchart for particles analysis 1.*

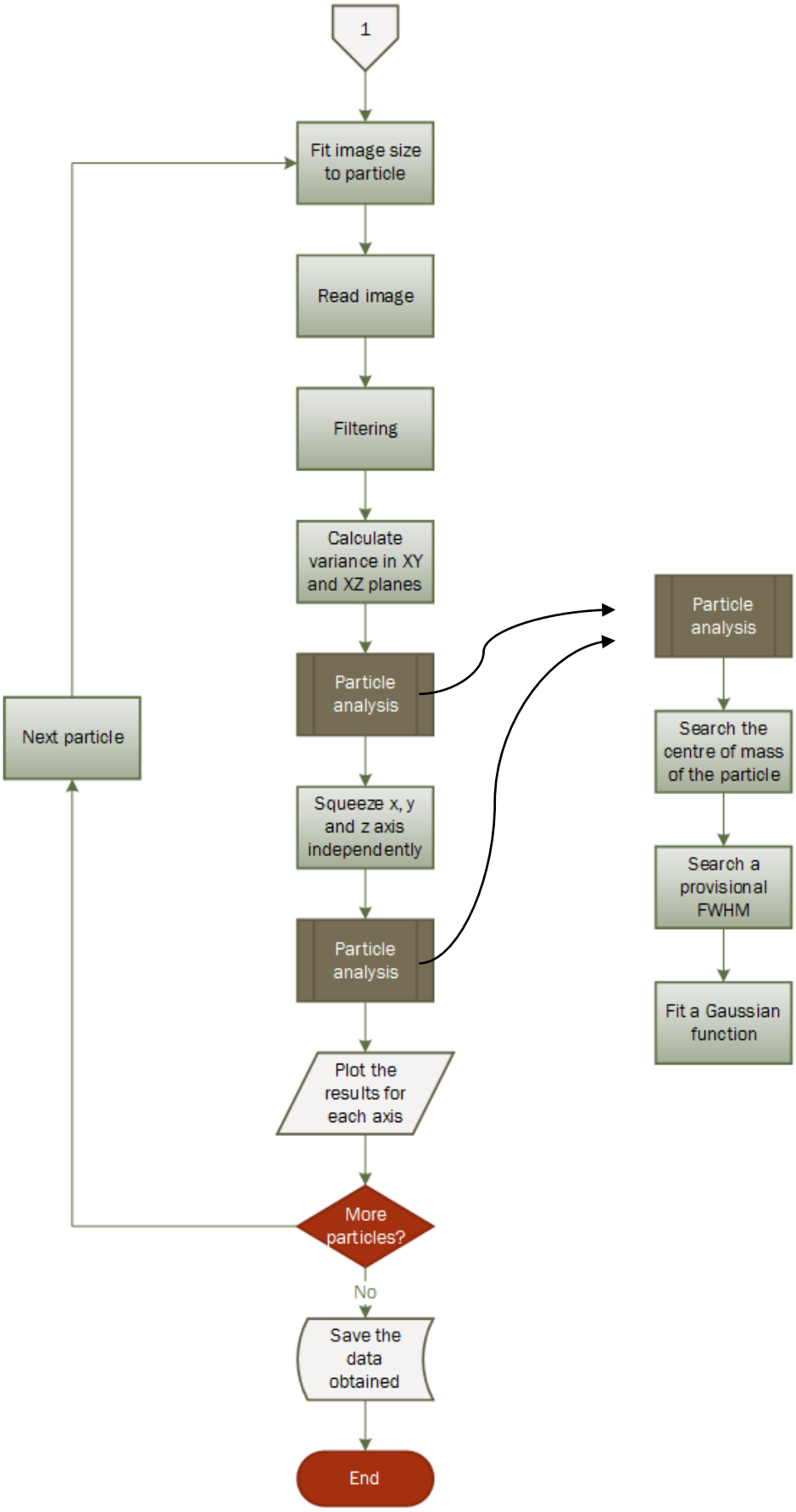


*Figure 4.3: Flowchart for particles analysis 2.*

Before starting the script, the image of interest should be selected in the code. For this purpose, both the folder and the name of the image should be correctly introduced in the code.

In this way, once the program is executed, it can automatically detect the pixel size of the image by knowing which magnification was used, as stated in the image name. If the pixel size is not defined for the magnification in use, or if the magnification is not defined correctly in the name of the image, the correct one can be introduced in the code.

Once these initial parameters are set, you are asked if you want to select your particles. The reason is that you may already have a file with the positions, and you just want to use the code for the analysis of the particles at these positions. If it is the first time that the image is used, the positions should be selected. In this case the program will read the 3D image and the variance of the image will be calculated and then filtered with the median. In this way the particles are more easily selected, firstly because in some cases (especially when the SNR is very small) the variance is more notable in the places where there are particles, and secondly because the median filter remove some of the noise that prevent the correct localizations of such particles.

The next step is the selection of the particles to be analyzed. For this an interactive image like the one shown in Figure 4.4 will appear. At the left it can be seen the XY plane of the stack obtained after using the variance and the filtering step. It is also squeezed in the z direction, so that all the particles existing in the 3D image are seen. At the right, an image similar to the left one is displayed, but in this case it corresponds to the XZ plane, and it has been squeezed in the y direction. The considerations mentioned above for the selection of the particles should be carefully taken into account at this step. In this way the user should first choose a point in the XY plane, and automatically the XZ plane is adjusted in size to the pixels surrounding the point selected. The user should then select the point corresponding to the center of the particle in the XZ plane. It is not very important to click exactly on the center of the particle, since the center of mass will be automatically calculated later. Once the particle has been defined in both planes, the user has four options:

a) Press “k” (keep): you keep the last position and the image appears again for selecting a new position.
b) Press “d” (discard): you discard the last position and the image appears again for selecting a new position.
c) Press “q” (keeps and quit): you keep the last position, and stop selecting particles.
d) Press “x” (discard and quit): you discard the last position, and stop selecting particles.

In this way different particles can be selected until either “q” or “x” is pressed.

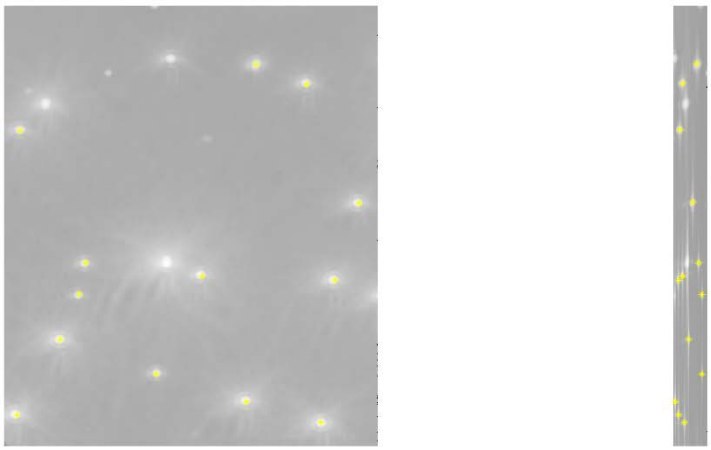

*Figure 4.4: Selection of the particles in the XY plane (left) and in the XZ plane (right).*

Once the user has finished selecting the particles, he can choose whether he want to save these positions or not. If the positions are saved, they can be used in later analysis. This option can be useful when some modifications are done to the program, or some additional parameters are desired that can be obtained from the positions of the particles.

Whether particles are selected or loaded from the corresponding Matlab file, the program will start calculating the parameters needed for characterizing the resolution of the system. From this point on, the program will iterate the same algorithm for every particle selected, so that the first step is to adjust the image size to the particle used in the current iteration, and in this way one particle remains in focus. For this purpose the original image (without the variance) is read and included in the matrix created with the desired size, for then being filtered with a median so that noise does not change the shape of the Gaussian fitted over the PSF.

Although there exist some Matlab functions for fitting a Gaussian, a custom method was developed for some of the reasons mentioned above, so that the width of such Gaussian function was as exact as possible. As the particle corresponds to a Gaussian function in 3D, the first approximation for fitting it was using the Matlab function "fminsearch", which makes use of the simplex search method proposed in [47] and does not use analytical or numerical gradients. By means of the algorithm used in this function, it was tried to compare the data of the particle with the formula of a 3D Gaussian function, defined by Formula 4.5.

$$f(x,y,z) = (I_0 - b) \cdot e^{-\frac{(x-x_0)^2+(y-y_0)^2}{2 \cdot {w_{xy}}^2} - \frac{(z-z_0)^2}{2 \cdot {w_z}^2}} + b \qquad 4.5$$

The position in each of the axis is determined by x, y and z, using $x_0$, $y_0$ and $z_0$ as the center. $I_0$ is the height of the function's peak, b is the background, and $w_{xy}$ and $w_z$

are the standard deviations for the XY plane and the z axis respectively. Note that both x and y axis have been defined together because as explained before, both of them define the lateral resolution, and their standard deviation is supposed to be the same, whereas the z axis is defined apart because it defines the axial resolution determined by $w_z$. In contrast to the normal definition of a Gaussian function, in which "b" would stand for the value the function asymptotically approaches far from the peak, in this approach this value is due to the background. Accordingly, $I_0$ is taken as the value of the particle in the center of mass, and it is correct to take as the amplitude of the function this intensity minus de background ($I_0$-b).

The problem of this approach is that besides being computationally very expensive, it hardly ever finds a global minimum, as it has to deal with many parameters. Consequently the result often corresponds to a local minimum that is far from the desired result. Thereupon a second approach was used, consisting in a separate analysis of a 2D Gaussian function in the XY plane (lateral resolution), and a second 1D Gaussian function in the z axis (axial resolution), defined respectively by Equation 4.6 and Equation 4.7.

$$f(x,y) = (I_0 - b) \cdot e^{-\frac{(x-x_0)^2+(y-y_0)^2}{2 \cdot {w_{xy}}^2}} + b \tag{4.6}$$

$$f(z) = (I_0 - b) \cdot e^{--\frac{(z-z_0)^2}{2 \cdot {w_z}^2}} + b \tag{4.7}$$

With these two functions in mind, it is much easier to fit the Gaussian function to the data, as the method is both fast and reliable. The problem resides in the combination of the parameters obtained after fitting each set of data, because when changing the parameters of one axis, some of the parameters corresponding to other axis are also moved. After testing different methods, it was found that this fact strongly depended on the initial conditions, it is, the parameters with which the function started.

According to this information, the method implemented has two steps. In the first one, the initial conditions are set by using the variance of the image as before. The middle stack is used for obtaining the initial conditions for both the x and the y axis by means of the 2D Gaussian function, whereas the z axis corresponding to the middle of the image is used for obtaining the initial conditions for the axial resolution, what is done by means of the 1D Gaussian function. In fact, another set of initial conditions is needed for this method, although they do not need to be very robust. They are obtained in the following way:

- The positions are found by using the concept of center of mass in the variance image. For each coordinate r, and being the variance of the image $I_{var}$, the positions are defined by Formula 4.8.

$$r_{cm} = \frac{\sum_{i=1}^{N} I_{var}(r_i) \cdot r_i}{\sum_{i=1}^{N} I_{var}(r_i)} \quad 4.8$$

- $I_0$ corresponds to the peak of the Gaussian function, and it is taken from the intensity at the center of mass.
- b corresponds to the background and is calculated as the mean of all the pixels far from the center of mass of the corresponding particle.
- The standard deviations ($w_{xy}$ and $w_z$) are calculated in a fast way by looking for the distance between the points corresponding to half the height of the Gaussian. For this purpose, the PSF is divided in two halves, a left one and a right one, so that just by finding the mentioned position in each one and adding the distances we can obtain this value.

Once the initial conditions have been set, the process is repeated, but besides using different initial parameters, the desired set of data are different. Finally, Formula 4.3 is used for obtaining the value of the FWHM from the standard deviation of the Gaussian function fitted in each of the axes.

### 4.2.3 Sectioning capability of the light sheet

Although the particles used here are considered to be measured as a PSF, it is not always the case. In order to have a more robust result about the axial resolution of the system, it can be compared with the profile of the beam waist, so that the sectioning capability of the lightsheet is measured. A complementary protocol is proposed here for determining the width of such waist; at the same time that a simplification is proved for showing that the profile is very similar in an axial and a lateral view.

For this purpose fluorescent beads of 500 nm are introduced in a bath of agarose, so that the camera can capture an image with the shape of the laser through the cuvette. Although the purpose of this experiment is to determine the axial resolution of the system by observing the shape of the laser in front of the camera, with this method only the lateral plane can be examined. The following steps are proposed for being able to determine the axial profile of the lightsheet by imaging the lateral one.

**First step**

Firstly, the diameter of the laser is doubled by placing two convergent lens, where the second one has twice the focal distance of the first one, as shown in Figure 4.5.

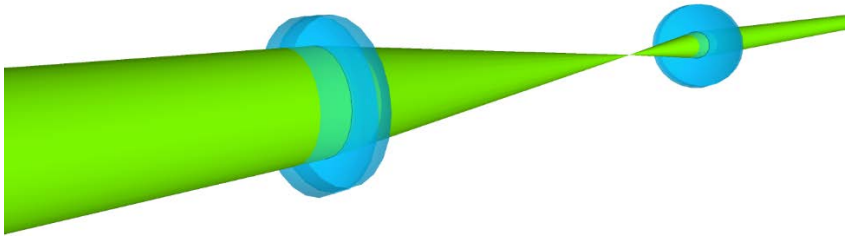

*Figure 4.5: Amplification of the laser by using two convergent lens. The second one (at the right) has twice the focal length of the first one (at the left).*

The cylindrical lens in charge of producing the lightsheet is then removed, so that the laser acquires the shape shown in Figure 4.6.

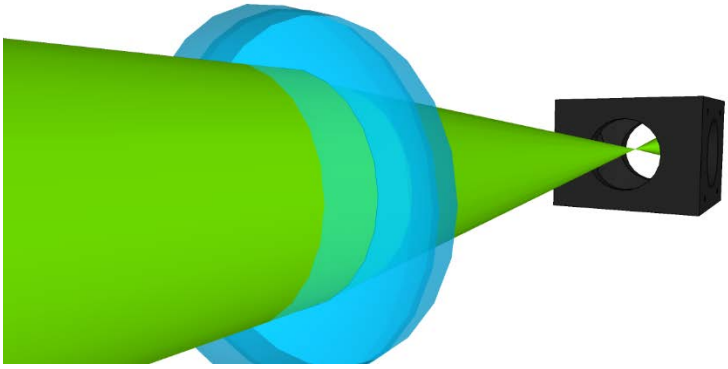

*Figure 4.6: Shape of the laser illuminating the sample after removing the cylindrical lens.*

Finally, the focus lens is moved for placing the tip of the cone of light in front of the camera, so that an image can be obtained similar to the one shown in Figure 4.7. Images are taken at 5x, 10x and 20x magnification for being able of comparing the resolution for each objective.

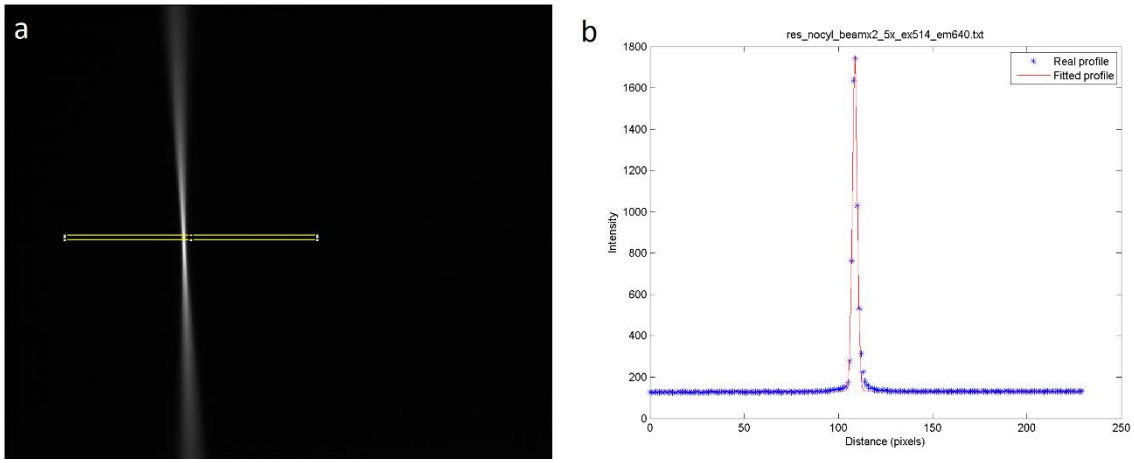


*Figure 4.7: a) Image of the laser with 5x objective. b) Profile of the laser in the ROI shown in yellow.*

**Second step**

A slit is placed before the lens in charge of focusing the laser, so that the laser is narrowed in the axial direction. This corresponds to the actual setup of the SPIM, in which the slit creates a narrower and more homogeneous light sheet. Figure 4.8 shows both the image captured by the camera and the Gaussian fit of the PSF corresponding to the profile of the light sheet created.

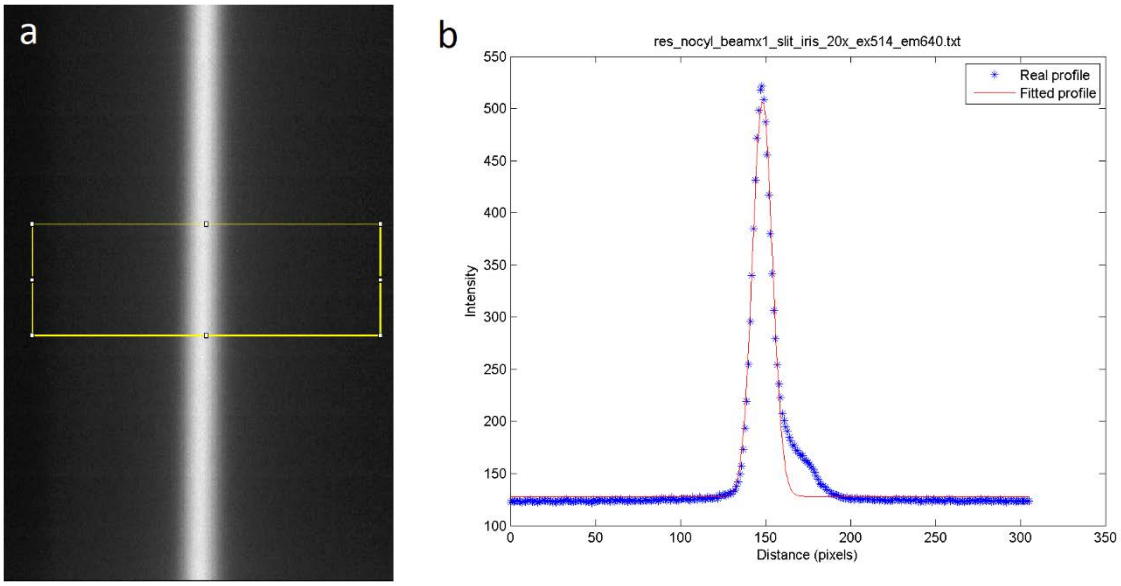


*Figure 4.8: a) Image of the laser when a slit is used with 20x objective. b) Profile of the laser in the ROI shown in yellow.*

Although the profile shown corresponds to an image in the lateral plane, the FWHM obtained can be also used for the axial plane. For showing this a third step is carried out.

**Third step**

In order to show that the width of the lightsheet in the lateral plane is similar to that of the axial plane, in this step an iris is used with the same aperture than the slit used in the second step. In this way the light sheet is also narrowed both axially and laterally. Figure 4.9 shows this effect in the lateral plane.

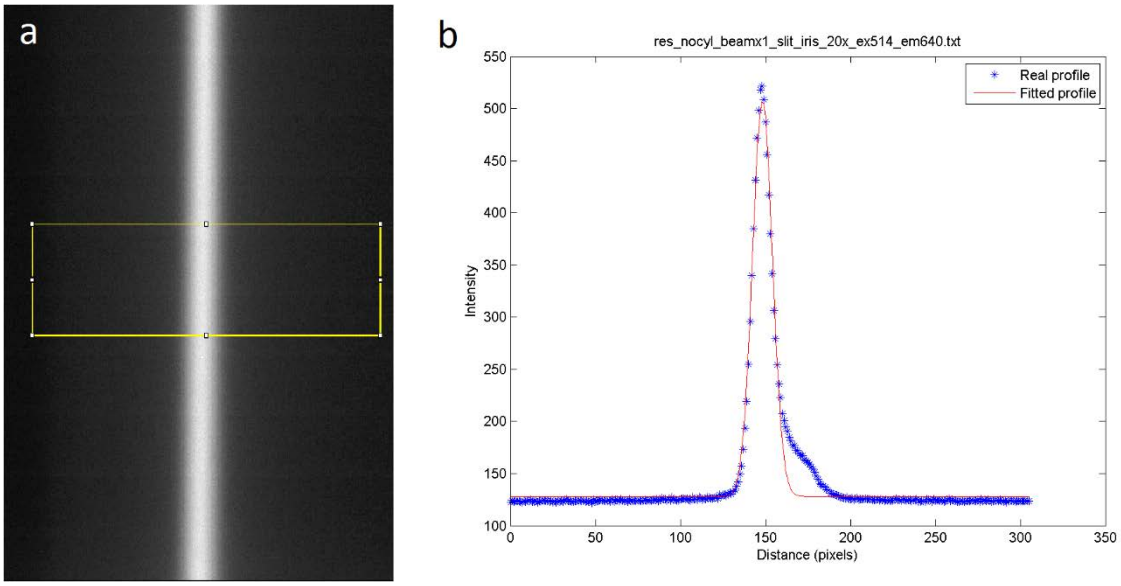


*Figure 4.9: a) Image of the laser when an iris is used with 20x objective. b) Profile of the laser in the ROI shown in yellow.*

It can be noted that the SNR is smaller in this step. The reason is that the iris limits more light than the slit does, although it is not an inconvenience for measuring the spatial resolution.

## 4.3 EXPERIMENTAL RESULTS

The resulting data for each particle should look like those shown in Figure 4.10 and Figure 4.11. In the first one a 2D representation is shown, in which both the original image and the fitted one are shown in the XZ plane (above) and in the XY plane (below), in such a way that both the axial and the lateral resolution can be studied together.

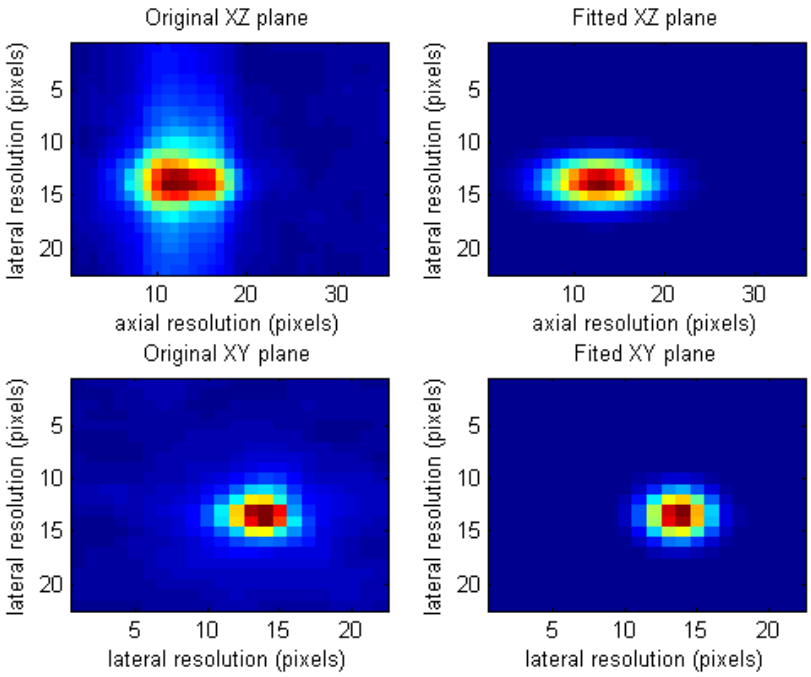


*Figure 4.10: 2D representation of the resulting data.*

In Figure 4.11 the same data is represented in 1D, for detecting the shape of the profile. Such profiles are taken from a line crossing the peak of the function along each axis, what is the same as taking a profile across the middle of each of the images in Figure 4.10.

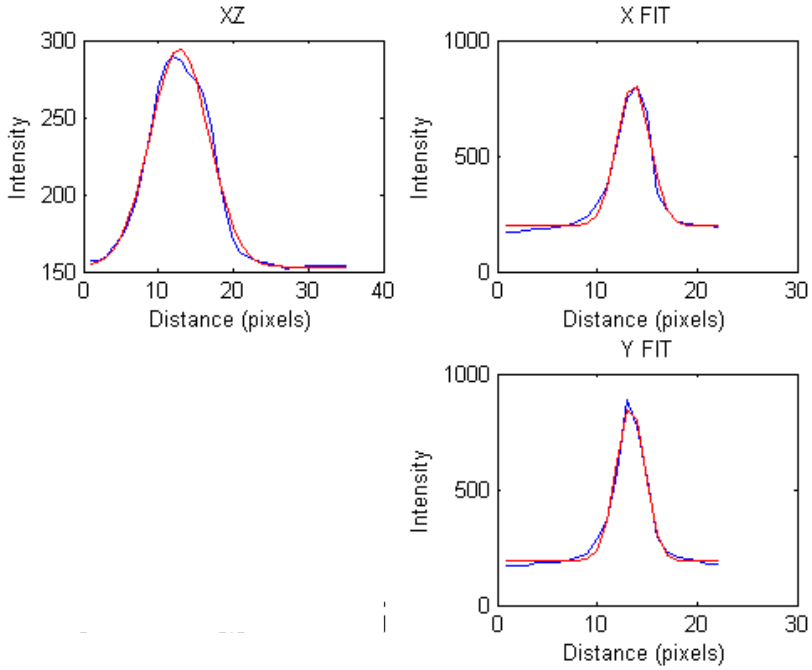


*Figure 4.11: 1D representation of the resulting data.*

Far from giving a useful analysis, these graphs provide an insight of how the resolution looks like for every particle. In this way if a strange shape is detected, the

corresponding particle can be rapidly deleted. For a deeper analysis all the results are stored in a variable, so that when the resolution of the system is to be analyzed, it is enough by using the average in such variable. Furthermore, if several particles have been selected, statistically reliable data will result.

Figure 4.12 shows an image of one of the particles selected in XY and XZ planes for the 5x magnification, as well as its corresponding analysis when this method is used with the samples described in 4.2.1 Sample preparation.

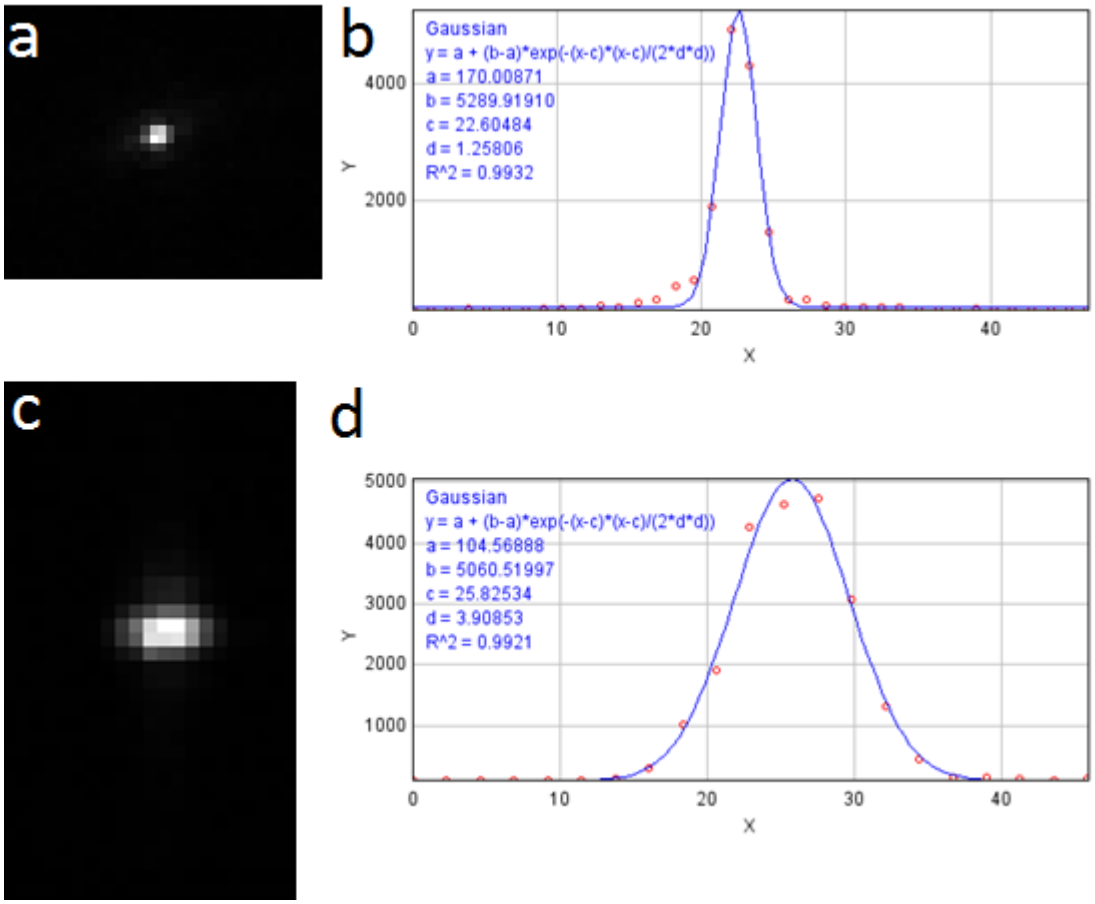


*Figure 4.12: Results for images obtained with 5x magnification. a) XY plane of the fluorescent bead selected. b) Gaussian fit of the image in (a). c) XZ plane of the fluorescent bead selected. d) Gaussian fit of the image in (c).*

As expected, the Gaussian in the XZ plane is wider than that in the XY plane due to the asymmetries of the system. When several particles are selected and an analysis is carried out in the images captured with the 5x and a 10x objectives, the results displayed in Table 4.1 are obtained.

| | 5x | 10x |
|---|---|---|
| Field of View | 280 µm | 85 µm |
| Approx. Width of Sheet | 7.77 µm | 7.05 µm |
| XY resolution | 2.96 µm | 2.92 µm |
| Z resolution | 9.2 µm | 9.6 µm |

*Table 4.1: Data resulting from the resolution analysis of different samples.*

The most appreciable difference between both objectives resides in the FOV, with a difference of 230%. The resolution of the system is just slightly influenced by the magnification used having a 1.37% of difference in the lateral resolution and a 4.17% of difference in the axial resolution. The fact that the axial resolution is worse for the 10x objective is surely due to the fact that particles are not monodisperse, and when any of them is selected outside the FOV, the resolutions worsen linearly with the distance from the center.

The difference between the approximate widths of the sheet of light is of 18%, indicating that the sectioning capability of the system slightly increases with the magnification used. These values are obtained from section 4.2.3, from which Table 3.2 is obtained after a study of the lightsheet under different circumstances. It contains the FWHM resulting from the profiles of the light sheets in the different steps and with the different magnifications used.

| | 5x | 10x | 20x |
|---|---|---|---|
| First step | 7.77 | 7.05 | 5.99 |
| Second step | - | 21.69 | 15.71 |
| Third step | - | 17.83 | 9.04 |

*Table 4.2: FWHM for the profile obtained after each step and with the different objectives.*

For a deeper analysis, particles corresponding to sample F in section 6 are used for studying if there exists a distribution of the FWHM inside the same sample.

Figure 4.13 shows two dispersion plots in 3D that allow the study of the dependence between the FWHM (the lateral one at left, and the axial one at right). Although a dependence does not seem to exist, a more quantitative study is carried out in Table 4.3, where the correlation is studied in pairs for the resolution and the distances from the center in both planes. In this way it can be observed that indeed a correlation does not exist between the values of the FWHM and the distance. The higher correlation is given for the dependence between the axial FWHM and the axial distance, but a value of 0.24 is not significant at all.

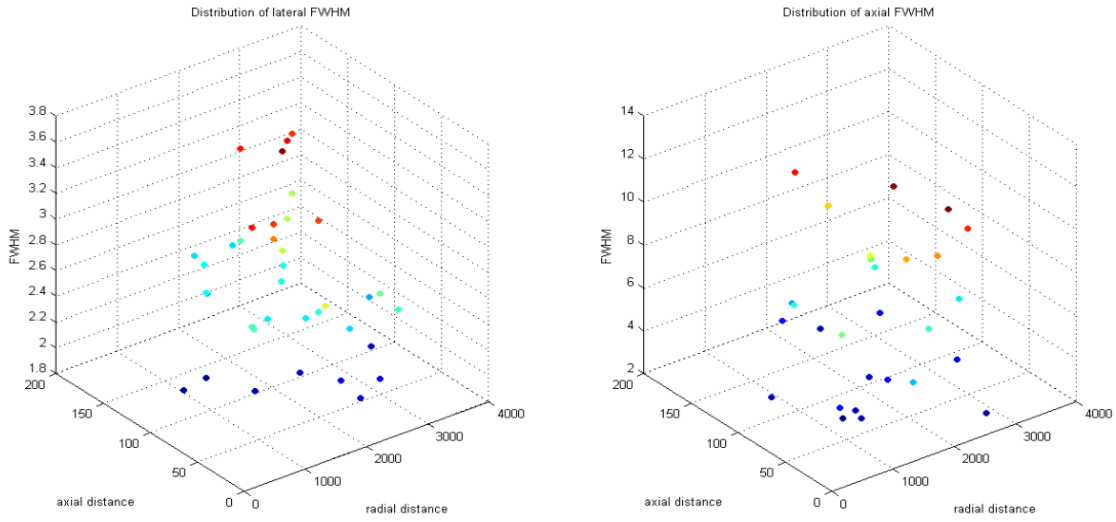


*Figure 4.13: Distribution of the resolution along the sample. a) The lateral FWHM is compared with the radial and the axial distances. b) The axial FWHM is compared with the radial and the axial distances.*

| | Radial distance | Axial distance |
|---|---|---|
| Lateral FWHM | 0.0667 | 0.1224 |
| Axial FWHM | 0.092 | -0.2435 |

*Table 4.3: Correlation between the resolution in each plane and the distances from the center, both in radial and axial directions.*

The histograms shown in Figure 4.14 give account of the distribution of the FWHM obtained for the lateral and axial planes respectively. A relatively homogeneous distribution is observed for the lateral plane (Figure 4.14a), since most of the values are close to 3 µm of FWHM. Figure 4.10b shows that the distribution is not so good for the axial plane, although it is to be expected, because this value strongly depends on the width of the lightsheet, and it can vary significantly from a particle to another.

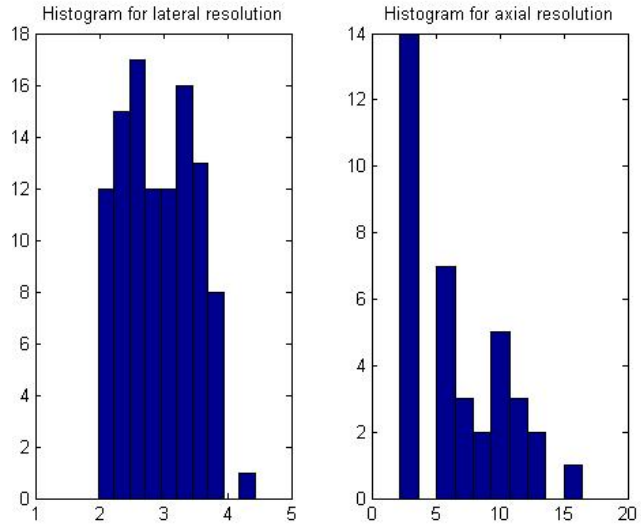


*Figure 4.14: Histograms for the lateral FWHM (a) and the axial FWHM (b).*

## 4.4 Resolution Comparison between Laser Sheet Microscopy and Optical Projection Tomography

Different methods for obtaining tomographic acquisitions by means of optical imaging are used nowadays. Although some standards exist for establishing which one should be used for a specific situation, it is still not clear in the literature which advantages one technique has over another, and more importantly, under which conditions is it more convenient to use each technique. In this work the resolution of two of the most popular 3D optical systems at this time, SPIM and OPT, is compared.

It has already seen in section 4.3 that the dependence between resolution and magnification in SPIM is very weak, and the FWHM of the PSF decreases very slightly when the magnification is smaller. Furthermore, the fact that in SPIM there is no need to focusing on the whole object allows for the use of higher NA. In this way, one of the most important differences between SPIM and OPT regarding their resolution is that in the former, the FWHM is nearly constant for different samples sizes, whereas in the later the FWHM is directly related with it. The reason is that in OPT at least half the sample has to be in focus for a correct acquisition, and this can only be achieved by using a small NA. In this way, a numerical study is carried out for comparing the resolution of both SPIM and OPT based on the NA (Numerical Aperture) required for the study.

Figure 4.15 shows the size achievable for each NA, limiting the use of OPT to small NA. On the other hand, in SPIM there is no need to focusing on the whole object, which enables the use of high NA objectives.

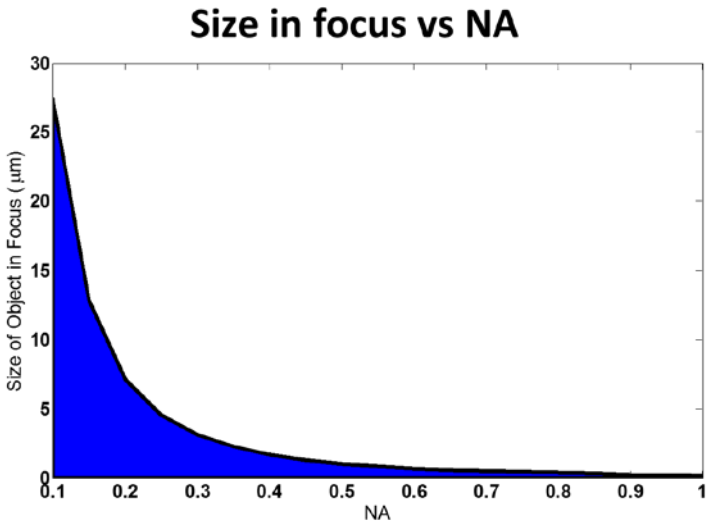


*Figure 4.15: Size of the object in focus vs NA. A small NA should be used for imaging bigger objects.*

In this way, Figure 4.16 depicts the focusing capability of both OPT and SPIM through a plane crossing the detection axis and parallel to it. The use of a low NA in OPT (Figure 4.16a) lead to a profile in which the whole axis is in focus. Such a broad region in focus leads to a bad spatial resolution. On the other hand, high NA used in SPIM (Figure 4.16b) creates a profile similar to a 2D Gaussian function. This means that the region in focus is a point, which has an enormous resolution compared with the profile shown in Figure 4.16a, and this resolution decays as a Gaussian with the distance from the center. It can also be noted that in the axis of detection the decay factor is smaller than in the axis perpendicular to it. It is due to the cone of acceptance described in section 1.1.2, and when the NA is lower, the Gaussian is wider in this axis (lower decay factor), until the point in which a very low NA creates the profile of Figure 4.16a.

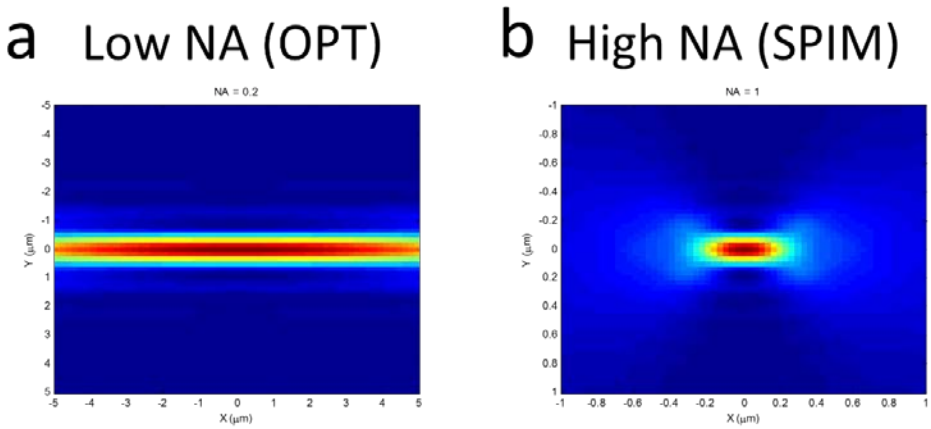


*Figure 4.16: Representation of the region in focus in a plane parallel to the detection objective and coincident with the detection axis. A low NA is used in (a), corresponding to OPT, and a high NA is used in (b), corresponding to SPIM. Red regions correspond to regions that are focused, whereas blue regions are out-of-focus.*

Whereas in Figure 4.16 are shown two graphical cases of the dependence between the NA used and the maximum resolution achievable by the system, a deeper study is shown in Figure 4.17. In this case, the resolution (expressed as the FWHM of the PSF) is compared with the size of the object in focus, which at the same time is related with the NA as shown in Figure 4.15. In SPIM the in-plane resolution increases with the magnification used, but is not affected by the size of the sample being studied. On the other hand, in OPT the resolution worsens proportionally with the size of the object due to the fact that the depth of field (volume in focus) must also increase.

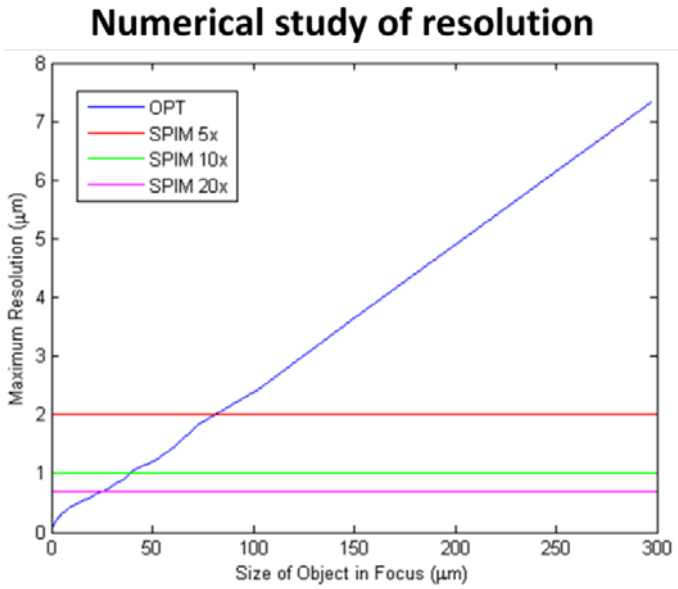


*Figure 4.17: Comparison between the maximum resolution achievable by the system and the size of the object in focus for OPT (in blue), and three different magnifications for SPIM: 5x (in red), 10x (in green) and 20x (in pink).*

# 5 PROTOCOL FOR ESTABLISHING PSF

## 5.1 INTRODUCTION

The resolution of an image system is mainly determined by the FWHM of its PSF but the method used for measuring it can diverge. It leads to unreliable results that are substantially due to difficulties for handling imperfections that usually arise when imaging a sample. Here a protocol is presented for determining the maximum resolution achievable by an optical tomographic system such as SPIM.

The tools used in section 4 are included here, so that similar results can be obtained by following a series of easy steps. This protocol is based on the one proposed in [36] for confocal microscopy. It consists in identifying different particles in the sample by making use of an image processing software developed in MATLAB, which use them for a latter mathematical analysis that results in the desired parameters.

For obtaining a quantitative measurement of the resolution, the concept of FWHM was used as explained in section 4. With the same protocol, the contrast resolution can also be determined by means of the Michelson contrast expression, given in Formula 4.4.

## 5.2 MATERIALS

REAGENTS

- Fluorescent beads with 500 nm diameter
- Distilled water ($dH_2O$)
- Low melting temperature agarose
- Lens cleaner

EQUIPMENT

- SPIM
- Computer
- Conical tubes, 7 ml
- Flask, more than 100 ml
- Eppendorf
- ImageJ software (http://imagej.nih.gov/ij/)
- Matlab software for particles analysis
- Latex or nitrile gloves
- Balance
- Microwave
- Pipettes, 1ml and 10 ml

- Micropipette
- Capillary tube

## 5.3 PREPARATION OF THE FLUORESCENT BEADS

Timing: 1 h 30 min

1. A flask is filled with 100 ml of $dH_2O$ (distilled water).
2. Place a weighting paper in the balance, and place 1 gram of low melting agarose on it as shown in Figure 5.1a.

   IMPORTANT STEP: Low melting temperature agarose should be used that does not solidify at ambient temperature, as it stands in liquid state for a while, allowing you to introduce the fluorescent beads. Otherwise you will not have enough time for placing the fluorescent beads inside.
3. Pour out the agarose in the flask and stir it for mixing the content.
4. As agarose does not dissolve very well at room temperature, use the microwave for heating up the mixture approximately 30 seconds and stir it again. Repeat until the agarose is completely dissolved. It should look like the one shown in Figure 5.1b.

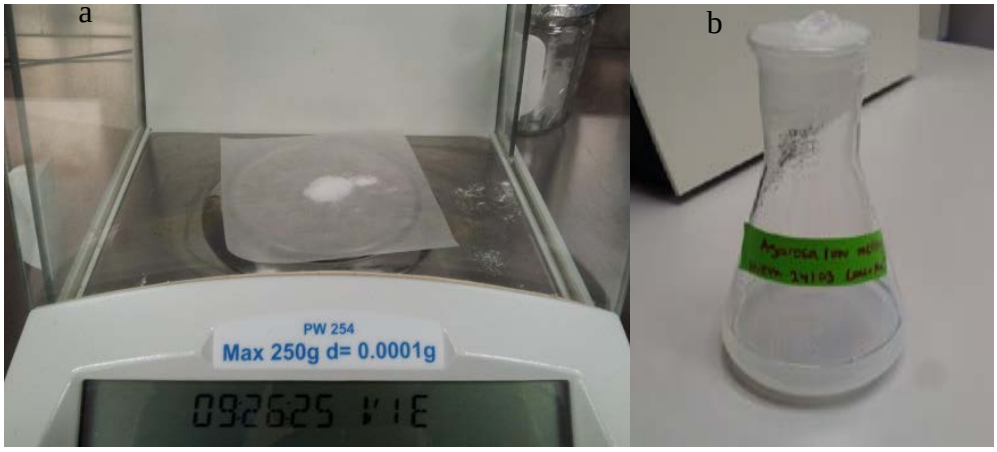


*Figure 5.1: a) Agarose on the balance. b) Dissolved agarose.*

5. Use a 1 mL pipette for placing 100 µL of dissolved agarose in an Eppendorf.
6. Place 2 µL of the fluorescent beads in the Eppendorf with dissolved agarose. For this step use a micropipette with a very small tip. Then mix the sample with the same micropipette very smoothly, as otherwise bubbles can form. Also take care of the liquid state of the sample, because when it hardens, it means that it is solidifying, and you should stop.

   IMPORTANT STEP: You should have the fluorescent beads prepared beforehand, so you can introduce them in the Eppendorf as fast as possible when they are required, because when such a small volume of agarose is placed, it solidifies very fast. If the agarose has already started to solidify, it will be very

difficult to dissolve the fluorescent beads, and some bubbles will form that will affect negatively to the final image.

7. Use a 10 mL pipette for placing 6 mL of the dissolved agarose in a conical tube of 7 mL.
8. Place 2 µL of the sample in the Eppendorf from step 6 in the conical tube, and mix it. As in step 6, a micropipette with a very small tip should be used. In this case mix the sample with a bigger pipette, as the sample is larger. Take care of distributing the fluorescent beads across the whole sample.
9. Wait more than 1 hour for the sample to solidify. The result after this step should be as shown in Figure 5.2.

*Figure 5.2: Fluorescent beads in conical tube.*

10. Use a capillary tube for extracting the sample. If you find difficulties for doing it, you can try sticking the capillary tube into the conical tube, and then turning it several times until a sample remain fixed inside the capillary tube.
11. Use a cylindrical object with a diameter smaller than the capillary tube (it could be a smaller capillary tube) for pushing the sample down, so that it stick slightly out of the capillary tube. In this way the sample should look like in Figure 5.3, and the mismatch between refraction indexes will be smaller, because the sample will be finally immersed in agarose.

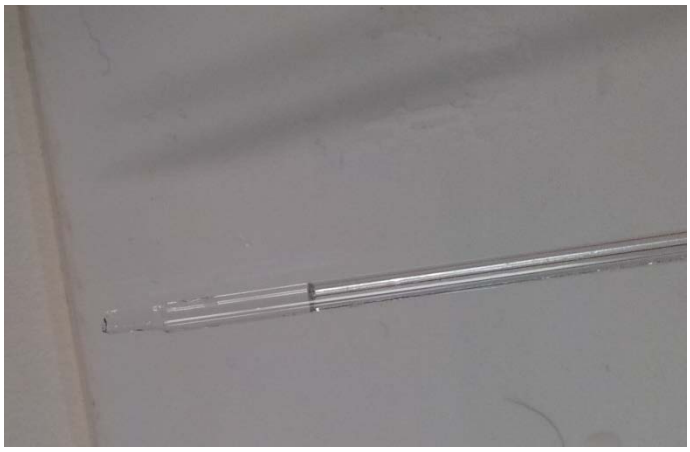

*Figure 5.3: Fluorescent beads sample in capillary tube.*

NOTE: The goal for steps 5-8 is creating a concentration of 1/150000 of fluorescent beads in dissolved agarose, so that other methods leading to the same concentration are also valid. The same happen for steps 1-2, in which a concentration of agarose in water is required at 1%.

## 5.4 SPIM SETUP

Timing: 2 h 30 min

1. Turn on the microscope and choose the green laser. Allow the laser to warm up for 1 hour.
2. Clean the objective lens. This should be done with a lens paper, ensuring that there is no dust in the lens, as it would be otherwise damaged. In a first stage the lens cleaner can be applied on the lens paper, and later $dH_2O$ is applied for removing residues from the lens cleaner.
3. Adjust the laser to focus the desired FOV. This should be done in several stages. First, you should ensure that the laser hits the center of the objective that will focus it. For this purpose a voltage can be used with x and y components that move the laser in the horizontal and vertical directions respectively. Next, the waist of the light sheet should appear in the center of the FOV by moving the objective in charge of focusing the laser.

   IMPORTANT STEP: If the waist of the light sheet is not well focused in the middle of the sample, the resolution would be badly affected, since the light sheet would be broadened and consequently would illuminate out of focus particles.
4. Adjust the width of the slit. For this step it is convenient to take away the cylindrical lens, so that you can see a cone of light. When the pinhole is properly adjusted, it can be seen how the waist of the cone of light is minimum in the middle of the image. Measure the width of the lightsheet for a later comparison

with the PSF obtained for the fluorescent beads. Further details about this procedure are given in section 4.2.3. Once the slit is adjusted, the cylindrical lens can be carefully placed again.

5. A cuvette of water with agarose is put in the place where the sample will be finally imaged. In this way the refraction mismatch between the sample and the media will be smaller.
6. Once the system is prepared, the sample can be placed. For this purpose, you can use a piece that fits both in the sample holder and in the capillary tube. Then you can move it until the sample is placed in the waist of the light sheet and it is focused. The complete setup is shown in Figure 3.1, Figure 3.2 and Figure 3.3. For further details about the system setup, see section 3.

## 5.5 INSTRUMENT SETUP

Timing: 1 h 30 min

1. Ensure that you have selected the green light as excitation, with a wavelength of 532 nm. Select an emission filter that collect light with a wavelength of 607 nm, it is, orange light.
2. Place the 10x objective and move it so that it focuses the fluorescent beads. You can use as clue that the variance in the image is maximum when it is well focused.
3. Set up the image acquisition instruction so that the sample is moved 2 μm for each step, or less if the system allows it. In this way the axial resolution is good enough at the same time that you ensure that this distance is real.

   IMPORTANT STEP: If you select a smaller distance the axial resolution could be better, but you risk that the system do not respond properly and for some stacks the image does not change because the motors have not moved. You can also record the image as a video whereas the sample is moving continuously, so that you avoid the vibrations produced with the steps, but you have the same problem that before, it is, you cannot be sure that the position recorded for each stack is the real one.
4. Select the 2x2 binning mode. Accordingly the SNR will increase, although the spatial resolution decreases. For optimal intensity information, it is best to collect 16-bit images. Finally set the image size to 1272x1080 pixels.
5. Ensure of focusing the fluorescent beads at the middle of the FOV for the best PSF characterization. Otherwise some artefacts can be observed in the PSF shape.
6. Adjust the laser power so that the intensity of the microspheres is approximately 75% of the maximum image intensity.

IMPORTANT STEP: Ensure that you select the laser power so that none of the particles are saturated. For detecting if there is saturation you can plot the profile a particle, and if the peak is flat, then you should reduce the power.

7. Scan a 0.2 mm depth image with the middle in your focus point; it is, 0.1 mm to each direction of the z axis.

## 5.6 DATA ANALYSIS

Timing: 1 h

1. Use the ImageJ software for visualizing the image obtained. ImageJ is a free software that can be downloaded at http://imagej.nih.gov/ij/. You can use the orthogonal views (Go to Image → Stacks → Orthogonal Views, or press Ctrl + Shift + H with your image selected) for determining if the image is correct. You should see your particles as shown in Figure 5.4.

   IMPORTANT STEP: If you see notable differences, for instance because you have a bad resolution in any axis, you should start from the beginning paying a lot of attention to every step. A very typical problem is that an asymmetric PSF is obtained in the axial direction. Although it is mostly due to some of the mismatches between refraction indexes, if the effect is very notable, you can try cleaning the objective lens and apply new immersion media, making sure that there are no bubbles in it.

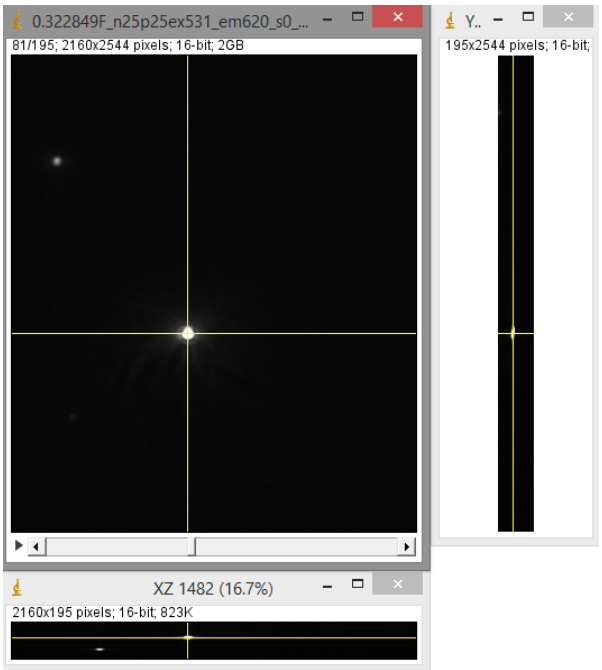


*Figure 5.4: Visualization of fluorescent beads in ImageJ.*

2. Open with Matlab the “particles_selection.m” script, correctly writing the name of your image and the folder where it is located. An image similar to the one

shown in Figure 5.5 will appear, which shows the variance of the particles, so you can select the approximate location of the particles to be analyzed. You should first select the center of a particle in the XY plane shown at the left, and then in the YZ plane shown at the right. Once the point has been defined in both planes, you have four options:

a. Press “k” (keep): you keep the last position and the image appears again for selecting a new position.
b. Press “d” (discard): you discard the last position and the image appears again for selecting a new position.
c. Press “q” (keeps and quit): you keep the last position, and stop selecting particles.
d. Press “x” (discard and quit): you discard the last position, and stop selecting particles.

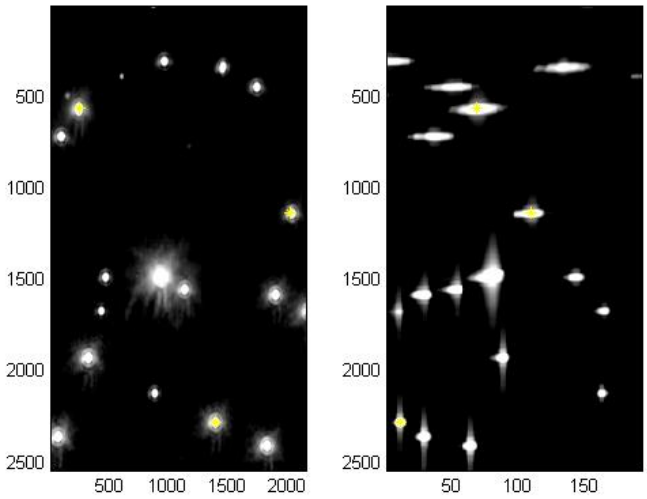


*Figure 5.5: Selection of the particles.*

3. Once you stop selecting particles, the program will ask you if you want to save the positions. If it is the first time you analyze this image, you should do so, because in this way you will be able to analyze them again later without the need of selecting the particles again.
4. The software will calculate separately the FWHM of each particle by fitting a Gaussian function over its PSF, as shown in Figure 5.6, and it will produce a Matlab file with all the data for later analysis. The most important variables are wxy, which contains the FWHM of the particle in the XY plane, and wz, which contains the FWHM of the particle in the z axis. If the number of particles selected is great enough, you will end up having a good statistic of the resolution of your system.

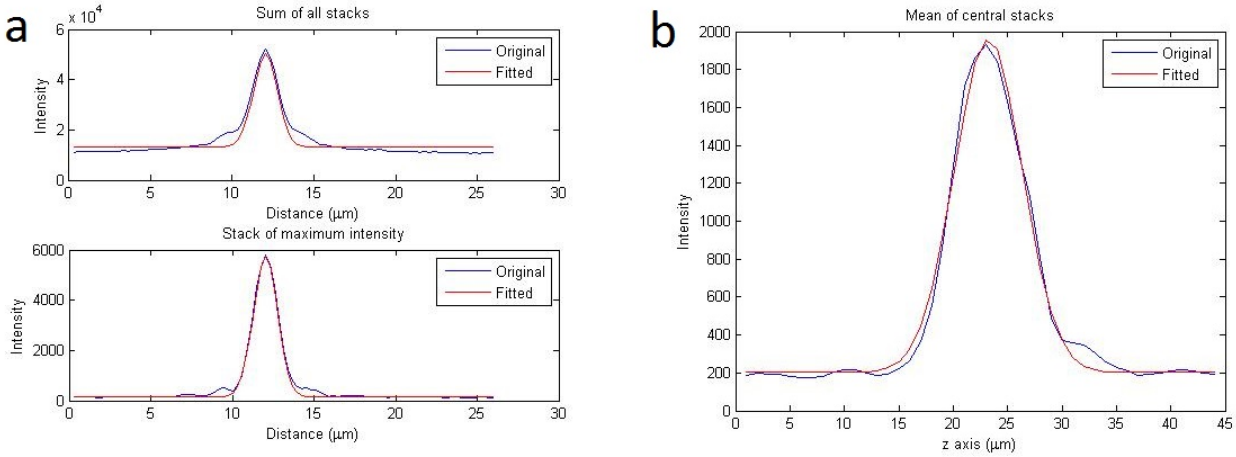


*Figure 5.6: PSF and corresponding Gaussian fitting for the XY plane (a) and the z axis (b).*

# 6 EFFECT OF SCATTERING ON PSF

## 6.1 INTRODUCTION

One of the most common problems when using SPIM is the effect of scattering in the resolution. Scattering is produced in biological tissues due to the mismatches in the refractive indexes existing between different layers, and results in a deviation of the straight path of light. This deviation limits the penetration depth of the system by producing a blur in both the illumination and the detection processes, so that the resolution of the system is limited by this effect [48].

For defining the effect of the scattering quantitatively there are some terms which are especially useful. If a scattering particle is considered with a geometrical size defined by A in $cm^2$, the effective cross-section ($\sigma$) is determined by Formula 6.1.

$$\sigma = Q \cdot A \tag{6.1}$$

Where Q is a proportionality constant called scattering efficiency. $\sigma$ can be understood as the size of the shadow of the scattering object. The most important term for defining the scattering is however the scattering coefficient ($\mu$), which is at the same time related with $\sigma$ and the volume density of the scattering matter ($\rho$) by Formula 6.2.

$$\mu = \rho \cdot \sigma \tag{6.2}$$

The units of the scattering coefficient are $cm^{-1}$, so that it can easily define the transmission of light (T) as a function of the distance traveled by a photon (L) with Formula 6.3.

$$T = e^{-\mu L} \tag{6.3}$$

This formula explain how light is transmitted across a sample, and the fact that it is defined by a decay exponential means that the intensity will diminish with the distance traveled, and if the scattering is more notable, the attenuation effect will be higher. Consequently, the decaying exponential effect in the transmission of light increases with the scattering coefficient.

Nevertheless, the scattering coefficient explains the behavior of transmission of light only under ideal conditions, but the fact is there exists an anisotropy factor (g) that plays an important effect here. This factor explains how much scattering occurs in the forward direction compared to the backward direction, and it is related with the transparency of the sample, so that a very transparent particle will scatter in the forward direction, whereas an opaque particle would scatter predominantly in the backward direction. Numerically g is a dimensionless factor expressed as the average of the cosine

of the angles with which light is scattered, so that when g = -1 means that all light is back-scattered, and when g=0 means that the particle has an isotropic behavior and all light is scattered in the forward direction. With all this in mind, the reduced scattering coefficient is defined by Formula 6.4.

$$\mu^* = \mu \cdot (1 - g) \qquad 6.4$$

Additionally the mean free path (l) can be extracted from the scattering coefficient. This factor determines the average distance that light has to travel until it suffers the next scattering event, so it is measured in cm, and is calculated as the inverse of the scattering coefficient. Another parameter called the reduced scattering mean free path (l*) can also be defined as the inverse of the reduced scattering coefficient. More information about these definitions can be found in [49].

The purpose of this experiment is to characterize experimentally how the scattering of light affects the resolution; in such a way that a quantified model exists that allows to discern if it is worth using SPIM as a function of the amount of the scattering existing in the sample. For this purpose, the resolution of samples containing different degrees of scattering is analyzed, so that a clear relationship can be made between the parameters described here and the maximum resolution achievable by the system.

## 6.2 SAMPLE PREPARATION

Different samples were prepared with a progressively higher effect of scattering. To this end, $TiO_2$ was used at six different concentrations, in such a way that by increasing this concentration the scattering effect is more notable.

The protocol proposed in section 5 was used for the resolution study. In this case, fluorescent particles of 0.1% $NaN_3$ with a mean size of 2 µm were prepared from stock with 2.5% in weight. The excitation wavelength to be used for these particles is 575 nm, and their emission wavelength is 610 nm. The scattering cross-section is $\sigma$ = 374 $cm^2$, and the anisotropy of particles is g = 0.9. The particles are dissolved in agarose following the protocol described, where they reach an index of refraction of 1.3438. In order to prevent some of the effects that the crystal interface of the cuvette does in the light sheet, the sample is placed 5.9 mm away from it.

Other parameters depend on the concentration of scattering material used. Table 6.1 shows the different parameters describing the scattering effect for each of the samples prepared.

| Sample | A | B | C | D | E | F |
|---|---|---|---|---|---|---|
| [C]% | 1% | 0,75% | 0,50% | 0,25% | 0,10% | 0,05% |
| l (mm) | 4,69 | 6,25 | 9,38 | 18,76 | 46,9 | 93,8 |
| l* (mm) | 46,9 | 62,5 | 93,8 | 187,6 | 469 | 938 |
| μ ($mm^{-1}$) | 0,213 | 0,16 | 0,106 | 0,053 | 0,021 | 0,010 |
| μ* ($mm^{-1}$) | 0,0213 | 0,016 | 0,0106 | 0,0053 | 0,0021 | 0,001 |

*Table 6.1: Parameters for the different samples prepared.*

Once the different samples have been imaged, it can be proceeded with the analysis as described in section 5.6, so that different set of data are obtained for different amounts of scattering.

## 6.3 EXPERIMENTAL RESULTS

Samples A, B and C have a characteristic behavior that is analyzed in section 6.4, so that only samples D, E and F are considered in this part.

Once the protocol for establishing the PSF has been followed, all the data corresponding to the resolution in each axis is available, as well as the properties of the fluorescent beads in each sample. Consequently we have a map for the particles selected in each image, as shown in Figure 6.1. What is shown in this image is each particle at its position, but the size shown for each particle does not correspond to their actual size. Instead, they are represented as an ellipsoid whose axes are equal to the FWHM of the corresponding fluorescent bead and in the correspondent dimension. Although this image does not provide any statistical data by itself, it is important for understanding the approximate distribution of the fluorescent beads inside each sample, as well as the heterogeneity existing, as some of the particles have sizes very different to the mean. This fact will be seen later when the standard deviation is analyzed. However, it is important to take into account that there exists a trend for the FWHM to be greater as the particles move away from the center. Although in an ideal situation this should not happen, the reason is that the light sheet is narrower at the center, and consequently its sectioning capability is better than at the edges of the FOV. Steps 3 and 4 in section 5.4 of the protocol are crucial for this effect not to happen.

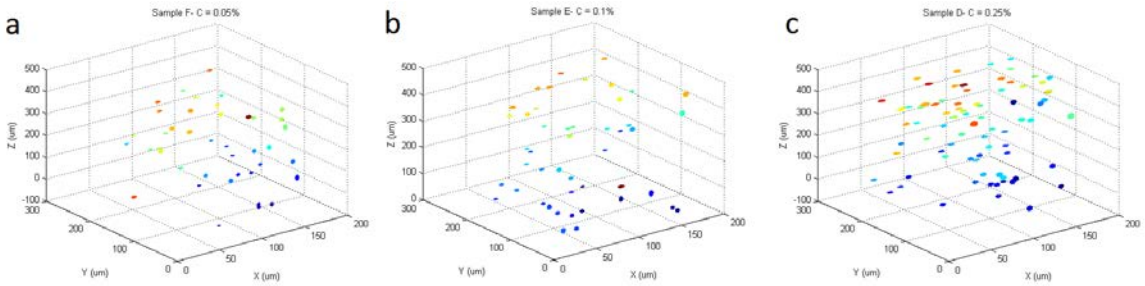


*Figure 6.1: Position of fluorescent beads in the image corresponding to: a) Sample F: μ=0,0107 mm$^{-1}$ b) Sample E: μ=0,0213 mm$^{-1}$ c) Sample D: μ=0,0533 mm$^{-1}$. The sizes of the particles in this figure correspond to the standard deviation of the Gaussian fitted over each of them, by taking into account that it is different in each dimension.*

The next step is studying how all the data extracted from the fluorescent beads depends on the amount of scattering existing in the sample. As explained, the FWHM is different in the axial and in the lateral planes because it depends on different factors, so it is first analyzed in the XY plane. In Figure 6.2 a clear dependence can be seen by which the FWHM increases with the axial distance, and at the same time, it is even greater when the concentration is increased.

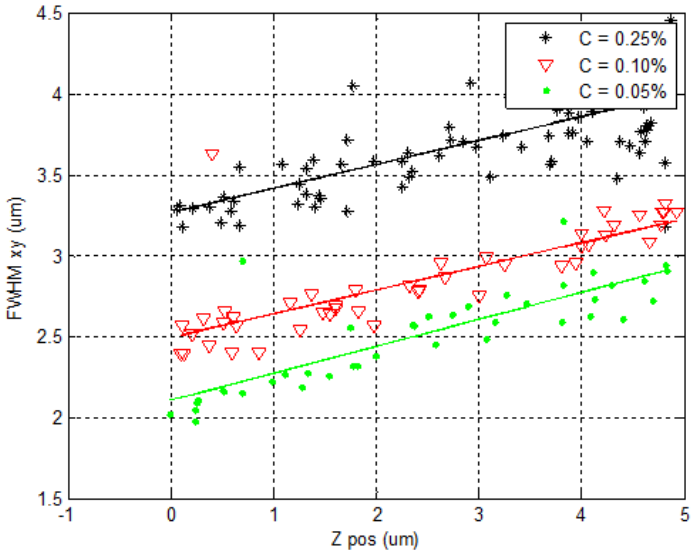


*Figure 6.2: Dependence of the FWHM in the XY plane with the axial distance in a dispersion graph where the data of each sample have been fitted.*

Once the dependence of the FWHM with the axial distance has been discussed, the mean at every position is taken for studying the dependence of the resolution in the XY plane with the scattering coefficient (μ). As it has been shown that μ depends on the axial position, if it is averaged and the position is not taken into account, it is to be expected that it includes a lot of standard deviation. Figure 6.3 depicts the study of the FWHM vs μ, where the effect of the mentioned standard deviation is obvious. In spite of the high standard deviation, a clear dependence of the resolution with the scattering

coefficient is observed, so that the FWHM increases linearly with the scattering coefficient.

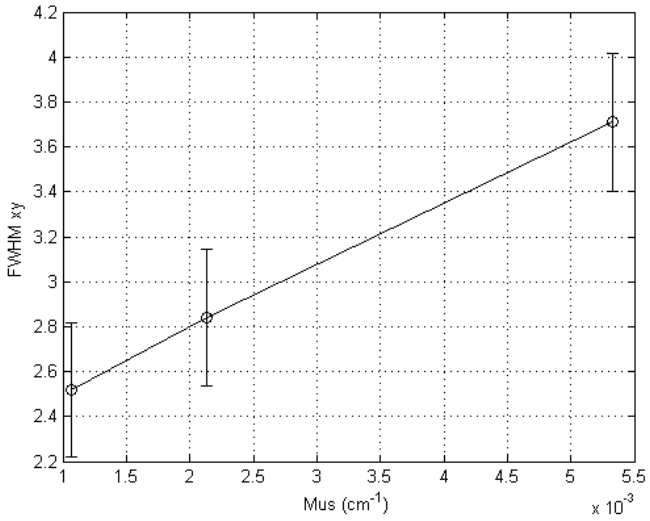


*Figure 6.3: FWHM in the XY plane vs Scattering Coefficient (μ). For these plots the FWHM at every axial distance has been averaged.*

When looking at the resolution in the axial direction (z axis) it is even more difficult to reach a conclusion due to the huge dispersion of the data (Figure 6.4). Consequently, a linear fit does not make sense due to the enormous standard deviation, and a dependence of the axial FWHM with the z position cannot be established.

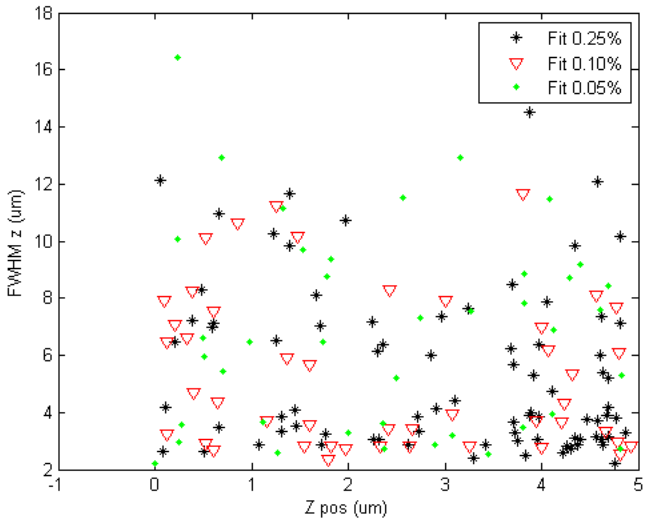


*Figure 6.4: Dependence of the FWHM in the axial direction with the axial distance in a dispersion graph, where only the three samples with smallest scattering (D, E and F) have been taken into account.*

As there is not a clear dependence between the axial FWHM direction and the z position, information is not lost when it is considered constant in every position, and the dependence is to be established with the scattering coefficient. Figure 6.11 shows this

relationship, and although the FWHM is seen to decrease with the scattering coefficient, it is important to take into account that this is an effect of the uncertainty, as it is supposed to be constant.

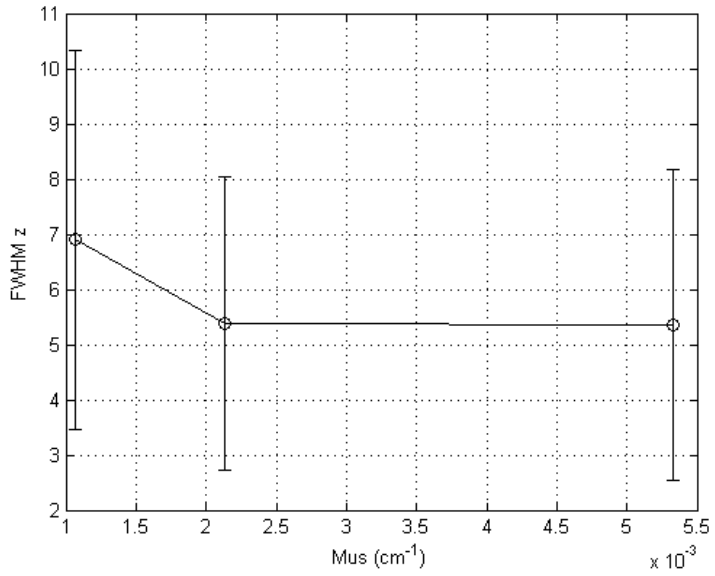


*Figure 6.5: FWHM in axial direction vs Scattering Coefficient (μ). For these plots the FWHM at every axial distance has been averaged.*

The protocol followed does not only give data about the spatial resolution, but also about the contrast resolution. In this way, the contrast for every particle was analyzed based on the Michelson Formula named before. Figure 6.6 is obtained when the results of every particle in each sample are averaged. It shows how the contrast is reduced by increasing the scattering.

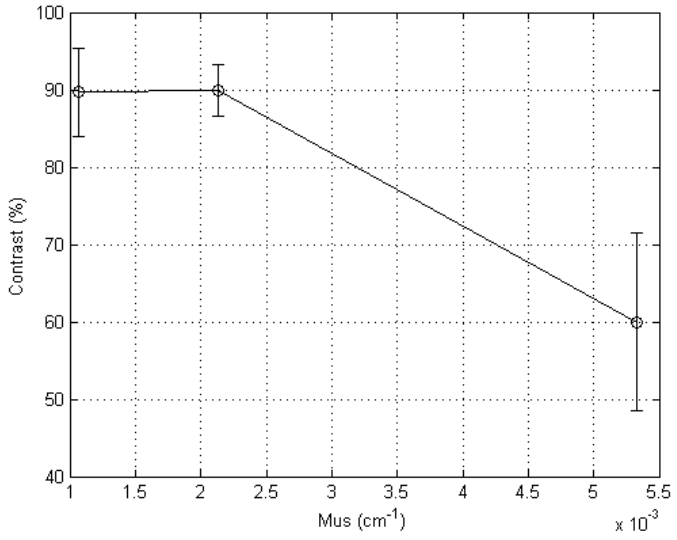


*Figure 6.6: Contrast resolution vs scattering coefficient.*

## 6.4 EFFECT OF FLUORESCENT AND SCATTERING PARTICLES

The fluorescent beads used for this experiment have the characteristic of producing further scattering by themselves. In this way, when they emit light, they also excite surrounding particles. A direct consequence is that fluorescence increases with scattering, and in this way the results change drastically if the concentration of fluorescent beads is increased, as they will be closer between them. This is the case for samples A, B and C, which besides affecting the resolution with scattering, they further affect it with the fluorescent particles they contain.

Consequently, two experiment were mixed. In the first one the scattering increases progressively for each sample, corresponding to the goal of this analysis. However, in a second one the amount of fluorophores also increases for each sample, but this parameter cannot be extracted from the existing data. As a consequence, the resolution measured is not only due to an increase of scattering, but also depend on the amount of fluorescent beads, and as this parameter cannot be controlled, the experiments cannot be separated.

The reason why the amount of fluorophores affects to the resolution is that fluorescence increases with scattering, and consequently the background illumination is higher. The problem is that background illumination does not increase homogeneously, but it depends on the distance between particles; this effect can be understood with an example. If there are three particles aligned, and starting from the premise that the intensity of each one decays like a Gaussian function, in the center of the middle particle the background intensity will be much smaller than on the sides. This means that the spatial resolution (FWHM) and the contrast resolution will depend on the distance between particles.

Figure 6.7 show this effect both in an ideal situation and in the experimental model. In an ideal situation (Figure 6.7a) the scattering would create a background illumination which is constant for the whole image, so that the formula for the Gaussian function corresponding to this PSF would be given by Formula 6.5.

$$f(x) = \left(\frac{1}{\sigma\sqrt{2\pi}} - b\right) \cdot exp\left[-\frac{(x - x_0)^2}{2\sigma^2}\right] + b \qquad 6.5$$

Where b is the background illumination. Such a Gaussian function has the same FWHM than the original one without scattering, since if both of them are normalized, they are exactly equal. Contrast resolution does change in this situation, since the background would make the difference in brightness smaller, and thus the contrast resolution is worsened.

On the other hand the experimental model is not like this. The fact that background illumination increases is due to the fluorescence emitted by surrounding particles as explained, and consequently it depends on the sum of the illumination of each particle at

a corresponding point. Figure 6.7b shows this effect for three fluorescent beads, where the tail of each PSF at the edges is added to the middle one, thus increasing its background in a non-homogeneous way, and resulting in the profile shown in red.

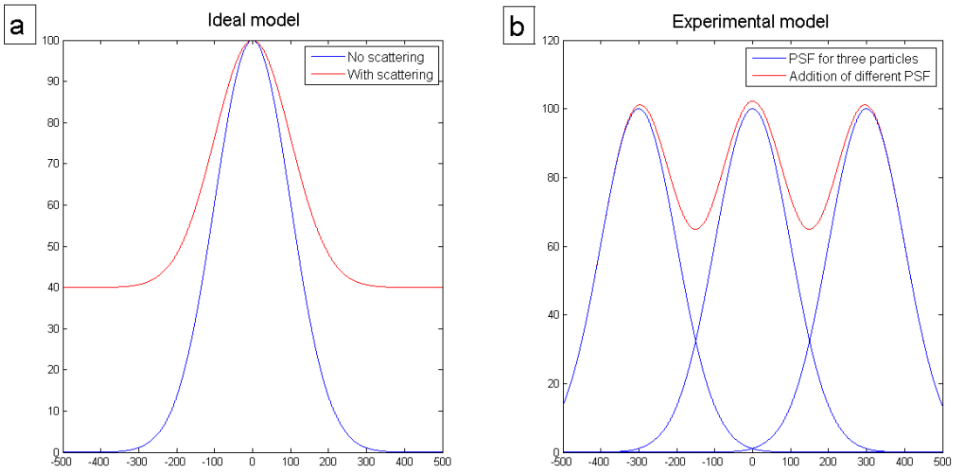


*Figure 6.7: PSF of a fluorescent beads in a scattering medium. a) Ideal model, the FWHM is the same that when there is not scattering. b) Experimental model, the FWHM is different when there is scattering.*

This is not what happens in a real scenario in which a biological sample is imaged with SPIM, as there could be more scattering, but not more fluorescence. Consequently, samples in which fluorescent beads are close enough for producing this effect (samples A, B and C) should be rejected, so that only samples D, E and F are valid for comparing this situation with a normal SPIM image. This is why only samples D, E and F are considered for studying the effect of scattering in the PSF, whereas all the samples are used here for studying the effect of this kind of fluorescent beads in the resolution of the system.

Figure 6.8 helps to understand how the distribution of particles can imply affect to the illumination of fluorescent beads between them for samples with higher scattering coefficient. The reason why there is a smaller number of particles in sample A is that due to the high scattering coefficient it is not easy to find particles for which the analysis can provide reliable result, but although they do not appear in the graph, the concentration of fluorescent beads is the highest.

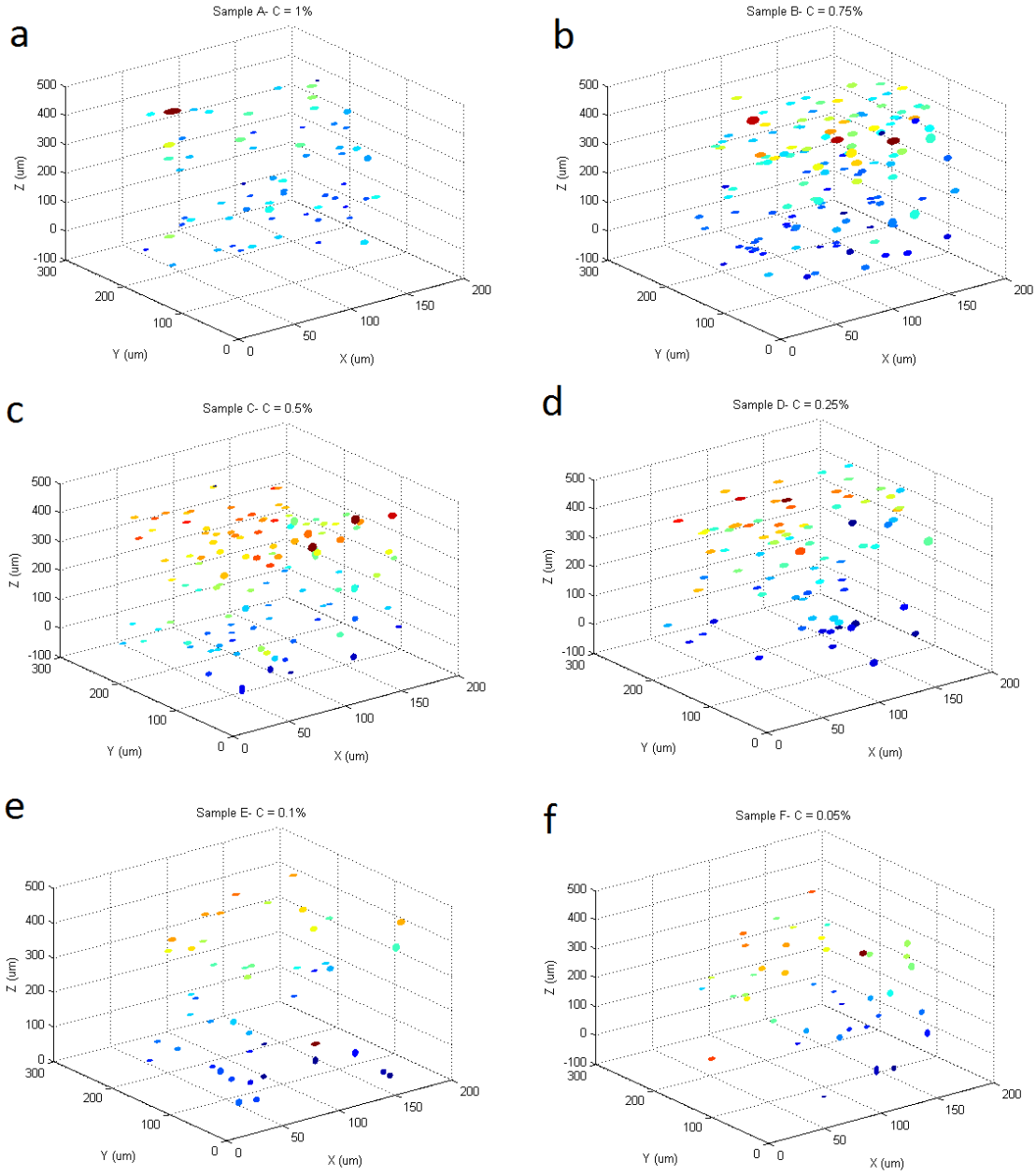


*Figure 6.8: Position of fluorescent beads in the image for the samples corresponding to: a) $\mu$=0,2132 $mm^{-1}$ b) $\mu$=0,16 $mm^{-1}$ c) $\mu$=0,1066 $mm^{-1}$ d) $\mu$=0,0533 $mm^{-1}$ e) $\mu$=0,0213 $mm^{-1}$ f) $\mu$=0,0107 $mm^{-1}$. The sizes of the particles in this figure correspond to the standard deviation of the Gaussian fitted over each of them, by taking into account that it is different in each dimension.*

Figure 6.9 represents the linear fits resulting from the dispersion graph in which the lateral resolution is compared with the axial position. In Figure 6.9a it can be appreciated the already mentioned dependence on both the z position and the scattering coefficient. However, when samples with more scattering are included in the analysis different effects are observed, as shown in Figure 6.9b. It is easy to see that samples A, B and C have a smaller FWHM than D, although their scattering coefficient is higher. It would imply that the resolution is better when scattering increases, but it does not make

sense at all. Furthermore, they are not related between them. It is, A has a greater FWHM than C, but smaller than D, what suggests that there is something wrong with the data.

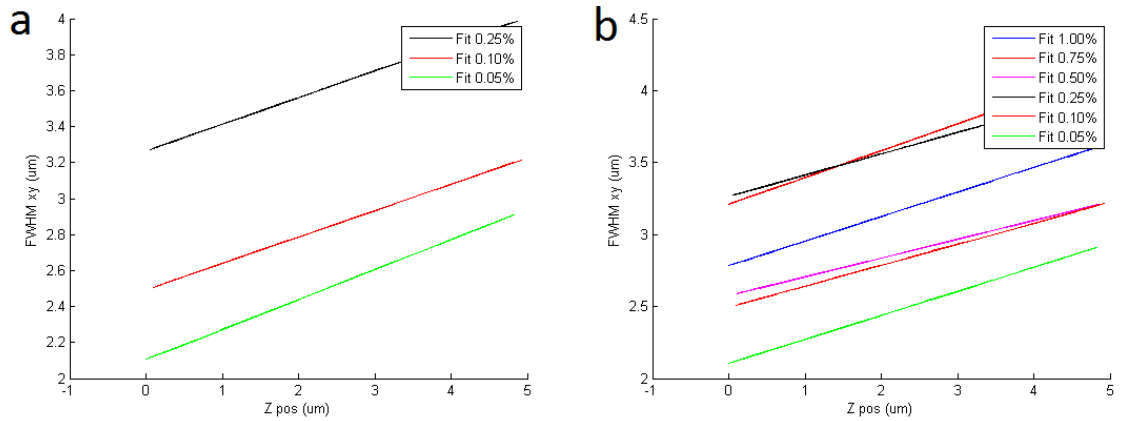


*Figure 6.9: Linear fit resulting from the dependence of the FWHM in the XY plane vs the axial direction for samples: a) D, E and F b) A, B, C, D, E and F.*

It is to be expected that lateral resolution worsens with the scattering coefficient, as is the case for samples D, E and F in Figure 6.10a. However, for samples having more scattering than D (see Figure 6.10b) anything makes sense, since resolution is seen to be better in C and A, whilst it should be worse.

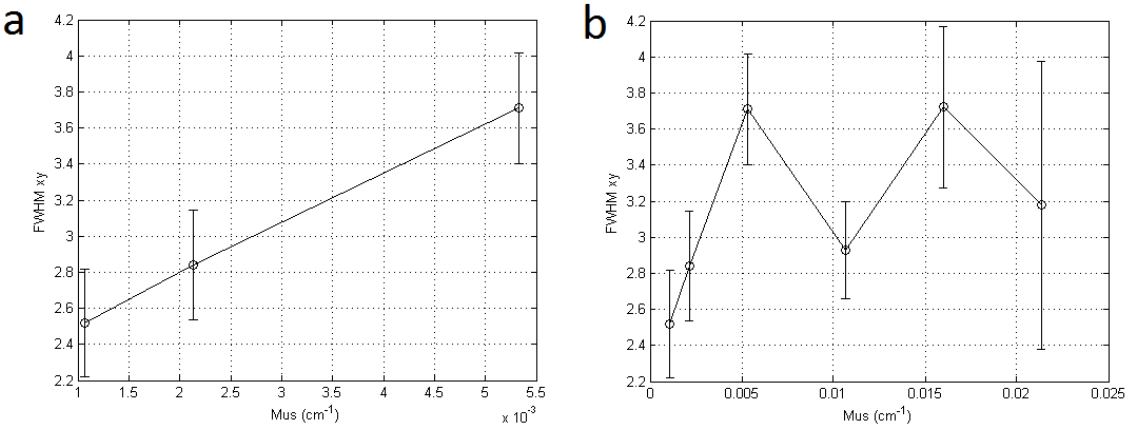


*Figure 6.10: FWHM in the XY plane vs Scattering Coefficient (μ). For these plots the FWHM at every axial distance has been averaged. a) Scattering coefficient for samples D, E and F are used. b) Scattering coefficient for all samples available are used.*

Figure 6.11 contains the data for the axial FWHM as a function of the scattering coefficient. In this case, the fact that fluorescence increases with an increase in the number of particles is not a problem, as the results are similar for every sample despite the properties of samples with higher scattering coefficients.

In Figure 6.11b all the samples are used, and although it is not as clear as in Figure 6.11a, there is also a tendency for the FWHM in the z axis to decrease with the scattering coefficient. Contrary to the situations found for the XY plane, the fact that the

dependence is different when samples with higher scattering are used is not the main problem here, but a greater uncertainty exists here due to the huge standard deviation existing in the data, that make it difficult to reach a conclusion. The origin of this standard deviation has been already discussed in section 6.3.

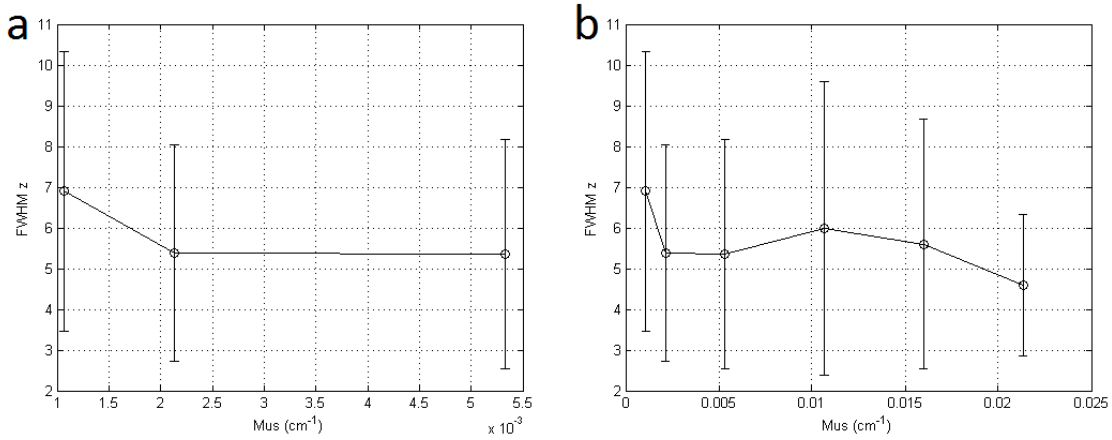


*Figure 6.11: FWHM in axial direction vs Scattering Coefficient (μ). For these plots the FWHM at every axial distance has been averaged. a) Scattering coefficient for samples D, E and F are used. b) Scattering coefficient for all samples available are used.*

The contrast resolution does not seem to be affected by the effects of the additional samples either, since it is supposed to decrease by increasing the scattering coefficient as shown in Figure 6.12. However, the factor by which it diminishes is in part further influenced by the distance between the particles as shown in Figure 6.7, so it cannot be considered that the curve should have this exact shape in a real situation in which scattering exists.

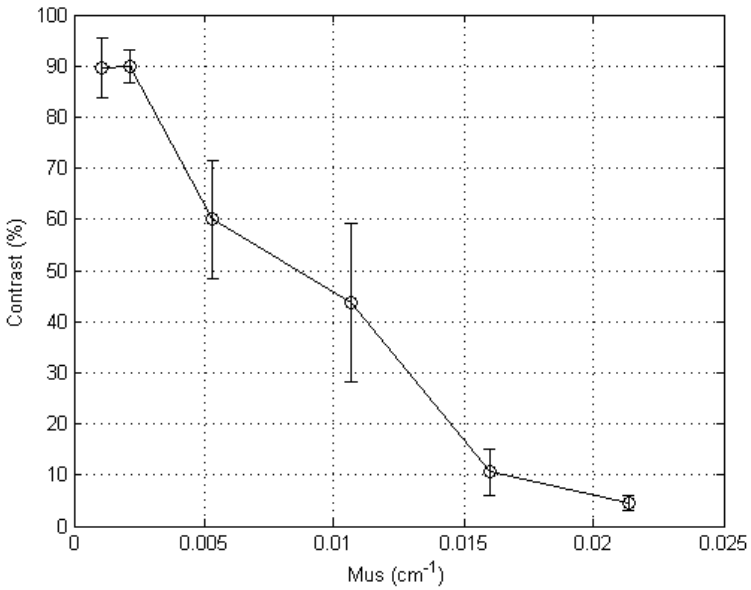


*Figure 6.12: Contrast resolution vs scattering coefficient for all the samples.*

This experiment cannot provide a reliable model for quantifying the effect of scattering in the resolution achievable by an optical tomography system, due to the undesired effects included. However, samples D, E and F are not affected by these problems, since the average distance between particles is big enough for their illumination not to affect the neighboring particles. Consequently, some useful conclusions can be reached if the figures that only include these particles are used.

# 7 CONCLUSIONS

## 7.1 CHARACTERIZATION OF OPTICAL SYSTEMS

The application of the method proposed for characterizing an optical system results in some data of great interest for determining some parameters that define the potential of an optical tomography system such as SPIM. By preparing the samples with fluorescent beads and analyzing them with the software presented, some conclusions can be discussed about the characteristics of the SPIM used in this experiment, which at the same time can be extrapolated for studying the behavior of similar systems.

The different steps followed for the study of the sectioning capability of the light sheet lead to the results shown in Table 4.2. It makes sense that in the first step the FWHM is so small compared with the values obtained in the second and third steps, because instead of having a sheet of light, the laser is focused in a single point; and this FWHM is in fact the width of such point. However, by looking at Figure 4.7a, it is quite clear that this configuration would only provide good results near the region where the FWHM is measured (in yellow), since the beam broaden as it moves away from the center.

Regarding the viability of using the slit aperture (second step) as a protocol for determining the width of the lightsheet, it can be observed in Table 4.2 that the FWHM obtained for this step is not entirely equal to the one obtained in the third step, where an iris was used. However, the difference is small enough to consider that the second step is a good approximation for determining the maximum axial resolution achievable by the system.

The fact that the sectioning capability of the system can be quantified with a single image of a lateral plane in the normal configuration of SPIM is a great advantage, since modifying the setup for placing an iris can take a lot of time, at the same time that a later calibration would be needed. When this technique is implemented in a protocol as described in section 4, it should be carried out rapidly and without the need of a technical knowledge about the manipulation of the system. Consequently, the simplification proposed here is very interesting for being included in the protocol.

Values from the first step in Table 4.2 are related to the actual width of the sheet and where it focuses. In fact, the camera captures the sum of the signal in the z axis within its depth of field, so that the combination of the width with the depth of field of the detector represents the axial resolution. Consequently they express that the z resolution is influenced by the magnification used, and in this way they can be incorporated in Table 4.1 with the data resulting from the PSF analysis of the fluorescent beads.

Altogether, data in Table 4.1 are useful for concluding that the resolution of SPIM is not highly influenced by the magnification used. Although it seems to improve

slightly when the magnification used is greater, the difference is so small (less than a 5%) that it can be considered negligible.

Regarding the distribution of the FWHM with position shown in Figure 4.13, it makes sense that a correlation is not obtained between the resolution and the distances in the different axes, because as long as the particles are selected inside the FOV, there does not exist any reason for their shape to depend on the position. Nevertheless some of them suffer this effect, because there could be some cases in which a particular fluorescent bead is selected excessively far from the center of the image. This behavior is explained in [37], where a model is proposed for determining the FWHM of the illumination beam as a function of the lateral position from the focal spot, as shown in Figure 7.1.

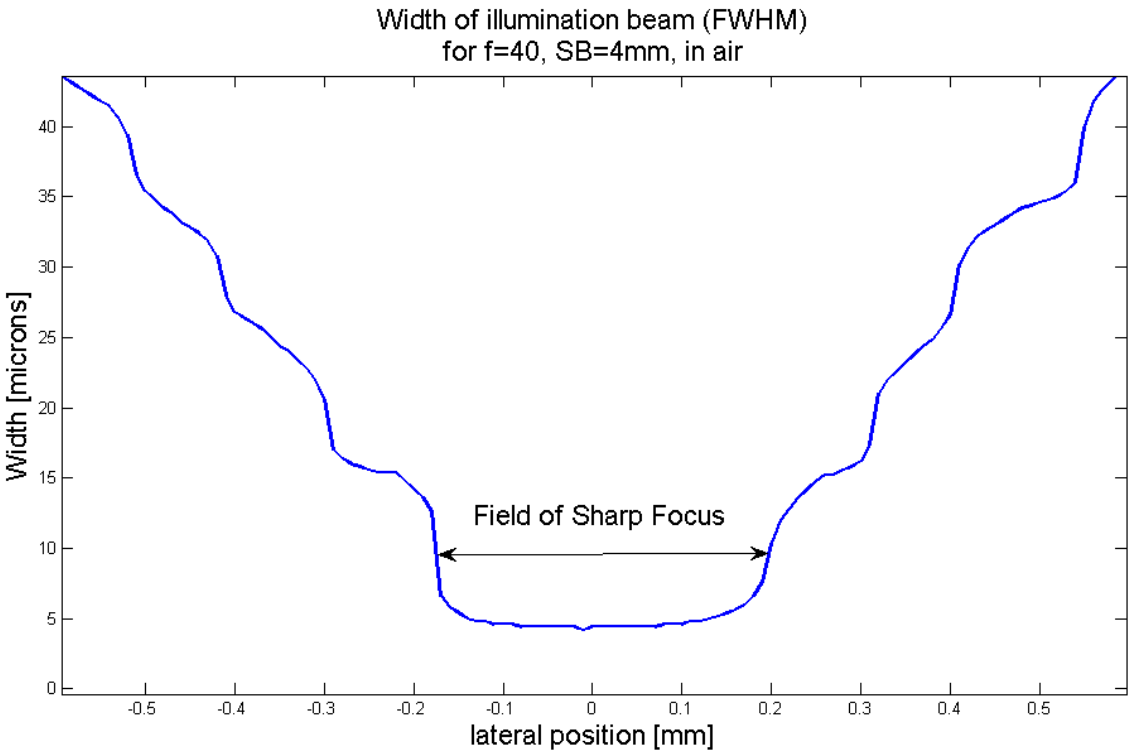


*Figure 7.1: FWHM of the illumination beam versus distance from the focal spot (by [37]).*

With the help of this graph and the histograms of Figure 4.14, it can be concluded that with a few exceptions (points that only have one or two counts at the edges of the histograms), most of the fluorescent beads selected are in what is referred in Figure 7.1 as Field of Sharp Focus, which correspond to the FOV.

Besides having thoroughly characterized a SPIM system, the theoretical comparison with OPT allows to understand the advantages and disadvantages of each technique. Therefore, it was shown that SPIM offers higher resolution capabilities, making it a better option for the study of small structures given in biological samples. On the other hand, OPT offers isotropic resolution and is more robust in the presence of scattering.

## 7.2 PROTOCOL FOR ESTABLISHING PSF

The protocol used was shown to give very accurate results, which fits perfectly when compared with the existing theoretical models, like the one proposed in [4]. Furthermore some optical problems can be detected and in this way studied with this protocol, as could be the imperfections that arise in the PSF when the refractive indices of the media of the objective lens and the specimen mismatch significantly (see [38]).

This protocol integrates most of the methods and results studied in this project in a series of steps that can be easily followed. In this way, any user can benefit from the analysis developed in section 4 without a deep knowledge about the different fields involved.

Altogether, this protocol can be followed as a standard for quantifying some properties related with the resolution of not only SPIM, but also some other optical tomographic systems like OPT.

## 7.3 EFFECT OF SCATTERING ON PSF

The analysis carried out in section 4, together with the protocol proposed in section 5 are of great importance for applications related with the resolution of a system. In this case, they were put into practice for studying how the scattering affect the PSF of a system, and consequently how an image with a specific amount of scattering is affected.

By observing Figure 6.3 it is quite clear that the lateral resolution worsens by increasing the amount of scattering material. It is to be expected, because when the axial distance increases, there exists more scattering between the particle being studied and the camera, and it makes the camera to record a particle that is more blurred than the original one. A more technical explanation consists in understanding that the mean free path (l) is smaller for greater concentrations of scattering, and being this parameter defined as the mean distance light has to travel for suffering the next scattering event, it is obvious that for higher concentrations of scattering the light emitted by the fluorescent beads will suffer more scattering events. Consequently, a blurring effect appears that produces a broadening of the Gaussian function defining the PSF.

The dependence seems to be linear. However it would make sense to think that if more data were available, a limit would exists in which the high scattering coefficient would make it impossible to measure a reliable PSF; and far from obtaining a quantification of the resolution in such an image, it could be considered that SPIM cannot provide a good image. Other techniques are more appropriate in situations in which the sample has a higher scattering coefficient, being OPT a good example.

Regarding the axial resolution, there is an issue related with the high dispersion of the data shown in Figure 6.4, which far from being a problem with the fitting function, it might be due to a problem aligning the sheet (see steps 3 and 4 in section 5.4).

Consequently the waist is thicker than expected, resulting in a bad sectioning capability. It is to be added to the fact that the procedure was not followed correctly, and instead of pushing the sample outside from the capillary tube as explained in step 11 of the protocol described in section 5.3, the sample containing the fluorescent beads remained inside. Consequently light had to travel across several interfaces (air, glass, bath and agarose), thus producing abnormalities in the axial resolution (see [38] for further details about this effect). All these effects result in an image whose fluorescence beads with very different FWHM, and consequently an enormous standard deviation of the data.

If the sectioning capability of the system is good, the axial resolution should not be greatly affected by the scattering coefficient. Indeed, Figure 6.5 supports that scattering does not have any influence in the axial resolution, because the difference in FWHM for different samples is smaller than the standard deviation, so that the resolution can be considered to be maintained as constant.

The fact that contrast resolution decreases with the scattering coefficient as shown in Figure 6.6 is to be expected, because light suffers more deviation events when the scattering material increases. At the same time, these deviations create a higher background illumination that makes the fluorescent beads less visible. This effect is graphically shown in Figure 6.7a (in red), where it is easily seen that the difference in illumination is smaller when scattering creates such background.

All in all, this experiment is very useful for quantifying the resolution in a real scenario where scattering exists. In fact, scattering is inherent in biomedical experiments due to the mismatches existing between different biological layers. Although clearing methods are used for avoiding these mismatches, they are far from completely removing scattering. Accordingly, the results obtained here can be useful for further characterizing different clearing methods.

This analysis is also useful for the material science field as a tool for characterizing materials in turbid media. Nevertheless, three samples do not provide enough data for extrapolating the result to samples where greater scattering coefficients exist, as different behaviors can appear.

# 8 FUTURE WORK

The scope of the methods suggested in this project for characterizing an optical system is far beyond the applications mentioned here. Besides scattering, biological samples used in optical tomography have several intrinsic parameters influencing the resolution of an image. Different models can be thus proposed for simulating many of the situations existing in these samples, for then quantifying as many parameters as possible by means of the protocol proposed in section 5.

As the protocol is easy to be used even by users without a thorough knowledge in the different fields that it covers, it can be considered as tacit knowledge, and in this way can be easily transferred between different research teams for collaboration purposes. This is very advantageous for future projects in which the knowledge of other teams is needed for specific results. A clear example could be the modeling of new parameters mentioned before, as other teams may develop samples with specific characteristic that can only be imaged in their own laboratories.

Regarding the study of the effect of scattering on the PSF in section 6, it has been seen that the results are very good as far as the three samples with the smallest scattering coefficient were used. As explained, it was due to a problem in the sample preparation, since two experiments were mixed, one that increases the amount of fluorophores and another one that increases the scattering. In order to obtain more reliable results, a new experiment should be done in a future in which the fluorescent concentration is maintained fixed, and only the scattering increases. In this way, a good quantification of the resolution could be obtained even for high values of scattering coefficient.

The analyses performed in this project are mainly focused in SPIM, but the conclusions concerning the behavior of the resolution under different scenarios, as well as the methods used for its analysis, are also valid for different optical tomography systems. However, the protocol for establishing the PSF is optimized for SPIM, and some changes should be done for it to be used in other systems. In this way, a number of protocols could be developed based on the one proposed here for SPIM, so that they are optimized for systems in which a clear demand of such a protocol exists.

Although nowadays SPIM has become a standard for many experiments, the importance of other systems in the field of optical tomography has also been mentioned. The reason is that some experiments require characteristics that are predominant in a specific system, for instance diSPIM has been shown to be an excellent option for microtubule tracking in live cells [27]. In section 4.4 a clear example of this ambiguity is given. Whereas SPIM is shown to be a better option than OPT for imaging bigger samples, OPT has a characteristic isotropic resolution that makes it superior to SPIM for many applications.

By taking these considerations into account, a new system could be proposed that takes advantage of both the light sheet of the SPIM and the acquisition method of OPT. Therefore, the resulting image would have an excellent resolution without being influenced by the size of the sample or by the direction (isotropic resolution); furthermore, photobleaching would be a minor problem due to the use of a lightsheet. The reconstruction technique for such a technique could be based on the Filtered Back Projection (FBP) used for fan beam CT.

## 8.1 INDUSTRIAL APPLICATIONS

Optical tomography systems are quite useful in biomedical companies, since they allow to study the behavior of different biological compounds, whether for the development of new drugs or for understanding the function of some structures in small animals, which at the same time can be useful for the treatment of a specific disease.

As already discussed, the protocol proposed here for establishing the PSF of an optical tomography system can be easily followed by any team owing this kind of equipment. As it includes most of the analysis presented here, it makes it possible to obtain meaningful results without the need of carrying out a deep study of the field. Furthermore, as no protocol has been published yet for measuring the resolution of SPIM, these studies are based on tedious analyses that provide less data and took longer than the method proposed here. Consequently, besides providing more useful data, the labor costs needed for completing it are much smaller.

For this reason, the protocol could become a standard for quantifying the resolution capabilities of different systems. It would imply that systems such as SPIM could carry a seal of quality given by this protocol. It would be especially interesting for companies that sell these systems, so that they could publicize them with this parameter included in the specifications. Furthermore, it would not only be useful for sellers, but also for teams having one of these systems, since they would be conscious of its capabilities in different scenarios without the need of carrying out the whole experiment.

For the impact of this protocol to be greater, a future project could consist in fully automatizing it, so that it could be followed even more easily. A software can be developed for this purpose, and it would be included in the SPIM controller. In this way a new option would be available in the user interface of the system, and the whole analysis would be carried out automatically just by clicking on this option. It implies that the system detects that a correct sample with fluorescent beads have been placed, for then focusing it by means of the image variance. As the dimensions of both the sample and the fluorescent beads would be known, the system could automatically take the 3D image. Finally, the analysis program would be initialized for analyzing the particles without the need of a user. One of the greatest difficulties would be to create a

software that discerns which particles are indeed appropriate for the study without human supervision.

In this context, there are two main reasons why a team in charge of an optical tomography system would desire to use the protocol proposed here for determining the PSF of their system. The first one is that they need the aforementioned seal of quality, and the second one that they want to put it in practice for studying how a specific parameter (that could be implicit in a product they commercialize) affects to the resolution of an optical system, as have been done here for the case of scattering.

# APPENDIX A

## A. particles_selection

```
%particles_selection
%This is the main program for particles analysis. It allows the user
interaction for selecting fluorescent beads
%in the image described in 'folder' and 'imName'. It ends up giving
the
%desired parameters for the particles selected.

folder = 'C:\Users\Álvaro\Documents\Carlos III\PFC\Scattering\Samples
Scattering_Exp\F\';

imName = '0.322849F_n25p25ex531_em620_s0_r1_o1_r';
FileTif = [folder imName '.tif'];
dxy = 0.08125; % Pixelsize in um (for the 80x in this case)
findPos = false;

objetive = imName(7:8);
if objetive == '50'
    dxy = 0.279398246778142; %Pixelsize in um/pixel
elseif objetive == '20'
    dxy = 0.633169418159987;
elseif objetive == '10'
    dxy = 1.25258180753014;
else
    disp('This objective does not exist. Check image name');
end

Zorig = 17;
Bead_Diameter = 0.5; %in um

InfoImage=imfinfo(FileTif);
Nx=InfoImage(1).Width;
Ny=InfoImage(1).Height;
%Nz=length(InfoImage)-1; %original
Nz=length(InfoImage)-3;
% Finding Pixelsize dZ:
Hdr = grump_readheader(InfoImage(2).ImageDescription);
Z0 = Hdr.z*1000;
refPos = [0 0 (Hdr.z-Zorig)]*1000;
Hdr = grump_readheader(InfoImage(Nz+1).ImageDescription);
Z1 = Hdr.z*1000;
dz = (Z1-Z0)/Nz;
%dz = (Z1-Z0)/(Nz-1);
pixelSize = [dxy,dxy,dz];
if objetive == '50'
    Nimgz = 26*ceil(Bead_Diameter/pixelSize(3)); %Images per bead
    Nimgxy = 26*ceil(Bead_Diameter/pixelSize(1)); %Pixels per bead
elseif objetive == '20'
    Nimgz = 30*ceil(Bead_Diameter/pixelSize(3)); %Images per bead
    Nimgxy = 30*ceil(Bead_Diameter/pixelSize(1)); %Pixels per bead

elseif objetive == '10'
    Nimgz = 26*ceil(Bead_Diameter/pixelSize(3)); %Images per bead
    Nimgxy = 26*ceil(Bead_Diameter/pixelSize(1)); %Pixels per bead
else
```

```
    disp('This objective does not exist. Check image name');
    Nimgz = 6*ceil(Bead_Diameter/pixelSize(3)); %Images per bead
    Nimgxy = 6*ceil(Bead_Diameter/pixelSize(1)); %Pixels per bead
end



%% Finding the positions
if findPos

    Ixyz = zeros(Ny,Nx,Nz,'uint16');
    for ii=1:Nz
        U = imread(FileTif,ii+1);
%         U = median2d(double(U));
        Ixyz(:,:,ii) = uint16(U);
    end

    % Fiding the XY variance
    Uvar = variance2d(Ixyz,3);
    Ixy = median2d(Uvar,5);
%     Ixy = squeeze(mean(Ixyz,3)); % the simple mean

    % Fiding the YZ variance (not really useful)
    Uvar = variance2d(Ixyz,2);
    Iyz = median2d(Uvar,5);
%     Iyz = squeeze(mean(Ixyz,2)); % the simple mean

%% Selecting the beads
    ip = 0; cont = true;
    Xpos = []; Ypos = []; Zpos = [];

    while cont
        figure(1)
        clf
        subplot(1,2,1)
        aux_Ixy = log(Ixy+1);
        aux_Ixy2 = aux_Ixy - min(aux_Ixy(:))+1;
        imagesc(log(aux_Ixy2)); caxis([7 11]);
        colormap gray
        %imshow(log(aux_Ixy2),[])
        hold on
        plot(Xpos,Ypos,'y*')
        subplot(1,2,2)
        aux_Iyz= log(Iyz+1);
        aux_Iyz2 = aux_Iyz - min(aux_Iyz(:))+1;
        imagesc(log(aux_Iyz2)); caxis([7 11]);
        colormap gray
        %imshow(log(aux_Iyz2),[])
        hold on
        plot(Zpos,Ypos,'y*')
        subplot(1,2,1)
        [xposXY,yposXY]=ginput(1);
        plot(xposXY,yposXY,'yo')

        % Now we have the xy position, we need to find the z:
        xini = ceil(xposXY-Nimgxy/2);
        xfin = ceil(xposXY+Nimgxy/2);
        Uvar = variance2d(Ixyz(:,xini:xfin,:),2);
        Iyzo = median2d(Uvar,5);
```

```
        % Iyzo = Iyz;
        Iyzo(ceil(yposXY-1):ceil(yposXY+1),:) = max(Iyzo(:));

        subplot(1,2,2)
        hold off
        imagesc(log(Iyzo)); caxis([7 11]);
        hold on
        [zposYZ,yposYZ] = ginput(1);
        plot(zposYZ,yposYZ,'yo')

        K = input('Keep/Discard/Keep & Quit/Discard & quit
(k/d/q/x)','s');

        switch K
            case {'k','K'}
                ip = ip+1;
                posy = (yposXY + yposYZ)/2;
                Xpos(ip) = xposXY;
                Ypos(ip) = posy;
                Zpos(ip) = zposYZ;
                cont = true;
            case {'q','Q'}
                ip = ip+1;
                posy = (yposXY + yposYZ)/2;
                Xpos(ip) = xposXY;
                Ypos(ip) = posy;
                Zpos(ip) = zposYZ;
                cont = false;
            case {'x'}
                cont = false;
            case {'d'}
              % do nothing
        end
    end % End while


%     txt = ['m=forward; n=backward; \n' ...
%            'q=quit; z=undo; s or w=save; \n'...
%            'p=H contrast up; l=H contrast down;\n'...
%            'o=L contrast up; k=L contrast down;\n'];
%     disp(txt);
%     % Finding the positions to use in this file
%     istart = 1;
%     stop = false;
%     ii = istart;
%     irec = ii;
%     ii0 = 0;
%     Xpos = []; Ypos = []; Zpos = [];
%     while ~stop && ii<=NumberImages
%         if ii0~=ii
%             U = imread(FileTif,ii+1);
%             imagesc(log(double(U)));
%             axis xy
%             title([num2str(ii) ' of ' num2str(NumberImages)])
%             ii0 = ii;
%             hold on
%             plot(Xpos,Ypos,'wo')
%             plot(Xpos,Ypos,'wx')
%             hold off
```

```
%         end
%         pause(0.1)
%         [posx,posy,K]=ginput(1);
%         if ~isscalar(K), K=0; end
%         switch K
%             case 1% there has been a mouse click;
%                 Xpos(irec) = round(posx);
%                 Ypos(irec) = round(posy);
%                 Zpos(irec) = ii;
%                 disp([num2str([ii, posx, posy])]);
%                 irec = irec+1;
%             otherwise
%                 Kc = char(K);
%                 switch Kc
%                     case 'm'
%                         ii = ii+1;
%                     case 'n'
%                         ii = ii-1;
%                     case 'z'
%                         irec = irec-1;
%                         Xpos = Xpos(1:irec);
%                         Ypos = Ypos(1:irec);
%                         Zpos = Zpos(1:irec);
%                     case 'q'
%                         stop = true;
%                     case {'s','w'}
%                         save([imName
'_Pos.mat'],'Xpos','Ypos','Zpos','FileTif','NumberImages','pixelSize')
;
%                 end
%         end
%     end

    S = input('Save the positions?: (y/n) ','s');
    if strcmp(S,'y')
        save([folder imName
'_Pos.mat'],'Xpos','Ypos','Zpos','FileTif','Nz','pixelSize');
    end
else
    % Load positions:
    load([folder imName '_Pos.mat']);
end

%% Finding the FWHM of each of the beads:
Xpos = round(Xpos); Ypos = round(Ypos); Zpos = round(Zpos);
for ip=1:length(Xpos)
    iz = 0;
    xini = max([(Xpos(ip)-Nimgxy/2) 1]);
    xfin = min([(Xpos(ip)+ Nimgxy/2) Nx]);
    yini = max([(Ypos(ip)-Nimgxy/2) 1]);
    yfin = min([(Ypos(ip)+ Nimgxy/2) Ny]);
    zini = max([(Zpos(ip)-Nimgz/2) 1]);
    zfin = min([(Zpos(ip)+ Nimgz/2) Nz]);

    totalImage = zeros((yfin-yini+1),(xfin-xini+1),(zfin-zini+1));
    for ii = 1:(2*Nimgz)
        if ((Zpos(ip)+ii-Nimgz/2)>1)&&((Zpos(ip)+ii-Nimgz/2)<Nz)
            iz = iz+1;
            U = imread(FileTif,1+Zpos(ip)+ii-Nimgz/2);
            U = double(U(yini:yfin,xini:xfin));
```

```
            Uc = median2d(U);
            totalImage(:,:,iz) = Uc;
        end
    end
    % Doing the median on the zx dimension:
    for iy=1:size(totalImage,1)
        Uz = squeeze(totalImage(iy,:,:));
        Uz = median2d(Uz);
        totalImage(iy,:,:) = Uz;
    end
    % Trimming:
    totalImage = totalImage([3:(end-3)],[3:(end-3)],[3:(end-3)]);

    Ixyz = smooth3(totalImage,'gaussian',[5 5 5]);

    close all
    [mfit3D,fimXYZ,fmin] = imResolution(Ixyz,totalImage,pixelSize);


    Xfit(ip) = (mfit3D(1)-1)*pixelSize(1)+refPos(1); %um
    Yfit(ip) = (mfit3D(2)-1)*pixelSize(2)+refPos(2); %um
    Zfit(ip) = (mfit3D(3)-1)*pixelSize(3)+refPos(3); %um
    wxy(ip) = 2*sqrt(2*log(2))*mfit3D(4)*pixelSize(1); % conversion
from sigma in gaussian to FWHM in um
    wz(ip) =  2*sqrt(2*log(2))*mfit3D(5)*pixelSize(3); %um
    Io(ip) = mfit3D(6);
    b(ip) = mfit3D(7);
    err(ip) = fmin;
end
asdfasdf
save([folder imName
'_Results.mat'],'Xpos','Ypos','Zpos','FileTif','Nz','pixelSize','Xfit'
,'Yfit','Zfit',...
                                    'wxy','wz','Io','b','err');
```

## B. grump_readheader

```
function Hdr = grump_readheader(desc)
% This function obtain the information needed from the header in the
Tiff
% file

%desc is the information contained in the File containing the
description
%of the image
%Hdr contains the position of the sample which is imaged

indx = findstr(desc,'#');

switch length(indx)
    case 16
        Hdr.Imax = str2double(desc((indx(1)+1):(indx(2)-1)));
        Hdr.Imin = str2double(desc((indx(2)+1):(indx(3)-1)));
        Hdr.Pow = str2double(desc((indx(3)+1):(indx(4)-1)));
        Hdr.Exp = str2double(desc((indx(4)+1):(indx(5)-1)));
        Hdr.Text = desc((indx(5)+1):(indx(6)-1));
        Hdr.Date = desc((indx(6)+1):(indx(7)-1));
        % Converting Time to total in days with year zero as
reference:
        Hdr.days = datenum(Hdr.Date);
        Hdr.Pow = str2double(desc((indx(7)+5):(indx(8)-1)));
        Hdr.Exp = str2double(desc((indx(8)+5):(indx(9)-1)));
        Hdr.Gain = str2double(desc((indx(9)+6):(indx(10)-1)));
        Hdr.x = str2double(desc((indx(10)+3):(indx(11)-1)));
        Hdr.y = str2double(desc((indx(11)+3):(indx(12)-1)));
        Hdr.z = str2double(desc((indx(12)+3):(indx(13)-1)));
        Hdr.r = str2double(desc((indx(13)+3):(indx(14)-1)));
        Hdr.f = str2double(desc((indx(14)+3):(indx(15)-1)));
        Hdr.dx = str2double(desc((indx(15)+4):(indx(16)-1)));
        Hdr.tilt = str2double(desc((indx(16)+6):end));
    otherwise
        Hdr = [];
end;


%Dstr = Hdr.Date;
```

## C. imResolution

```
function [mfit3D,fimXYZ,fmin,fPlotx,fPloty,fPlotz] =
imResolution(FinalImage,OrigImage,pixelSize)
%This function analyzes the particles selected for giving a desciption
of
%their PSF

%mfit3D is the most important output, as it contains the values for
the
%FWHM in the different axes.
%fimXYZ contain a fit of the different profiles: fPlotx, fPloty and
fPlotz
%fmin is the difference used between the real profile and the Gassian
%fitted

[Ny,Nx,Nz] = size(FinalImage);

vx = [1:Nx].*pixelSize(1);
vy = [1:Ny].*pixelSize(2);
vz = [1:Nz].*pixelSize(3);

% ----- XY (preliminary) ------------------------------------------
----------------
% Using the variance to find the center and approx FWHM:

[vXY,mXY] = variance2d(FinalImage,3);

imXY = vXY;

[xcmRef,ycmRef] = searchCM(imXY);

[FWHMxy,~,~,maxXY,minXY] = searchFWHM(imXY,xcmRef,ycmRef);
inivalxy = [xcmRef,ycmRef,FWHMxy/2,maxXY,minXY];

[mfitxy,fimXY] = gfitxy(double(imXY),inivalxy,'wxy');

% now we have the XY value, we need to find the Z position:
% ----- XZ ------------------------------------------------------------
--
% Fitting now the Z position (we found the X and Y)
[vXZ,mXZ] = variance2d(FinalImage,1);
imXZ = mXZ;
sumZ = sum(imXZ,1);

[mfitxz,fPlotxz] = gfit(sumZ);

[xcmRefXZ,ycmRefXZ] = searchCM(imXZ);
%[~,~,~,maxxz,minxz] = zFWHM(imXZ,xcmRefXZ,ycmRefXZ);

% Using the result to find the fwhm at a single plane:
ifit = (round(mfitxy(2))-1):(round(mfitxy(2))+1);
ifit = ifit(find((ifit>0).*(ifit<size(imXZ,1))));
vPlotxz = double(mean(imXZ(ifit,:),1));
inival1Dxz = [mfitxz(1),mfitxz(2),max(vPlotxz(:)),min(vPlotxz(:))];
[mfit1Dxz,fPlotxz,fminxz] = gfit(vPlotxz,inival1Dxz);
%inivalxz = [mfitxz(1),mfitxy(1),mfitxy(3),maxxz,minxz];
```

```
%[mfitxz2D,fimXZ] = gfitxy(double(imXZ),inivalxz,'wxwy');

% ----- YZ ------------------------------------------------------------
--
% [vYZ,mYZ] = variance2d(FinalImage,2);
% sumZ = sum(mYZ,1);
% [mfityz,fPlotyz] = gfit(sumZ);
%
% [xcmRefYZ,ycmRefYZ] = searchCM(mYZ);
% %[~,~,~,maxyz,minyz] = zFWHM(imYZ,xcmRefYZ,ycmRefYZ);
%
% % Using the result to find the fwhm at a single plane:
% inival1Dyz = [mfityz(1),mfitxy(3),max(mYZ(:)),min(mYZ(:))];
% vPlotyz = double(mYZ(round(mfitxz(1)),:));
% [mfit1Dyz,fPlotyz,fminyz] = gfit(vPlotyz,inival1Dyz);
% % inivalyz = [mfityz(1),mfitxy(2),mfitxy(3),maxyz,minyz];
% % [mfityz2D,fimYZ] = gfitxy(double(imYZ),inivalyz,'wxwy');
%
% % ------ XY (final) -----
% zo = (mfit1Dxz(1)/fminxz + mfit1Dyz(1)/fminyz)/(1/fminxz +
1/fminyz);
zo = mfit1Dxz(1);

% Using the result to find the fwhm at a single plane:
imXY = OrigImage(:,:,ceil(zo));


ifit = (round(mfitxy(2))-1):(round(mfitxy(2))+1);
ifit = ifit(find((ifit>0).*(ifit<size(imXY,1))));
vPlotx = double(mean(imXY(ifit,:),1));
inival1Dx = [mfitxy(1),mfitxy(3),max(vPlotx(:)),min(vPlotx(:))];
[mfit1Dx,fPlotx,fminx] = gfit(vPlotx,inival1Dx);

% Using the result to find the fwhm at a single plane:

ifit = (round(mfitxy(1))-1):(round(mfitxy(1))+1);
ifit = ifit(find((ifit>0).*(ifit<size(imXY,2))));
vPloty = double(mean(imXY(:,ifit),2));
inival1Dy = [mfitxy(2),mfitxy(3),max(vPloty(:)),min(vPloty(:))];
[mfit1Dy,fPloty,fminy] = gfit(vPloty,inival1Dy);



% ----- XYZ Together --------------------------------------------------
------------
% Now we try to fit all together in 3D:

xo = mfitxy(1);
yo = mfitxy(2);
%zo = (mfit1Dxz(1)/fminxz + mfit1Dyz(1)/fminyz)/(1/fminxz+1/fminyz);
%Weighted average
zo = mfit1Dxz(1);
wx = mfit1Dx(2);
wy = mfit1Dy(2);
wxy = (wx/fminx + wy/fminy)/(1/fminx + 1/fminy); %Weighted average;
%wz = (mfit1Dxz(2)/fminxz + mfit1Dyz(2)/fminyz)/(1/fminxz+1/fminyz);
%Weighted average
wz = mfit1Dxz(2);
```

```
Io = [mfit1Dx(3) mfit1Dy(3) mfit1Dxz(3)];
b = [mfit1Dx(4) mfit1Dy(4) mfit1Dxz(4)];
fmin = [fminx fminy fminxz];
% Io = [mfit1Dx(3) mfit1Dy(3) mfit1Dxz(3) mfit1Dyz(3)];
% b = [mfit1Dx(4) mfit1Dy(4) mfit1Dxz(4) mfit1Dyz(4)];
%fmin = [fminx fminy fminxz fminyz];

if yo<0
    yo = 1;
elseif yo>size(OrigImage,1)
    yo = size(OrigImage,1);
end
if xo<0
    xo = 1;
elseif xo>size(OrigImage,2)
    xo = size(OrigImage,2);
end
if zo<0
    zo = 1;
elseif zo>size(OrigImage,3)
    zo = size(OrigImage,3);
end
% Fitting the central images:
Xcut = double(squeeze(OrigImage(round(yo),:,round(zo))));
Ycut = double(squeeze(OrigImage(:,round(xo),round(zo))));
Zcut = double(squeeze(OrigImage(round(yo),round(xo),:)));
inival1Dx = [xo,wxy,Io,b];
[mfit1Dx,fPlotx,fminx] = gfit_all(Xcut,inival1Dx);
xo = mfit1Dx(1);
wx = mfit1Dx(2);
Ix = mfit1Dx(3);
bx = mfit1Dx(4);
inival1Dy = [yo,wxy,Io,b];
[mfit1Dy,fPloty,fminy] = gfit_all(Ycut,inival1Dy);
yo = mfit1Dy(1);
wy = mfit1Dy(2);
Iy = mfit1Dy(3);
by = mfit1Dy(4);
inival1Dz = [zo,wz,Io,b];
[mfit1Dz,fPlotz,fminz] = gfit_all(Zcut,inival1Dz);
zo = mfit1Dz(1);
wz = mfit1Dz(2);
Iz = mfit1Dz(3);
bz = mfit1Dz(4);
wxy = (wx./fminx + wy./fminy)./(1./fminx + 1./fminy);
b = (bx./fminx + by./fminy)./(1./fminx + 1./fminy);
Io = (Ix./fminx + Iy./fminy)./(1./fminx + 1./fminy);
fmin = (fminx + fminy + fminz)./3;
fimXYZ = [];

%Skipping this:
%inivalIob = [xo yo zo wxy wz Io b];
%[mfitIob,fimXYZ,fmin] = gfitxy(double(OrigImage),inivalIob,'Iob');

% inival3D = [xo yo zo wxy wz mfitIob(1) mfitIob(2)];
% [mfit3D,fimXYZ,fmin] = gfitxy(double(FinalImage),inival3D,'all3D');
% Io = mfitIob(6);
% b = mfitIob(7);

mfit3D(1) = xo;
```

```
mfit3D(2) = yo;
mfit3D(3) = zo;
mfit3D(4) = wx;
mfit3D(5) = wz;
mfit3D(6) = wz;
mfit3D(7) = Io;
mfit3D(8) = b;

figure
subplot(221)
plot(Xcut)
hold on
plot(fPlotx,'r')
title('X FIT')
subplot(223)
%plot(vPlotyz)
%hold on
%plot(fPlotyz,'r')
%title('YZ')
subplot(222)
plot(Ycut)
hold on
plot(fPloty,'r')
title('Y FIT')
subplot(224)
plot(Zcut)
hold on
plot(fPlotz,'r')
title('Z FIT')

% figure
% subplot(221)
% imagesc(squeeze(sum(OrigImage,1)))
% subplot(222)
% imagesc(squeeze(sum(fimXYZ,1)))
% subplot(223)
% imagesc(squeeze(sum(OrigImage,3)))
% subplot(224)
% imagesc(squeeze(sum(fimXYZ,3)))
%
pause(0.5)

end



function [xcmRef,ycmRef] = searchCM(im2D,x,y)

% im2D = double(im2D);
% [hx,hy] = hist(im2D(:));
% im2D = im2D-hy(3);
% im2D(im2D<0) = 0;

if nargin<2
    x = round(size(im2D,2)/2);
    y = round(size(im2D,1)/2);
end

im2D = median2d(im2D,5);
```

```
sizeX = size(im2D,2);
sizeY = size(im2D,1);
im2D = im2D-min(im2D(:));

%center of mass coordinates are calculated
auxX = (1:sizeX)'-x;
auxY = (1:sizeY)'-y;
xcm = round(sum(double(im2D)*auxX)/sum(im2D(:)));
ycm = round(sum(double(im2D')*auxY)/sum(im2D(:)));

xcmRef = xcm-min(auxX)+1;
ycmRef = ycm-min(auxY)+1;
end

function [width,stdWidth,R,maxIm,minIm] =
searchFWHM(subIm,xcmRef,ycmRef)
% Find the radius from the center xcm,ycm
[X,Y] = meshgrid(1:size(subIm,2),1:size(subIm,1));
R = sqrt((X-xcmRef).^2 + (Y-ycmRef).^2);

% From I vs R now WE can find the fwhm, with an error

maxIm = double(subIm(ycmRef,xcmRef));
minIm = mean(subIm(find(R>(0.8*max(R(:))))));
val = (maxIm+minIm)/2;

%An approximate value to half maximum is looked for

findClosest = abs(double(subIm)-val);
b = 0.1*maxIm; %value included above and below the desired one
posClosest = R(findClosest<b);
meanWidth = mean(posClosest(:));
stdWidth = std(posClosest);

%The FWHM is computed witht the following formula
width = meanWidth*2;
end

function [width,stdWidth,vPlot,maxIm,minIm] = zFWHM(subIm,xcm,ycm)
vPlot = subIm(ycm-
round(0.1*size(subIm,1)):ycm+round(0.1*size(subIm,1)),:);%vector
containing the row of the image corresponding to the maximum value
vPlot = mean(vPlot,1);
maxIm = double(subIm(ycm,xcm));
minIm = mean(vPlot(find((vPlot-min(vPlot(:)))<0.1*(maxIm-
min(vPlot(:))))));

%vPlot is divided in a left and right part corresponding to the
maximum
%point, so that points at both sides of the maximum can be obtained
vPlotL = vPlot(1:xcm);
vPlotR = vPlot(xcm+1:end);
%An approximate value to half maximum is looked for
val = (maxIm+minIm)/2;
findClosestL = abs(vPlotL-val); %vector which defines who far the
value is from the desired one
closestL = min(findClosestL);
```

```
posClosestL = find(findClosestL==closestL); %position for the left
part
if numel(posClosestL)==0
    keyboard
end
posClosestL = posClosestL(1);

%same for right part
findClosestR = abs(vPlotR-val);
closestR = min(findClosestR);
posClosestR = find(findClosestR==closestR);
posClosestR = posClosestR(1);

%The FWHM is computed witht the following formula
width = posClosestR + length(findClosestL)-posClosestL;
stdWidth = 0;
end
```

## D. gfit

```
function [mfit,fPlot,fmin] = gfit(Usub,inival)
%gfit creates a Gaussian fit in 1D

%mfit contains the parameters describing the Gaussian function
%fPlot is the fit created
%fmin is the difference used between the real profile and the Gassian
%fitted

Nx=length(Usub);

if nargin<2 || isempty(inival),
    xpix = (1:Nx);
    xcm = round(sum(double(Usub(:)-min(Usub(:))).*xpix(:))/sum(Usub-
min(Usub(:))));
    xcm = xcm+Nx/2;
    [Umax,mpos] = max(Usub(:));
    inival = [mpos,10,Umax,min(Usub(:))];
end

xpix = 1:Nx;

mfit = fminsearch(@gw_find,inival,[],Usub,xpix);
if mfit(1)<1, mfit(1) = 1; end;
if mfit(1)>Nx, mfit(1) = Nx; end;

% mfit(2) = mfit(2)*2;
[fmin,fPlot] = gw_find(mfit,Usub,xpix);


% clf
% % figure(23)
% plot(vz,Usub)
% hold on
% plot(vz,fPlot,'r')
% title('Mean of central stacks')
% xlabel('Distance (\mum)');
% ylabel('Intensity');
% legend('Original','Fitted');

% xo = mfit(1);
% wx = mfit(2);
% Io = mfit(3);
% b = mfit(4);

% figure(21)
% clf
% plot(Usub)
% hold on
% plot(fPlot,'r')
% ---
end

function [fmin,Ig] = gw_find(inival,U,xpix)

xo = inival(1);
wx = inival(2);
```

```
Io = inival(3);
b = inival(4);
Ig = (Io-b).*exp(-(xpix-xo).^2/(2*wx.^2))+b;

fmin = (sum((U(:)-Ig(:)).^2))/sum(Ig(:)) + exp(-(Io-b)) +...
    (xo<1)*exp(-xo*100);


%
% figure(23)
% clf
% plot(xpix,U)
% hold on
% plot(xpix,Ig,'r')
% title('Mean of central stacks')
% legend('Original','Fitted');
end
```

## E. gfit_all

```
function [mfit,fPlot,fmin] = gfit_all(Usub,inival)
%gfit_all creates a Gaussian fit in all the axes

%mfit contains the parameters describing the Gaussian function
%fPlot is the fit created
%fmin is the difference used between the real profile and the Gassian
%fitted

Nx=length(Usub);

if nargin<2 || isempty(inival),
    xpix = (1:Nx);
    xcm = round(sum(double(Usub(:)-min(Usub(:))).*xpix(:))/sum(Usub-
min(Usub(:))));
    xcm = xcm+Nx/2;
    [Umax,mpos] = max(Usub(:));
    inival = [mpos,10,Umax,min(Usub(Usub>0))];
end

xpix = 1:Nx;

[x,h] = hist(Usub(:),10);
Umin = mean(h(1));

mfit = fminsearch(@gw_find,inival,[],Usub,xpix,Umin);
if mfit(1)<1, mfit(1) = 1; end;
if mfit(1)>Nx, mfit(1) = Nx; end;

% mfit(2) = mfit(2)*2;
[fmin,fPlot] = gw_find(mfit,Usub,xpix,Umin);


% clf
% % figure(23)
% plot(vz,Usub)
% hold on
% plot(vz,fPlot,'r')
% title('Mean of central stacks')
% xlabel('Distance (\mum)');
% ylabel('Intensity');
% legend('Original','Fitted');

% xo = mfit(1);
% wx = mfit(2);
% Io = mfit(3);
% b = mfit(4);

% figure(21)
% clf
% plot(Usub)
% hold on
% plot(fPlot,'r')
% ---
end

function [fmin,Ig] = gw_find(inival,U,xpix,Umin)
```

```
%b =min(U(:));
xo = inival(1);
wx = inival(2);
Io = inival(3);
b = inival(4);
Ig = (Io-b).*exp(-(xpix-xo).^2/(2*wx.^2))+b;

if size(U)~=size(Ig)
    Ig = permute(Ig,[2 1]);
end
idx = find(U>Umin);
fmin = sqrt(sum((U(idx)-Ig(idx)).^2))/length(Ig(idx)) + exp(-(Io-b))
+...
    (xo<1)*exp(-xo*100) + (b<0)*exp(-b);



% figure(23)
% clf
% plot(xpix,U)
% hold on
% plot(xpix,Ig,'r')
% plot(xpix(idx),Ig(idx),'ro')
% title('Mean of central stacks')
% legend('Original','Fitted');
end
```

## F. gfitxy

```
function [mfit,fimXY,fmin] = gfitxy(Usub,inival,what2fit)
%gfit creates a Gaussian fit in 2D for cases 'wxy' and 'wxwy'

%mfit contains the parameters describing the Gaussian function
%fimXY is the fit created
%fmin is the difference used between the real profile and the Gassian
%fitted

if nargin<3
    what2fit = 'wxy';
end

switch what2fit
    case 'wxy'

        [Nx,Ny]=size(Usub);
        [xpix,ypix]=meshgrid(1:Ny,1:Nx);

        if nargin<2 || isempty(inival),
            inival = [Nx/2, Ny/2, 10, max(Usub(:)), min(Usub(:))];
        end

        mfit = fminsearch(@gwxy_find,inival,[],Usub,xpix,ypix);

        if mfit(1)<1, mfit(1) = 1; end
        if mfit(2)<1, mfit(2) = 1; end
        if mfit(1)>Nx, mfit(1) = Nx; end
        if mfit(2)>Ny, mfit(2) = Ny; end;

        % mfit(3) = mfit(3)*2;
        [fmin,fimXY] = gwxy_find(mfit,Usub,xpix,ypix);

    case 'wxwy'

        [Nx,Ny]=size(Usub);
        [xpix,ypix]=meshgrid(1:Ny,1:Nx);

        xpos = inival(1);
        ypos = inival(2);
        inivalw = [10, 10, max(Usub(:)), min(Usub(:))];

        wfit =
fminsearch(@gwxwy_find,inivalw,[],Usub,xpix,ypix,xpos,ypos);
        [fmin,fimXY] = gwxwy_find(wfit,Usub,xpix,ypix,xpos,ypos);
        mfit(1) = inival(1);
        mfit(2) = inival(2);
        mfit(3) = wfit(1);
        mfit(4) = wfit(2);
        mfit(5) = wfit(3);
        mfit(6) = wfit(4);

    case 'Iob'

        [Nx,Ny,Nz]=size(Usub);
        [xpix,ypix,zpix]=meshgrid(1:Ny,1:Nx,1:Nz);
```

```
        xpos = inival(1);
        ypos = inival(2);
        zpos = inival(3);
        wxy = inival(4);
        wz = inival(5);
        inivalI = [max(Usub(:)), min(Usub(:))];

        Ifit =
fminsearch(@gIob_find,inivalI,[],Usub,xpix,ypix,zpix,xpos,ypos,zpos,wx
y,wz);
        [fmin,fimXY] =
gIob_find(Ifit,Usub,xpix,ypix,zpix,xpos,ypos,zpos,wxy,wz);
        mfit(1:5) = inival(1:5);
        mfit(6) = Ifit(1);
        mfit(7) = Ifit(2);

    case {'all3D','all3d'}

        [Nx,Ny,Nz]=size(Usub);
        [xpix,ypix,zpix]=meshgrid(1:Ny,1:Nx,1:Nz);

        mfit = fminsearch(@g3d_find,inival,[],Usub,xpix,ypix,zpix);
        [fmin,fimXY] = g3d_find(mfit,Usub,xpix,ypix,zpix);
end


% figure(20)
% yo = mfit(2);
% clf
% subplot(211)
% plot(vx,sum(Usub))
% hold on
% plot(vxf,sum(fimXY),'r')
% title('Sum of all stacks')
% xlabel('Distance (\mum)');
% ylabel('Intensity');
% legend('Original','Fitted');
% % plot(idx,Igxy(idx),'r.')
%
% subplot(212)
% plot(Usub(round(yo+round(size(Usub,1)/2)),:))
% hold on
% plot(fimXY(round(yo+round(size(Usub,1)/2)),:),'r')
% title('Stack of maximum intensity')
% xlabel('Distance (\mum)');
% ylabel('Intensity');
% legend('Original','Fitted');

% yo = mfit(2);
% figure(20)
% subplot(211)
% clf
% plot(sum(Usub))
% hold on
% plot(sum(fimXY),'r')
%
% subplot(212)
% clf
```

```
% plot(Usub(round(yo+round(size(Usub,1)/2)),:))
% hold on
% plot(fimXY(round(yo+round(size(Usub,1)/2)),:),'r')
% title('XY fit')
return
% ---

function [fmin,Ig] = gwxy_find(inival,U,xpix,ypix)

xo = inival(1);
yo = inival(2);
wxy = inival(3);
Io = inival(4);
b = inival(5);
Ig = (Io-b).*exp(-((xpix-xo).^2 + (ypix-yo).^2)./(2*wxy.^2)) + b;

Igxy = (Ig);
Uxy = (U);

%Igxy = Ig(round(yo+round(size(U,1)/2)),:);
%Uxy = U(round(yo+round(size(U,1)/2)),:);

%idx = find(Uxy>(0.0*max(Uxy(:)-min(Uxy(:)))+min(Uxy(:))));
%fmin = sqrt(sum((U(:)-Ig(:)).^2))/length(U(:));
fxy = (Igxy(:)-Uxy(:));
fmin = sqrt(sum(fxy(:).^2))./length(Igxy(:)) + exp(-(Io-b)) + ...
    (xo<0).*exp(-xo*100) + (yo<0).*exp(-yo*100) +
(xo>size(xpix,1)).*exp(xo) + (yo>size(ypix,2)).*exp(yo);

% idx = find(Uxy>(0.05*max(Uxy-min(Uxy(:)))+min(Uxy(:))));
%
% %fmin = sqrt(sum((U(:)-Ig(:)).^2))/length(U(:));
% fxy = abs(Igxy(idx)-Uxy(idx));
%
% fmin = mean(fxy(:).^2)/max(U(:)).^2;
%
% fmin = round(fmin*100)/100;

% figure(20)
% clf
% subplot(221)
% plot(sum(U))
% hold on
% plot(sum(Ig),'r')
% title('Sum of all stacks')
% legend('Original','Fitted');
% % plot(idx,Igxy(idx),'r.')
% subplot(222)
% plot(U(round(yo+round(size(U,1)/2)),:))
% hold on
% plot(Ig(round(yo+round(size(U,1)/2)),:),'r')
% title('Stack of maximum intensity')
% legend('Original','Fitted');
% subplot(223)
% plot(sum(U,2))
% hold on
% plot(sum(Ig,2),'r')
% title('Sum of all stacks')
% legend('Original','Fitted');
```

```
% % plot(idx,Igxy(idx),'r.')
% subplot(224)
% plot(U(:,round(xo+round(size(U,2)/2))))
% hold on
% plot(Ig(:,round(xo+round(size(U,2)/2))),'r')
% title('Stack of maximum intensity')
% legend('Original','Fitted');

function [fmin,Ig] = gwxwy_find(inival,U,xpix,ypix,xo,yo)

wx = inival(1);
wy = inival(2);
Io = inival(3);
b = inival(4);
Ig = (Io-b).*exp(-((xpix-xo).^2./(2*wx.^2))).*exp(-((ypix-
yo).^2./(2*wy.^2))) + b;

fmin = sqrt(sum((U(:)-Ig(:)).^2))./sum(Ig(:)) + exp(-(Io-b));

function [fmin,Ig] = g3d_find(inival,U,xpix,ypix,zpix)

xo = inival(1);
yo = inival(2);
zo = inival(3);
wxy = inival(4);
wz = inival(5);
Io = inival(6);
b = inival(7);

Ig = (Io-b).*exp(-((xpix-xo).^2 + (ypix-yo).^2)./(2*wxy.^2)).*...
    exp(-(zpix-zo).^2./(2*wz.^2)) + b;

fmin = sqrt(sum((U(:)-Ig(:)).^2))./length(Ig(:)) + exp(-(Io-b)) + ...
    (xo<0).*exp(-xo*100) + (yo<0).*exp(-yo*100) + (zo<0).*exp(-zo*100)
+ ...
    (xo>length(xpix)).*exp(xo) + (yo>length(ypix)).*exp(yo) +
(zo>length(zpix)).*exp(zo);

% figure(20)
% clf
% subplot(221)
% imagesc(squeeze(sum(U,1)))
% subplot(222)
% imagesc(squeeze(sum(Ig,1)))
% subplot(223)
% imagesc(squeeze(sum(U,3)))
% subplot(224)
% imagesc(squeeze(sum(Ig,3)))
return

function [fmin,Ig] =
gIob_find(inival,U,xpix,ypix,zpix,xo,yo,zo,wxy,wz)

Io = inival(1);
b = inival(2);

Ig = (Io-b).*exp(-((xpix-xo).^2 + (ypix-yo).^2)./(2*wxy.^2)).*...
    exp(-(zpix-zo).^2./(2*wz.^2)) + b;
```

```
fmin = sqrt(sum((U(:)-Ig(:)).^2)./sum(Ig(:)) + exp(-(Io-b)) + ...
    (xo<0).*exp(-xo*100) + (yo<0).*exp(-yo*100) + (zo<0).*exp(-zo*100)
+ ...
    (xo>length(xpix)).*exp(xo) + (yo>length(ypix)).*exp(yo) +
(zo>length(zpix)).*exp(zo);

% figure(20)
% clf
% subplot(221)
% imagesc(squeeze(sum(U,1)))
% subplot(222)
% imagesc(squeeze(sum(Ig,1)))
% subplot(223)
% imagesc(squeeze(sum(U,3)))
% subplot(224)
% imagesc(squeeze(sum(Ig,3)))
return
```

# ACRONYMS

SPIM: Selective Plane Illumination Microscopy

OPT: Optical Projection Tomography

PSF: Point Spread Function

FWHM: Full Width at Half Maximum

MTF: Modulated Transfer Function

OTF: Optical Transfer Function

ERF: Edge Response Function

LSFM: Light Sheet Fluorescent Microscopy

FOV: Field Of View

FBP: Filtered Back Projection

MLEM: Maximum Likelihood Expectation Maximization

ROI: Region Of Interest

NA: Numerical Aperture

# BIBLIOGRAPHY


[1] A. Van Helden, S. Dupre, and R. Van Gent, "The Origins of the Telescope," p. 43, 2011.

[2] S. Bradbury, "The Evolution of the Microscope," *Pergamon Press*, p. 357, 1967.

[3] Zeiss Group Microscopes Business Unit, *Anticipating the Future*. Jena, Germany, 1996, p. 34.

[4] D. Murphy, "Differential interference contrast (DIC) microscopy and modulation contrast microscopy," *Fundam. Light Microsc. Digit. Imaging*, no. Wiley-Liss, New York, pp. 153–168, 2001.

[5] Nikon, "Introduction to Fluorescence Microscopy," *MicroscopyU*, 2008. [Online]. Available: http://www.microscopyu.com/articles/fluorescence/fluorescenceintro.html.

[6] J. Kapuscinski, "DAPI: a DNA-specific fluorescent probe.," *Biotech. Histochem.*, vol. 70, pp. 220–233, 1995.

[7] D. Axelrod, "Cell-substrate contacts illuminated by total internal reflection fluorescence.," *J. Cell Biol.*, vol. 89, pp. 141–145, 1981.

[8] M. Davidson and M. Abramowitz, "Optical Microscopy," *Microscopy Resource Center Olympus*, 1999. .

[9] C. F. Bohren and D. R. Huffman, *Absorption and scattering of light by small particles*, vol. 1. 1983, p. xiv, 530 p.

[10] M. Davidson and K. Spring, "Working Distance and Parfocal Length," *MicroscopyU Nikon*. [Online]. Available: http://www.microscopyu.com/articles/formulas/formulasworkingparfocal.html.

[11] W. Abramowithz, *Contrast Methods in Microscopy: Transmitted Light*. Melville, New York: Olympus America, Inc., 1987, p. 31.

[12] Photomicrography: Instant Photography Through the Microscope. Cambridge, MA: Polaroid Corporation, 1995, p. 72.

[13] L. Gao, L. Shao, C. D. Higgins, J. S. Poulton, M. Peifer, M. W. Davidson, X. Wu, B. Goldstein, and E. Betzig, "Noninvasive imaging beyond the diffraction limit of 3D dynamics in thickly fluorescent specimens," *Cell*, vol. 151, pp. 1370–1385, 2012.

[14] M. B. Ahrens, M. B. Orger, D. N. Robson, J. M. Li, and P. J. Keller, “Whole-brain functional imaging at cellular resolution using light-sheet microscopy.,” *Nat. Methods*, vol. 10, pp. 413–20, 2013.

[15] T. V Truong, W. Supatto, D. S. Koos, J. M. Choi, and S. E. Fraser, “Deep and fast live imaging with two-photon scanned light-sheet microscopy.,” *Nat. Methods*, vol. 8, pp. 757–760, 2011.

[16] P. J. Verveer, J. Swoger, F. Pampaloni, K. Greger, M. Marcello, and E. H. K. Stelzer, “High-resolution three-dimensional imaging of large specimens with light sheet-based microscopy.,” *Nat. Methods*, vol. 4, pp. 311–313, 2007.

[17] S. Preibisch, S. Saalfeld, J. Schindelin, and P. Tomancak, “Software for bead-based registration of selective plane illumination microscopy data.,” *Nature methods*, vol. 7. pp. 418–419, 2010.

[18] P. J. Keller, A. D. Schmidt, A. Santella, K. Khairy, Z. Bao, J. Wittbrodt, and E. H. K. Stelzer, “Fast, high-contrast imaging of animal development with scanned light sheet-based structured-illumination microscopy.,” *Nat. Methods*, vol. 7, pp. 637–642, 2010.

[19] J. Sharpe, “Optical projection tomography.,” *Annu. Rev. Biomed. Eng.*, vol. 6, pp. 209–28, Jan. 2004.

[20] J. Sharpe, U. Ahlgren, P. Perry, B. Hill, A. Ross, J. Hecksher-Sørensen, R. Baldock, and D. Davidson, “Optical projection tomography as a tool for 3D microscopy and gene expression studies.,” *Science*, vol. 296, no. 5567, pp. 541–5, Apr. 2002.

[21] D. W. Holdsworth and M. M. Thornton, “Micro-CT in small animal and specimen imaging,” *Trends in Biotechnology*, vol. 20. 2002.

[22] L. W. Goldman, “Principles of CT and CT technology.,” *J. Nucl. Med. Technol.*, vol. 35, pp. 115–128; quiz 129–130, 2007.

[23] E. L. Ritman, “Current status of developments and applications of micro-CT.,” *Annu. Rev. Biomed. Eng.*, vol. 13, pp. 531–552, 2011.

[24] H. Siedentopf and R. Zsigmondy, “Uber Sichtbarmachung und Größenbestimmung ultramikoskopischer Teilchen, mit besonderer Anwendung auf Goldrubingläser,” *Ann. Phys.*, vol. 315, no. 1, pp. 1–39, 1902.

[25] W. Spaltenholz, Über das Durchsichtigmachen von menschlichen und tierischen Präparaten : nebst Anhang: Über Knochenfärbung. Leipzig: S. Hirzel, 1911.

[26] Y. Wu, A. Ghitani, R. Christensen, A. Santella, Z. Du, G. Rondeau, and Z. Bao, “Inverted selective plane illumination microscopy ( i SPIM ) enables coupled cell identity lineaging and neurodevelopmental imaging in Caenorhabditis elegans,” pp. 2–7.

[27] Y. Wu, P. Wawrzusin, J. Senseney, R. S. Fischer, R. Christensen, A. Santella, A. G. York, P. W. Winter, C. M. Waterman, Z. Bao, D. a Colón-Ramos, M. McAuliffe, and H. Shroff, “Spatially isotropic four-dimensional imaging with dual-view plane illumination microscopy.,” *Nat. Biotechnol.*, vol. 31, no. 11, pp. 1032–8, Nov. 2013.

[28] P. A. STOKSETH, “Properties of a Defocused Optical System,” *Journal of the Optical Society of America*, vol. 59. p. 1314, 1969.

[29] Y. Hiraoka, J. W. Sedat, and D. A. Agard, “Determination of three-dimensional imaging properties of a light microscope system. Partial confocal behavior in epifluorescence microscopy.,” *Biophys. J.*, vol. 57, pp. 325–333, 1990.

[30] J. G. McNally, C. Preza, J. A. Conchello, and L. J. Thomas, “Artifacts in computational optical-sectioning microscopy.,” *J. Opt. Soc. Am. A. Opt. Image Sci. Vis.*, vol. 11, pp. 1056–1067, 1994.

[31] P. Pankajakshan, L. Blanc-F??raud, Z. Kam, and J. Zerubia, “Point-spread function retrieval for fluorescence microscopy,” in *Proceedings - 2009 IEEE International Symposium on Biomedical Imaging: From Nano to Macro, ISBI 2009*, 2009, pp. 1095–1098.

[32] C. J. R. Sheppard and P. T??r??k, “An electromagnetic theory of imaging in fluorescence microscopy, and imaging in polarization fluorescence microscopy,” *Bioimaging*, vol. 5, pp. 205–218, 1997.

[33] P. Török, P. D. Higdon, and T. Wilson, “Theory for confocal and conventional microscopes imaging small dielectric scatterers,” *Journal of Modern Optics*, vol. 45. pp. 1681–1698, 1998.

[34] P. D. Higdon, P. T??r??k, and T. Wilson, “Imaging properties of high aperture multiphoton fluorescence scanning optical microscopes,” *J. Microsc.*, vol. 193, pp. 127–141, 1999.

[35] P. Török, P. D. Higdon, and T. Wilson, “On the general properties of polarised light conventional and confocal microscopes,” *Optics Communications*, vol. 148. pp. 300–315, 1998.

[36] R. W. Cole, T. Jinadasa, and C. M. Brown, “Measuring and interpreting point spread functions to determine confocal microscope resolution and ensure quality control.,” *Nat. Protoc.*, vol. 6, no. 12, pp. 1929–41, Dec. 2011.

[37] U. Leischner, W. Zieglgänsberger, and H. Dodt, “Resolution of ultramicroscopy and field of view analysis,” *PLoS One*, no. June, 2009.

[38] O. Haeberlé, M. Ammar, H. Furukawa, K. Tenjimbayashi, and P. Török, “The point spread function of optical microscopes imaging through stratified media.,” *Opt. Express*, vol. 11, no. 22, pp. 2964–9, Nov. 2003.

[39] L. Gao, L. Shao, B. Chen, and E. Betzig, “3D live fluorescence imaging of cellular dynamics using Bessel beam plane illumination microscopy,” pp. 1083–1101, 2014.

[40] M. Rieckher, U. J. Birk, H. Meyer, J. Ripoll, and N. Tavernarakis, “Microscopic optical projection tomography in vivo,” *PLoS One*, vol. 6, 2011.

[41] C. Vinegoni, C. Pitsouli, D. Razansky, N. Perrimon, and V. Ntziachristos, “In vivo imaging of Drosophila melanogaster pupae with mesoscopic fluorescence tomography.,” *Nat. Methods*, vol. 5, pp. 45–47, 2008.

[42] L. McGurk, H. Morrison, L. P. Keegan, J. Sharpe, and M. A. O’Connell, “Three-dimensional imaging of Drosophila melanogaster,” *PLoS One*, vol. 2, 2007.

[43] A. D. Leeper, J. Farrell, J. M. Dixon, S. E. Wedden, D. J. Harrison, and E. Katz, “Long-term Culture of Human Breast Cancer Specimens and Their Analysis Using Optical Projection Tomography.,” *J. Vis. Exp.*, 2011.

[44] A. Kokolakis, G. Zacharakis, K. Krasagakis, K. Lasithiotakis, R. Favicchio, G. Spiliopoulos, E. Giannikaki, J. Ripoll, and A. Tosca, “Prehistological evaluation of benign and malignant pigmented skin lesions with optical computed tomography,” *Journal of Biomedical Optics*, vol. 17. p. 066004, 2012.

[45] V. Ntziachristos, “Going deeper than microscopy: the optical imaging frontier in biology.,” *Nat. Methods*, vol. 7, pp. 603–614, 2010.

[46] A. Arranz, D. Dong, S. Zhu, M. Rudin, C. Tsatsanis, J. Tian, and J. Ripoll, “Helical optical projection tomography.,” *Opt. Express*, vol. 21, pp. 25912–25, 2013.

[47] J. C. Lagarias, J. A. Reeds, M. H. Wright, and P. E. Wright, “Convergence Properties of the Nelder--Mead Simplex Method in Low Dimensions,” *SIAM Journal on Optimization*, vol. 9. pp. 112–147, 1998.

[48] J. Huisken and D. Y. R. Stainier, “Selective plane illumination microscopy techniques in developmental biology.,” *Development*, vol. 136, no. 12, pp. 1963–75, Jun. 2009.

[49] J. Ripoll, “Scattering and Absorption,” in *Principles of Diffuse Light Propagation*, WORLD SCIENTIFIC, 2012, pp. 53–88.